DESIGN OF AIR-COOLED MICROCHANNEL CONDENSERS FOR MAL-DISTRIBUTED AIR FLOW CONDITIONS

A Thesis

Presented to

The Academic Faculty

by

Vishwanath Subramaniam

In Partial Fulfillment

of the Requirements for the Degree

Master of Science in Mechanical Engineering

Georgia Institute of Technology

July 2004

DESIGN OF AIR-COOLED MICROCHANNEL CONDENSERS FOR MAL-DISTRIBUTED AIR FLOW CONDITIONS

Approved by:

Dr. Srinivas Garimella, Chairman

Dr. Sheldon Jeter

Dr. Yogendra Joshi

Date Approved: July 09, 2004

TABLE OF CONTENTS

LIST OF TABLES

LIST OF FIGURES

NOMENCLATURE

A_{ba}	Air-side flow area blocked by fins
A_c	Total core face area
A_{da}	Air-side direct heat transfer area
A_{dt}	Tube-side direct heat transfer area
A_{effa}	Air-side effective heat transfer area
A_{efft}	Tube effective heat transfer area
A_{fa}	Total air-side free flow area
A_{ft}	Total tube inside free flow area
A_{ida}	Air-side indirect heat transfer area
A_{idt}	Tube indirect heat transfer area
A_t	Inside cross sectional area of each tube
C	Thermal capacity rate
c_h	Fin height
C_{ratio}	Ratio of thermal capacity rates
c_w	Fin depth
D_{ha}	Air-side hydraulic diameter
D_{ht}	Tube hydraulic diameter
f	Friction factor
f_p	Fin pitch

f_{thk}	Fin thickness
g	Acceleration due to gravity
G	Mass flux
h_{air}	Air-side heat transfer coefficient
h_{tube}	Tube-side heat transfer coefficient
j	Colburn j factor
k	Thermal conductivity
L_{cond}	Total condenser length
l_l	Louver length
l_p	Louver pitch
L_{seg}	Segment length
$mass_{fin}$	Mass of fins
$mass_{total}$	Total mass
$mass_{tube}$	Mass of tube
NTU	Number of heat transfer units
n_{tube_total}	Total number of tubes
N_u	Nusselt number
N_w	Number of webs
P	Pressure
per_a	Air-side wetted perimeter
per_t	Tube-side wetted perimeter
Pr	Prandtl number
Q_{actual}	Actual heat transferred per segment

Q_{max}	Maximum heat transfer possible per segment
r	Surface roughness
Re	Reynolds number
Re_{lp}	Reynolds number based on louver pitch
T_{ain}	Air inlet temperature
T_{aout}	Air outlet temperature
t_{hi}	Tube inner height
thk_t	Tube wall thickness
t_{ho}	Tube outer height
t_p	Tube pitch
t_{wi}	Tube inner width
v_{ratio}	Velocity ratio
w_t	Web thickness
web_{sp}	Web spacing
x	Quality

Greek Symbols

α	Aspect ratio
α_v	Void fraction
ε	Effectiveness
η_{fa}	Air side fin efficiency
η_{ft}	Tube side fin efficiency
θ	Louver angle

μ	Kinematic viscosity
ρ	Density
σ	Surface tension

Subscripts

a	Air
Al	Aluminum
cri	Critical
go	Gas only
in	Inlet
liq	Liquid
lo	Liquid only
max	Maximum
min	Minimum
out	Outlet
r	Refrigerant
t	Tube
TP	Two phase
Vap	Vapor

ACKNOWLEDGEMENTS

I would like to take this opportunity to express my sincere gratitude to my advisor Dr. Srinivas Garimella for his constant support and guidance in the course of this work. This thesis would not have been possible in the current form without his exhaustive reviews. I would also like to thank my committee members Dr. Sheldon Jeter and Dr. Yogendra Joshi for their co-operation.

Special thanks to all the members of STSL, who were always willing to lend a helping hand, when I required it. The warm and friendly atmosphere at STSL made working there a pleasure.

ABSTRACT

Air-cooled condensers are routinely designed for a variety of applications, including residential air-conditioning systems. Recent attempts at improving the performance of these heat exchangers have included the consideration of microchannel tube, multilouver fin heat exchangers instead of the more conventional round tube-plate fin designs. In most packaged air-conditioning systems, however, the condenser surrounds the compressor and other auxiliary parts in an outdoor unit, with an induced draft fan at the top of this enclosure. Such a configuration results in significant mal-distribution of the air flow arriving at the condenser, and leads to a decrease in performance. This work addresses the issue of mal-distribution by adapting the air-side geometry to the expected air flow distribution. A microchannel tube, multilouver fin condenser is first designed to transfer the desired heat rejection load for an air-conditioning system under uniform air flow conditions. Tube-side pass arrangements, tube dimensions, and fin and louver geometry are varied to arrive at a minimum mass, 2.54 kg condenser that delivers the desired heat load of 14.5 kW. The design model is then used to predict the performance of the condenser for a variety of air flow distributions across the heat exchanger. It is found that for a 50% air flow mal-distribution, the required condenser mass increases to 2.73 kg. The air-side geometry (fin density and height) of the condenser is then systematically changed to optimally distribute the air-side surface area across the condenser to best address the mal-distributed air flow. It is found that linear fin density and height variations from the

mean value of 40% and 20%, respectively, keeping the mean fin density and height the same, reduce the required condenser mass to 2.65 kg even for this mal-distributed air-flow case. The influence of geometry variations on heat transfer coefficients, fan power and other performance measures is discussed in detail to guide the judicious choice of surface area and tube-side flow area allocations for any potential air flow mal-distribution. The results from this study can be used for the design of air-cooled condensers under realistic flow conditions.

Chapter 1

INTRODUCTION

1.1 Microchannel Condensers

Microchannel-tube, multilouver-fin heat exchangers are fast replacing conventional round-tube, plate-fin condensers in air-conditioning applications. The larger air-side heat transfer coefficients due to the louvers and the larger surface area per unit volume of these tubes are believed to lead to more compact heat exchangers. The basic geometry of a microchannel condenser and multilouver fin is shown in Figure 1.1.

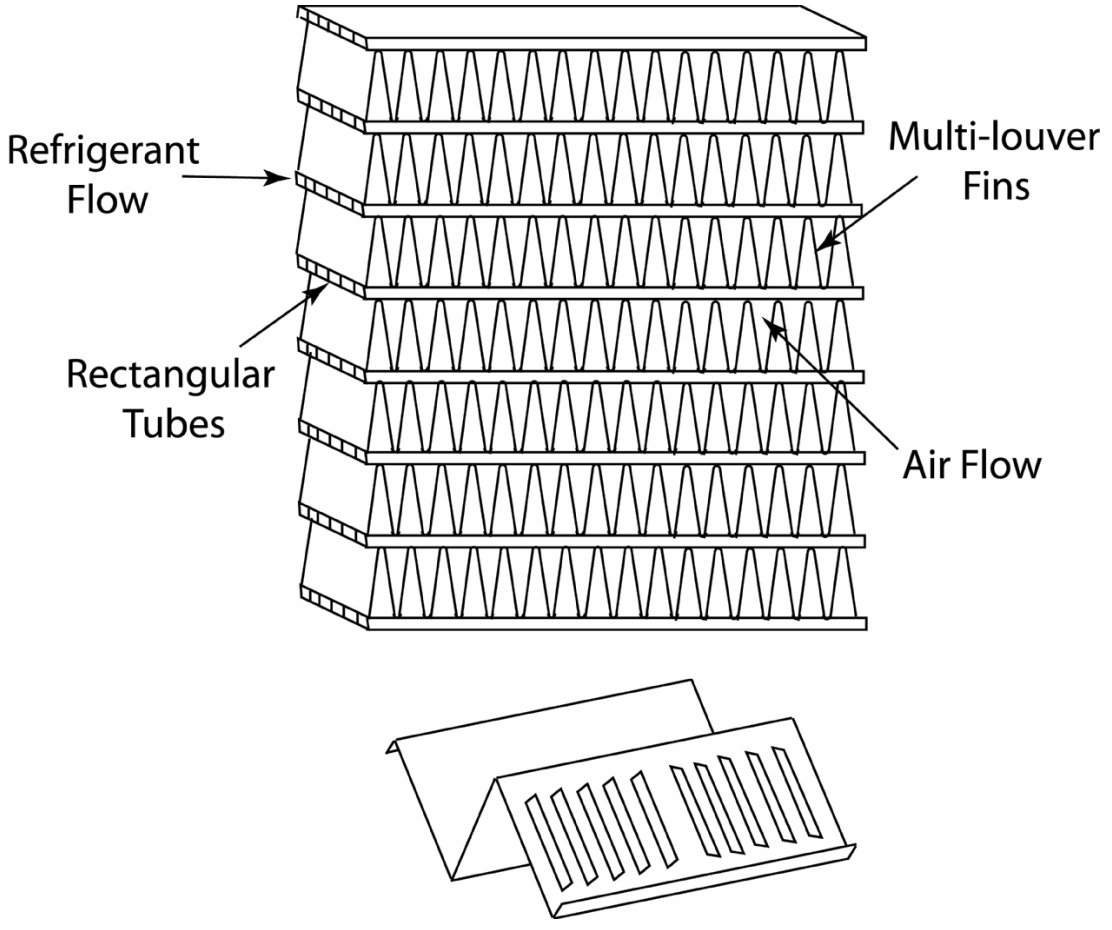

Figure 1. 1 Schematic of a Microchannel Condenser and Multilouver Fin

1.2 Need for Air Flow Mal-Distribution Analysis

Figure 1.2 shows a typical condenser unit of an air conditioning system. The condenser coils are vertically placed along the four sidewalls of the condenser unit. Air flow over the condenser coils is generated by an induced draft fan placed at the top of the unit. This configuration results in a non-uniform air flow through the condenser coils. Hence a uniform air flow distribution, which is assumed in most theoretical studies, is an idealization. A study of the condenser performance for mal-distributed air flow conditions is required.

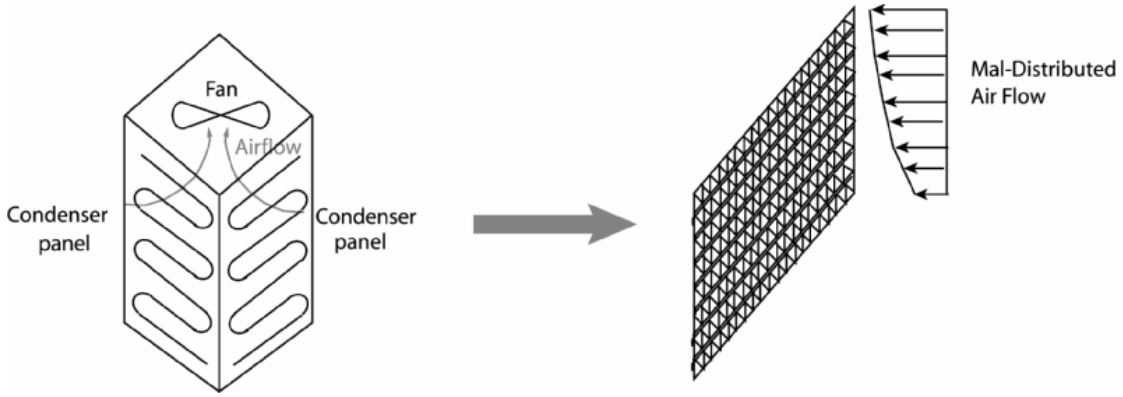

Figure 1. 2 Cause of Air Flow Mal-distribution

1.3 Thesis Outline

The thesis is organized as follows:

Chapter 1 introduces the microchannel, multi-louvered fin condenser geometry and explains the need to study its performance under mal-distributed air flow conditions.

Chapter 2 reviews the literature on the various applications of microchannel heat exchangers and discusses their advantages over conventional geometries. The chapter also reviews literature on the study of performance of conventional heat exchangers under mal-distributed air flow conditions. In addition, the chapter also identifies the need

for the current research on the study of the effect of air flow maldistributions on microchannel condensers.

Chapter 3 describes the heat transfer and pressure drop models and the calculation scheme used to evaluate the heat duty of a particular microchannel condenser. It also outlines a design procedure to obtain an optimum geometry that which delivers the design heat duty with minimum mass under uniform air flow conditions.

Chapter 4 analyzes the performance of the condenser for various linearly mal-distributed air flows.

Chapter 5 describes a procedure to design a condenser that performs optimally under mal-distributed air flow conditions. This is done by varying the air-side geometrical parameters such as fin density and fin height along the condenser height.

Chapter 6 provides conclusions from the current study and recommendations for further research.

Chapter 2

LITERATURE REVIEW

2.1 Literature on Microchannel Condensers

Garimella and Coleman (1998) studied the design and optimization of air-cooled, round-tube condensers for ammonia-water absorption heat pumps. They studied the performance of these systems with flat, wavy, louvered and annular fins. The goal of their optimization was to obtain the design heat duty of 18 kW with the minimum mass heat exchanger possible. It was found that wavy fins resulted in the smallest heat exchanger mass among the fin geometries considered within the constraints of the allowable pressure drop. According to the authors, this is because of secondary flows induced by the wavy fins, which increase the air-side heat transfer coefficient and result in a lower mass of the heat exchanger.

Garimella et al. (1997) also considered the substitution of conventional air-coupled single-phase exchangers for residential absorption heat pumps with such flat-tube, multilouver-fin heat exchangers. They demonstrated that the use of these flat-tube heat exchangers led to a 59 percent reduction in the heat exchanger mass compared to a round-tube, wavy-fin heat exchanger.

Condensation of ammonia in flat-tube, multi-louver fin heat exchangers was investigated by Garimella and Wicht (1995), who optimized the various geometric parameters to obtain a design heat duty of 21 kW with lowest heat exchanger mass. They found that tube and fin depth and fin spacing had a significant effect on heat exchanger performance. The heat exchanger mass was reduced from a nominal value of 19.0 kg to

17.7 kg by optimizing the geometric parameters. Also the available air flow was shown to have a significant effect on performance. A 20% decrease in air flow resulted in a 60% increase in the heat exchanger mass.

Jiang and Garimella (2001) investigated air-coupled and hydronically coupled heat pumps using microchannel tube, multilouver fin heat exchangers as evaporators and condensers with refrigerant R-22 and compared them with conventional round-tube systems. In the hydronically coupled system, the refrigerant in the evaporator transferred heat to an intermediate ethylene-glycol loop, which is connected to the indoor/outdoor air through air-to-hydronic fluid heat exchangers. They found that the indoor and outdoor units of the air-coupled microchannel system could be packaged in one-half and one-third the volume required for a conventional system, respectively. The evaporator and condenser of the hydronically coupled system were found to require 35% and 65% less material than the air-coupled system respectively, due to higher heat transfer coefficients in these counterflow heat exchangers with microchannels on both sides. The refrigerant charge required was found to be 20% and 90% lower in the air-coupled and the hydronically-coupled systems respectively, as compared to a conventional round-tube system.

Kim and Bullard (2002b) compared the performance of a microchannel condenser with a finned-tube condenser for a window room air conditioner using refrigerant R22. They concluded that the heat transfer rates per unit core volume are 14 to 331% higher for microchannel condensers as compared to conventional finned round-tube condensers. Also the refrigerant charge, condenser core volume and mass were found to be 35, 55 and 35% lower respectively for the microchannel condenser.

Kim and Groll (2003) tested a 3-ton (10.5 kW) residential split heat pump system with refrigerant R-22 using a baseline spine-fin heat exchanger and a microchannel heat exchanger for the indoor and outdoor heat exchangers. The microchannel heat exchangers were tested for vertically placed and 15^{o} angularly placed configurations with 6 and 8 fins per cm. The microchannel heat exchangers had about 23% less face area and 32% less refrigerant-side volume as compared to the baseline heat exchanger. In the cooling mode, the COP was found to increase from 1% to almost 6% for the microchannel heat exchangers depending on fin density and heat exchanger orientation. The 15% angular installation was found to perform better than the vertical installation, as the air-flow to the heat exchanger was more normal in the angular installation. This closeness to normal air-flow increased the air-side heat transfer due to increased interruption of the thermal boundary layer on the louvered fins. Also the 8 fins per cm system was found to perform better than the 6 fins per cm system. In the heating mode, the performance of the microchannel heat exchanger system was found to be lower than that of the baseline case. Also the vertical installation was found to offer a better performance than the 15% angular installation. The 8 fins per cm system was found to offer a better performance than the 6 fins per cm system in the vertically placed configuration, while the two were found to offer the same performance in the angularly placed case. In the heating mode, the baseline system was also found to have a lower frequency of defrost cycles as compared to the case with microchannel heat exchangers. Among the microchannel heat exchangers, the vertically placed 6 fins per cm system was found to have the lowest frequency of defrost cycles in the heating mode, followed by the 8 fins per cm vertically

placed system, 6 fins per cm angularly placed system and 8 fins per cm angularly placed system in that order.

2.2 Literature on Air Flow Mal-distribution

Elgowainy (2001) performed a three dimensional simulation of the air flow distribution over the face of tube-fin heat exchangers in typical outdoor units of residential air-conditioning and heat pump systems. In order to simulate the air flow through the heat exchanger coil, the coil was modeled as a porous wall with a pressure loss coefficient. The air volume flow rates obtained from the model were compared with experimental results to verify the model. The heat transfer coefficient and pressure drop were studied based on localized simulations of the flow through one tube-fin section. The area-averaged heat transfer coefficient for non-uniform air flow was found to be 1.5% and 0.9% less than that predicted based on a uniform velocity distribution. The mass-averaged pressure drop for non-uniform air flow was found to be 9% and 8% less than that predicted based on a uniform velocity distribution.

Lee et al. (2003) numerically analyzed the heat transfer characteristics of fin and tube evaporators with refrigerant R-407C for two-dimensional air flow mal-distributions. The simulation results for the uniform air flow case using refrigerants R-22 and R-407C were compared with test data to validate the numerical scheme. The maximum difference between the cooling capacities predicted by simulation and experiments was found to be 5.4%. The evaporator performance was analyzed for uniform, concave, convex and inclined velocity profiles with a constant average air velocity of 1.2 m/s. The uniform air

flow distribution was found to have the highest heat transfer rate and air flow mal-distribution was found to decrease the heat transfer rate by a maximum of 6%.

Soler et al. (1983) developed a theoretical model to evaluate the temperature profile and heat duty for single-phase flow in a tube with non-uniform air flow on the outside.

$$T_t(x) = T_{si} + (T_{ti} - T_{si}) \cdot e^{-\int_0^x \gamma(y)dy} \quad (1)$$

$$Q = m_t C_{pt} (T_{ti} - T_{si}) \left[1 - e^{-\int_0^L \gamma(y)dy} \right] \quad (2)$$

where, T_{si} and T_{ti} are the shell-side and tube-side fluid inlet temperature, m_t and C_{pt} are the mass flow rate and specific heat capacity of the tube-side fluid and,

$$\gamma(x) = \frac{\phi(x) C_{ps} UP}{m_t C_{pt} (\phi(x) C_{ps} + 0.5UP)} \quad (3)$$

where, ϕ (x) is the shell-side mass flow rate of air per unit length of tube, C_{ps} is the specific heat capacity of air, U is the overall heat transfer coefficient and P is the equivalent perimeter of the tube including any effect of fins. The numerical form of the model was developed for a multiple tube pass, cross flow construction and the following discrete equations were obtained.

$$t_i = \frac{t_o (1 + \alpha_{jk} + \beta_{jk}) - 2\alpha_{jk} T_{sk}}{\Delta} \quad (4)$$

$$T_s(k+1) = \frac{2t_o\beta_{jk} + T_{sk}(1-\alpha_{jk}-\beta_{jk})}{\Delta} \quad (5)$$

where t_i and t_o are the segment inlet and outlet temperatures of the tube-side fluid and,

$$\Delta = 1 + \beta_{jk} - \alpha_{jk} \quad (6)$$

$$\alpha_{jk} = \frac{(UA)_{jk}}{2m_{tk}c_{pt,jk}} \quad (7)$$

$$\beta_{jk} = \frac{(UA)_{jk}}{2m_{sj}c_{ps,jk}} \quad (8)$$

Here j is the segment number in the direction of tube-side fluid flow in the first pass and k is the segment number in the direction of air flow.

A numerical example of flow of liquid metal eutectic of sodium potassium was considered in a 4-pass arrangement of finned tubes. Each pass consisted of three rows in a staggered array. These heat exchangers were similar to the ones designed for use in the Clinch River Breeder Reactor Project. For a given mass flow rate, the numerical results were similar for a given air flow profile and its mirror image about the central plane at half tube length. This was in agreement with theoretically derived results.

Beiler and Kroger (1996) studied the effect of mal-distributed air flow on the performance of a cross flow air-cooled heat exchanger with both fluids unmixed. They analyzed the tube rows separately in order to find the overall heat exchanger performance deterioration. This was done because in a multi-row heat exchanger the air-side heat transfer coefficient is different for different rows and is influenced by free stream turbulence and the row number. They used a performance factor that quantifies the decrease in heat exchanger performance due to air flow mal-distribution. The

performance factor was found to be higher for the downstream tube rows than for the inlet rows due to the non-uniform temperature profile caused due to non-uniform inlet air flow. In a two-tube-row bundle, for an NTU of 1.0, the performance factor for the first and second row were 0.6% and 1.4% respectively. The overall performance reduction due to the air flow mal-distributions was found to be less than 2%.

Berryman and Russell (1987) studied the effect of air flow mal-distribution on the performance of air-cooled heat exchangers used in process plants under forced draft or induced draft conditions. They experimentally determined that the standard deviation in the air flow velocities due to mal-distribution is in the range 10 – 20% for forced draft and in the range 12 – 22% for induced draft. With the help of a computer code, they determined the typical heat load dissipated by a heat exchanger for a constant air flow rate with varying degrees of air flow mal-distribution. Two types of tube-side flows were considered namely, single pass and four pass counter flow with air flowing upwards and fluid downwards. They found that for the mal-distributions that occur in practical situations, the effect on heat exchanger performance in only a few percent. They however state that the effect of air flow mal-distribution could be quite drastic in certain special cases like steam condensing under vacuum or for excessive localized cooling of viscous fluids. In the case of steam condensing under vacuum, different tubes of a row would have different cooling capacities due to varying air flow rates over them. However as the tube-side pressure drop across them is equal, the ends of tubes with excessive air flow could become full of non-condensibles and hence ineffective, if there is not adequate steam draw-off from all tubes. This would lead to a further loss in performance. In the case of excessive localized cooling of viscous fluids, the coolers are designed to avoid the

tube wall temperature from falling below the wax point of the tube-side fluid. Hence it is important to design the cooler based on the point on the cooler estimated to have the highest air flow rate.

Rabas (1987) numerically studied the effect of non-uniform inlet air flow and temperature distribution on the thermal performance of air-cooled, cross-flow condensers. The overall heat transfer coefficient was assumed to be proportional to the 0.6 power of the local air flow rate. The condenser performance was analyzed for one-dimensional and two-dimensional air flow and temperature mal-distributions. It was found that the non-uniform inlet flow distribution reduced the thermal performance of the condenser. However this deviation in performance due to non-uniformity was found to be small and even for extremely non-uniform inlet profiles, the reduction in the mean effectiveness of the condenser was found to be less that 7%. However, there was no information provided on the effect of non-uniform inlet air flow on the air-side pressure drop and fan power.

Chiou (1983) developed a mathematical model to study the effect of air flow mal-distributions on the heat transfer effectiveness of a multi-pass, cross-flow automobile air-conditioning condenser with flat tube/plate fin configuration. The performance of the condenser was evaluated for twelve typical two-dimensional air flow mal-distributions. The author deduced that the effect of air flow mal-distributions may be significant for these applications. The model developed in the paper can be used to estimate the effective UA of a condenser for mal-distributed conditions. This could be useful in designing condensers that function effectively in mal-distributed air flow conditions.

The literature reviewed in this chapter is summarized in Tables 2.1 and 2.2. From the above literature review we infer that flat-tube, multi-louvered, microchannel heat exchangers lead to significant savings in material, refrigerant and energy costs for a variety of applications. A number of researchers have analyzed the performance of these microchannel heat exchangers assuming a uniform air flow through them. Also a number of researchers have studied the performance of various commonly used heat exchangers under mal-distributed air flow conditions. They found that air flow mal-distribution changes the heat transfer rate in a heat exchanger by about 5-10% for commonly used heat exchangers. However there was no literature found on the performance of multi-louver finned microchannel heat exchangers under mal-distributed air flow conditions. As these heat exchangers are getting increasingly popular, the analysis of their performance under real life air flow conditions is essential. The present study strives to fill in this need by studying the performance of these flat-tube, multi-louver fin heat exchangers for residential air-conditioning applications under mal-distributed air flow conditions. The study also suggests design modifications to the heat exchanger so that it performs optimally under mal-distributed air flow conditions.

The next chapter describes the calculation procedure used to evaluate the heat duty of a microchannel tube, multilouver fin condenser of any given geometry. It then outlines a procedure to obtain the condenser geometry that delivers the required heat duty with minimum mass under uniform air flow conditions.

Table 2. 1 Literature on Microchannel Geometry

Author	Fluid	Application	Method	Comments
Garimella and Coleman (1998)	Ammonia-Water	Vapor Absorption Heat Pump	Analytical	Studied the design and optimization of air-cooled, round-tube condensers with flat, wavy, louvered and annular fins.
Garimella *et al.* (1997)	Hydronic fluid	Hydronic fluid-to-air heat exchangers in space conditioning	Analytical	Demonstrated that the use of flat-tube, multilouver-fin heat exchangers results in a 59% reduction in the condenser mass as compared to a round-tube, wavy-fin heat exchanger.
Garimella and Wicht (1995)	Ammonia	Condensation of Ammonia in Microchannel tubes	Analytical	Optimized the various geometric parameters in a Microchannel condenser to obtain the design heat duty of 21 kW with lowest condenser mass.
Jiang and Garimella (2001)	R-22	Air-coupled and Hydronically-coupled heat pumps	Analytical	Investigated the use of air-coupled and hydronically-coupled microchannel heat exchangers for the indoor and outdoor units of heat pumps
Kim and Bullard (2002b)	R-22	Window air-conditioner	Experimental	Compared the performance of a microchannel condenser with a finned-tube condenser.
Kim and Groll (2003)	R-22	Residential split heat pump	Experimental	Compared a baseline spine-fin heat exchanger with a microchannel heat exchanger for the indoor and outdoor units.

Table 2. 2 Literature on Air Flow Mal-Distribution

Author	Fluid	Geometry	Application	Method	Comments
Elgowainy (2001)	Air	Tube-fin heat exchangers	Residential Heat pumps	Numerical	Performed a 3D simulation of air flow over tube-fin heat exchangers.
Lee *et al.* (2003)	R-22, R-407C	Fin and Tube evaporators	Air-conditioning	Numerical and Experimental	Numerically analyzed the heat transfer characteristics of fin and tube evaporators for 2D air flow mal-distributions.
Soler *et al.* (1983)	Liquid metal eutectic of Sodium Potassium	Finned tubes, 4 pass	Nuclear Reactors	Numerical	Developed a theoretical model and its numerical form to evaluate the heat duty of multiple tube pass, cross-flow heat exchangers.
Beiler and Kroger (1996)	Air	Round-tube, finned, cross-flow	General air-cooled heat exchanger design	Experimental	Studied the effect of air flow mal-distribution on the performance of a crossflow heat exchanger.
Berryman and Russell (1987)	Air	Induced-draft and forced-draft, cross-flow	Process plant, air-cooled heat exchangers	Analytical	Studied the effect of air flow maldistribution.
Rabas (1987)	Air	Cross-flow condensers	Air-conditioning	Numerical	Studied the effect of 1D and 2D non-uniform inlet air flow and temperature distribution.
Chiou (1983)	Air	Flat-tube, plate-fin, cross-flow	Automobile air-conditioning	Numerical	Effect of air flow mal-distribution on multi-pass, cross-flow automobile air-conditioning condenser.

Chapter 3

DESIGN AND OPTIMIZATION OF MICROCHANNEL CONDENSERS

3.1 Microchannel Geometry

The schematic of a microchannel condenser was shown in Figure 1.1. The cross section of the microchannel tube is as shown in Figure 3.1. It consists of a series of rectangular paths separated by webs. In addition, fin and louver geometry details are presented in this figure, along with a representation of a segment used for the analyses described in subsequent sections.

3.2 Calculation Scheme

In an air-cooled condenser, the refrigerant properties change along the flow with change in refrigerant quality. Hence, in order to accurately determine the condenser performance, the tube is divided into a number of small segments along the direction of the refrigerant flow. The refrigerant properties are assumed to be constant within a segment. The refrigerant inlet condition is specified for the first segment. This inlet condition is shown in Table 3.1. The outlet condition for the segment is found by subtracting the enthalpy loss and pressure drop for the segment. The outlet condition of the previous segment acts as the inlet condition for the following segment. The average of the inlet and outlet refrigerant conditions is used to evaluate the constant refrigerant properties for the segment in order to calculate the heat duty and pressure drop for that segment. Since the outlet condition is not initially known, an initial assumption is made and an iterative scheme is used to refine the solution.

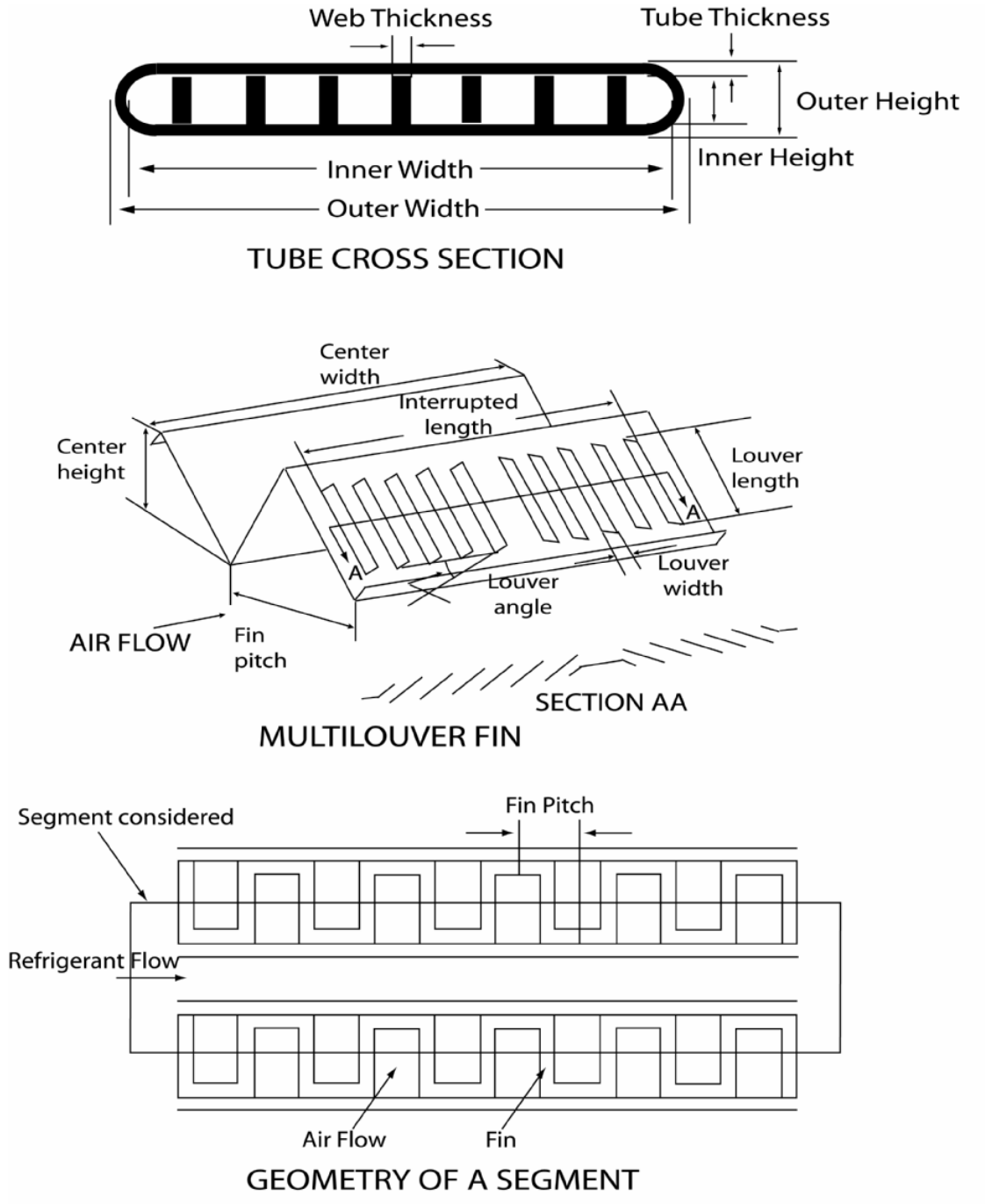

Figure 3. 1 Geometrical Details of a Microchannel Condenser

Table 3. 1 Inlet Conditions

Tube-side		Air-side	
Refrigerant mass flow rate	0.072 kg/s	Air mass flow rate	1.62 kg/s (3000 cfm)
Refrigerant inlet pressure	3.071 MPa	Air inlet temperature	35°C (95°F)
Refrigerant inlet enthalpy	477.85 kJ/kg	Allowable air pressure drop	49.77 Pa (0.2 in of H_2O)
Allowable refrigerant saturated temperature glide	1°C		
Absolute surface roughness of tube	0.0015 mm		

3.3 Tube Geometry

The cross section of a microchannel tube is as shown in Figure 3.1. The initial values of the geometric parameters are shown in Table 3.2. The sides of the tube are assumed to be semicircular with diameter equal to the tube height. Hence the total tube-side area is given by:

$$A_t = t_{hi}\left(t_{wi} - t_{hi}\right) + \frac{\pi}{4} t_{hi}^2 \qquad (9)$$

The tube free-flow area is obtained by subtracting the area occupied by the webs from the tube cross-sectional area.

$$A_{ft} = A_t - N_w t_{hi} w_t \qquad (10)$$

The tube-wetted perimeter is the total tube perimeter in contact with the refrigerant. This is given by:

Table 3. 2 Initial Values of the Geometric Parameters

Tube-side		**Fin**		**Louver**	
Inner tube height	1.4 mm (0.055 in)	Fin pitch	1.693 mm (0.067 in)	Louver angle	30^{o}
Inner tube depth	17.4 mm (0.69 in)	Fin height	12.4 mm (0.49 in)	Number of louvers per cm	13
Number of webs	10	Fin thickness	0.127 mm (0.005 in)	Louver width	0.8 mm (0.044 in)
Thickness of webs	0.318 mm (0.0125 in)	Fin depth	18 mm (0.71 in)		
Tube wall thickness	0.318 mm (0.0125 in)	Mass of fins	1.69 kg		
Tube length	1.04 (3.4 ft)				
Pass arrangement	17, 10, 5				
Mass of tubes	1.44 kg				
Total mass	3.13 kg				

$$per_t = \pi t_{hi} + 2\left(t_{wi} - t_{hi} - N_w w_t\right) + 2t_{hi} N_w \quad (11)$$

The hydraulic diameter is given by:

$$D_{ht} = \frac{4A_{ft}}{per_t} \quad (12)$$

The tube walls wetted directly by the refrigerant directly transfer heat from the refrigerant to the outside air. This constitutes the direct heat transfer area.

$$A_{dt} = 2\left(t_{wi} - t_{hi}\right)L_t + \pi t_{hi} L_t - 2N_w w_t L_t \quad (13)$$

The webs act as fins and help in transmitting heat from the refrigerant to the outside air. This constitutes the indirect heat transfer area.

$$A_{idt} = 2N_w t_{hi} L_t \quad (14)$$

The total heat transfer area is given by:

$$A_{efft} = A_{dt} + \eta_{ft} A_{idt} \tag{15}$$

where η_{ft} is the fin efficiency, given by:

$$\eta_{ft} = \frac{\tanh\left[\sqrt{\frac{2h_{tube}\left(L_{seg} + w_t\right)}{k_t w_t L_{seg}}}\frac{t_{hi}}{2}\right]}{\sqrt{\frac{2h_{tube}\left(L_{seg} + w_t\right)}{k_t w_t L_{seg}}}\frac{t_{hi}}{2}} \tag{16}$$

3.4 Air-side Geometry

The cross section of the tube outer surface is assumed to be as shown in Figure 3.1. The fins are assumed to be perfectly rectangular and at right angles to the tube outer surface. The face area of one tube and fin set in one segment is given by:

$$A_c = \left(t_{ho} + c_h\right)L_{seg} \tag{17}$$

Of this, the area blocked by the fins is given by:

$$A_{ba} = \frac{L_{seg}}{f_p}\left(c_h f_{thk} + \left(f_p - 2f_{thk}\right)f_{thk}\right) \tag{18}$$

The area available for air flow is the total area less the area blocked by the fins and the area occupied by the tube for refrigerant flow.

$$A_{fa} = A_c - \left(A_{ba} + t_{ho} L_{seg}\right) \tag{19}$$

The perimeter of the tube directly in contact with air is:

$$per_a = 2\left[\frac{L_{seg}}{f_p}\left(c_h - f_{thk}\right) + L_{seg} - L_{seg}\frac{f_{thk}}{f_p}\right] \tag{20}$$

The hydraulic diameter is given by:

$$D_{ha} = \frac{4A_{fa}}{per_a} \tag{21}$$

Part of the tube wall, which is in contact with the refrigerant on the inside surface and with air on the outside surface directly transfers heat from the refrigerant to the outside air. This constitutes the direct heat transfer area.

$$A_{da} = \left[2\left(t_{wo} - t_{ho}\right)\left[1 - \frac{f_{thk}}{f_p}\right] + \pi t_{ho} \right] L_{seg} \tag{22}$$

The fins also help in transferring heat from the refrigerant to the outside air. This constitutes the indirect heat transfer area.

$$A_{ida} = 2c_w \frac{1}{f_p}\left(c_h - f_{thk}\right) L_{seg} \tag{23}$$

The total outside heat transfer area is given by:

$$A_{effa} = A_{da} + \eta_{fa} A_{ida} \tag{24}$$

where η_{fa} is the fin efficiency given by:

$$\eta_{fa} = \frac{\tanh\left[\sqrt{\frac{2h_{air}\left(c_w + f_{thk}\right)}{k_t f_{thk} c_w}}\frac{c_h}{2}\right]}{\sqrt{\frac{2h_{air}\left(c_w + f_{thk}\right)}{k_t f_{thk} c_w}}\frac{c_h}{2}} \tag{25}$$

The total mass of the condenser is the sum of the mass of the tube and the mass of the outside fins. The mass of the tube is given by

$$mass_{tube} = n_{tube\_total} \cdot L_{cond} \cdot \rho_{Al}\left[2\left(t_{wi} - t_{hi}\right)thk_t + \pi t_{hi} thk_t + N_w w_t t_{hi}\right] \tag{26}$$

The mass of the fins is given by

$$mass_{fin} = n_{tube\_total} \cdot \rho_{Al} \cdot \frac{L_{cond}}{f_p}\left[c_w\left((c_h - f_{thk})f_{thk} + f_p f_{thk}\right)\right] \quad (27)$$

3.5 Refrigerant-side heat transfer coefficient and pressure drop

The refrigerant enters the condenser as superheated vapor and leaves as sub-cooled liquid. The refrigerant-side heat transfer and pressure drop calculations are done separately for the superheated vapor region, two-phase region and the sub-cooled liquid region. The properties of the refrigerant R410A were obtained from Lemmon (2002).

For the sub-cooled and the superheated flow regime, the correlations for heat transfer coefficient and pressure drop are different for the laminar and turbulent flow regimes. The critical Reynolds number that determines the transition criteria is found from the following equation (Bhatti and Shah 1987)

$$Re_{cri} = \frac{4650}{v_{ratio}} \quad (28)$$

The velocity ratio is found from the equation developed by Purday (1949)

$$v_{ratio} = \frac{m+1}{m}\frac{n+1}{n} \quad (29)$$

Natarajan and Lakshmanan (1972) developed the equations for m and n.

$$m = 1.7 + 0.5\alpha^{-1.4} \quad (30)$$

$$\begin{aligned} &\text{If } \alpha < \frac{1}{3} \text{ then } n = 2 \\ &\text{else } \quad n = 2 + 0.3\left(\alpha - \frac{1}{3}\right) \end{aligned} \quad (31)$$

where α is the aspect ratio, defined as

$$\alpha = \frac{t_{hi}}{web_{sp}} \tag{32}$$

The single-phase refrigerant-side Nusselt number for laminar flow is calculated using the following expression provided by Shah and Bhatti (1987)

$$Nu = 8.325\left(1 - 2.0241\alpha + 3.0853\alpha^2 - 2.4765\alpha^3 + 1.0578\alpha^4 - 0.1861\alpha^5\right) \tag{33}$$

For single-phase turbulent flow, the Nusselt number is found using the equation developed by Churchill (1977a)

$$Nu = \left[4.364^{10} + \left[\frac{e^{\frac{2200-Re}{365}}}{4.364^2} + \frac{1}{\left(6.3 + \frac{0.079(f/8)^{1/2}\,Re\,Pr}{\left(1+Pr^{4/5}\right)^{5/6}}\right)^2}\right]^{-5}\right]^{1/10} \tag{34}$$

where f is the friction factor calculated by Churchill (1977b)

$$f = 8\left[\left(\frac{8}{Re}\right)^{12} + \frac{1}{\left[\left(2.457\ln\left(\frac{1}{(7/Re)^{0.9} + (0.27\,r/D_{ht})}\right)\right)^{16} + \left(\frac{37530}{Re}\right)^{16}\right]^{1.5}}\right]^{1/12} \tag{35}$$

To compute single-phase pressure drop in the laminar regime, the following expression developed by Shah and London (1978) for rectangular ducts was used.

$$f = \frac{96}{Re}\left[1 - 1.3553\alpha + 1.9467\alpha^2 - 1.7012\alpha^3 + 0.9564\alpha^4 - 0.2537\alpha^5\right] \tag{36}$$

For turbulent flow, Bhatti and Shah (1987) suggested the following equation

$$f = (1.0875 - 0.1125\alpha)8\left[\left(\frac{8}{Re}\right)^{12} + \frac{1}{\left[\left(2.457\ln\left(\frac{1}{(7/Re)^{0.9} + (0.27\,r/D_{ht})}\right)\right)^{16} + \left(\frac{37530}{Re}\right)^{16}\right]^{1.5}}\right]^{1/12} \quad (37)$$

In the condensing region, the heat transfer coefficient for two-phase refrigerant flow was computed using the correlation developed by Shah (1979)

$$h_{tube} = 0.023\frac{k_{liq}}{D_{ht}}Re_{liq}^{0.8}\,Pr_{liq}^{0.4}\left[(1-x)^{0.8} + \frac{3.8x^{0.76}(1-x)^{0.04}}{\left(\frac{P}{P_{cri}}\right)^{0.38}}\right] \quad (38)$$

It should be noted that other two-phase heat transfer correlations were also considered; however, due to the applicable thermal resistances on the air-side and the refrigerant-side, the heat duty is not very sensitive to the correlation used for condensation heat transfer coefficient as will be demonstrated in a later part of this chapter. The pressure drop in the two-phase region consists of the frictional pressure drop and the deceleration pressure drop. The frictional pressure drop is calculated as follows (Friedel 1979)

$$\left(\frac{dp}{dx}\right)_{fric} = \phi_{lo}^2\left(\frac{dp}{dx}\right)_{lo} \quad (39)$$

where,

$$\phi_{lo}^2 = E + \frac{3.24FH}{Fr^{0.045}We^{0.035}} \quad (40)$$

$$We = \frac{G^2 D_{ht}}{\rho_{TP}\sigma} \quad (41)$$

$$Fr = \frac{G^2}{gD_{ht}\rho_{TP}^2} \quad (42)$$

$$\rho_{TP} = \left[\frac{x}{\rho_{vap}} + \frac{1-x}{\rho_{liq}}\right]^{-1} \quad (43)$$

$$H = \left(\frac{\rho_{liq}}{\rho_{vap}}\right)^{0.91}\left(\frac{\mu_{vap}}{\mu_{liq}}\right)^{0.19}\left(1-\frac{\mu_{vap}}{\mu_{liq}}\right)^{0.7} \quad (44)$$

$$F = x^{0.78}(1-x)^{0.24} \quad (45)$$

$$E = (1-x^2) + x^2\frac{\rho_{liq}f_{go}}{\rho_{vap}f_{lo}} \quad (46)$$

where, f_{go} and f_{lo} are the gas-only and liquid-only Darcy friction factors calculated using the Churchill (1977b) correlation

$$\left[\frac{dp}{dx}\right]_{lo} = \frac{f_{lo}G^2}{2D_{ht}\rho_{liq}} \quad (47)$$

$$\left[\frac{dp}{dx}\right]_{go} = \frac{f_{go}G^2}{2D_{ht}\rho_{vap}} \quad (48)$$

The deceleration pressure drop is given by

$$\left(\frac{dp}{dx}\right)_{dec} = G^2\left[\frac{x_{out}^{\ 2}}{\alpha_v \rho_{vap}} + \frac{(1-x_{out})^2}{(1-\alpha_v)\rho_{liq}}\right] - G^2\left[\frac{x_{in}^{\ 2}}{\alpha_v \rho_{vap}} + \frac{(1-x_{in})^2}{(1-\alpha_v)\rho_{liq}}\right] \quad (49)$$

where α_v is the void fraction, given by Butterworth (1975)

$$\alpha_v = \left[1 + 0.28\left(\frac{1-x}{x}\right)^{0.64}\left(\frac{\rho_{vap}}{\rho_{liq}}\right)^{0.36}\left(\frac{\mu_{liq}}{\mu_{vap}}\right)^{0.07}\right]^{-1} \quad (50)$$

In addition to the frictional and deceleration pressure drop, there is an additional pressure loss at the bends. The pressure drop at the bends for single phase flow is given by

$$\Delta P_{bend} = \frac{1}{2} k_{minor} \rho_r v_r^2 \quad (51)$$

where, k_{minor} is the minor loss coefficient for the bend. A minor loss coefficient of 0.2 was used in the current analyses.

The pressure drop for two-phase flow over a bend is calculated by using a multiplier as suggested by Rohsenow *et al.* (1985)

$$(\Delta P_{bend})_{two\_phase} = (\Delta P_{bend})_{liq}\left[1 + 2x\frac{\rho_{liq}}{\rho_r}\right] \quad (52)$$

3.6 Air-side heat transfer coefficient and pressure drop

Kim and Bullard (2002a) developed a correlation for Colburn j factor and friction factor for air flow over multilouvered fins. This is used to find the air-side heat transfer coefficient and pressure drop.

$$j = Re_{lp}^{-0.487}\left[\frac{\theta}{90}\right]^{0.257}\left[\frac{f_p}{l_p}\right]^{-0.13}\left[\frac{c_h}{l_p}\right]^{-0.29}\left[\frac{c_w}{l_p}\right]^{-0.235}\left[\frac{l_l}{l_p}\right]^{0.68}\left[\frac{t_p}{l_p}\right]^{-0.279}\left[\frac{f_{thk}}{l_p}\right]^{-0.05} \quad (53)$$

$$f = Re_{lp}^{-0.781}\left[\frac{\theta}{90}\right]^{0.444}\left[\frac{f_p}{l_p}\right]^{-1.682}\left[\frac{c_h}{l_p}\right]^{-1.22}\left[\frac{c_w}{l_p}\right]^{0.818}\left[\frac{l_l}{l_p}\right]^{1.97} \quad (54)$$

The Reynolds number Re_{lp} is based on the louver pitch. The pressure drop is obtained from the friction factor using the equation below:

$$\Delta p = \frac{f \cdot G_{air}{}^2 c_w}{2\rho \cdot l_p} \quad (55)$$

The pressure drop is then used to compute the ideal fan power required.

$$P_{fan} = \frac{\Delta p \cdot \dot{m}_{air}}{\rho} \quad (56)$$

Having calculated the tube-side and air-side heat transfer coefficients, the heat duty of each segment is calculated by the effectiveness-NTU method. The effectiveness relation for single-phase refrigerant flow is given below:

$$\varepsilon = 1 - \exp\left[\frac{1}{C}NTU^{0.22}\left\{\exp\left(-C \cdot NTU^{0.78}\right) - 1\right\}\right] \quad (57)$$

This is the effectiveness relationship for a cross flow, single-pass heat exchanger with both fluids unmixed. For two-phase refrigerant flow, the effectiveness relation is,

$$\varepsilon = 1 - \exp(-NTU) \quad (58)$$

The heat duty and fan power requirement for each segment are then summed to find the overall heat duty and fan power requirement for the condenser. The refrigerant inlet

enthalpy and pressure for the subsequent segment is obtained by subtracting the heat duty and the pressure drop of the current segment.

3.7 Segment Sensitivity

As stated above, the heat duty of the condenser was found by summing the segment heat duties. The accuracy of the calculation increases as the tube is divided to smaller and smaller segments. However this consumes more computational time. A plot of the calculated condenser heat duty against the number of segments is shown in Figure 3.2.

From the plot it is seen that there is a significant fluctuation in the heat duty with change in number of segments when each tube is segmented into less than 15 segments.

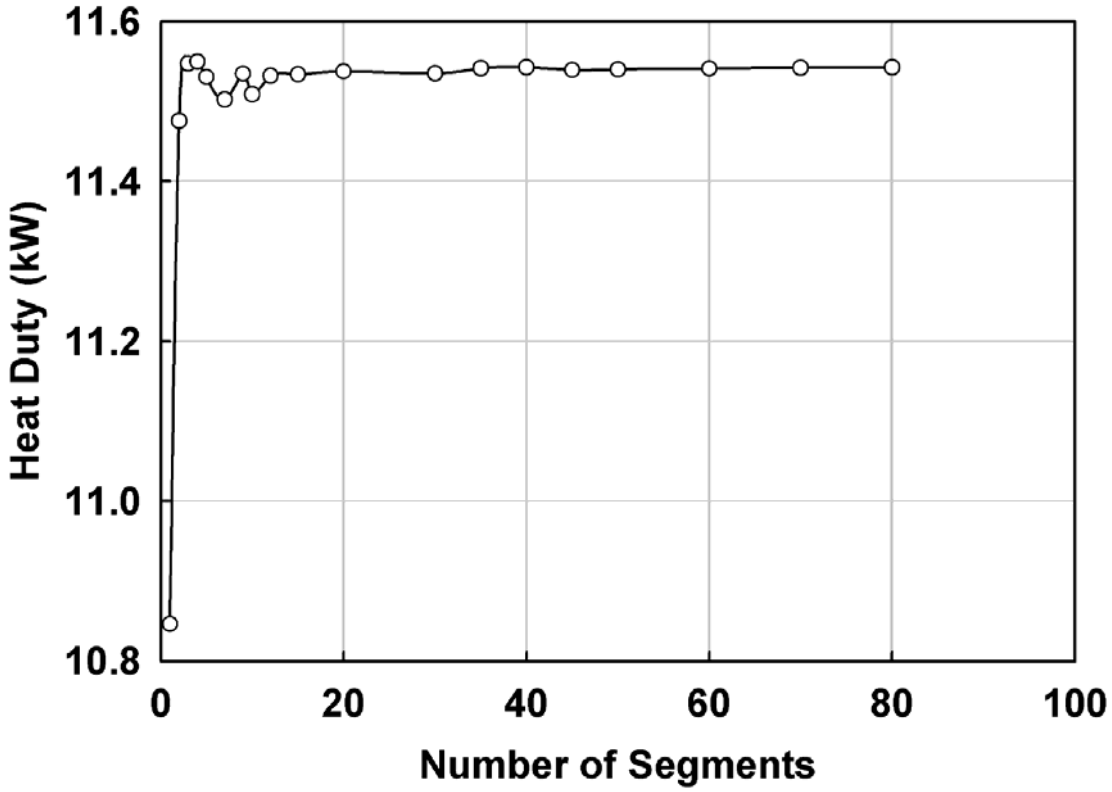

Figure 3. 2 Sensitivity of Computation to Segmentation

However for more than 15 segments, the calculated heat duty gradually converges to a steady value. Based on this analysis, the condenser was divided into 20 segments for this study.

3.8 Iterative Scheme and Stop Criteria

The tube-side and air-side heat transfer coefficients and pressure drop are functions of the refrigerant and air properties. These properties change significantly along the condenser with change in temperature and pressure. However the mean temperature and pressure for each segment is not known at the start of the calculation, but is a calculated quantity. Hence an iterative scheme is used to perform these calculations. For the first iteration, the refrigerant properties for the first segment are calculated at the refrigerant inlet condition. The refrigerant properties for the subsequent segments in the first iteration are calculated at the inlet condition at that segment, which is the calculated outlet condition of the previous segment. For the subsequent iterations, the refrigerant properties are calculated at the average refrigerant temperature and pressure obtained from the previous iteration.

The iterations are terminated when the difference between the calculated values of the variations in heat duty for each segment for successive iterations are less than the allowable error limit. An allowable error limit of 0.01 % was used for this study.

3.9 Baseline Calculations

Representative refrigerant and air inlet conditions were chosen (Table 3.1) for the design of a baseline combination of geometric parameters for the condenser design heat

duty of 14.5 kW. In addition, the maximum allowable refrigerant temperature glide during condensation was set at 1°C so that the driving temperature difference between the refrigerant and the air is not adversely affected due to excessive refrigerant pressure drop. Also the air velocity through the condenser core was not allowed to exceed 4 m/s.

Aluminum was chosen as the material for the heat exchanger due to its high thermal conductivity, low density and low cost. Table 3.2 shows the initial values of the geometric parameters considered. This configuration with a mass of 3.13 kg satisfies the design conditions and delivers a heat duty of 14.497 kW, with a subcooling of 5°C, and refrigerant-side pressure drop of 24 kPa (3.5 psi). The air-side pressure drop is 25 Pa (0.1" H_2O).

3.10 Heat Transfer Coefficient Variation along Condenser Length

Figure 3.3 shows the tube-side heat transfer coefficient and heat duty per segment calculated using the two-phase heat transfer correlations by Shah (1979), Traviss *et al.* (1973) and Soliman *et al.* (1968). There is a step increase in the tube-side heat transfer coefficient at every new pass, as the number of tubes per pass is lower in successive passes, resulting in a higher refrigerant mass flow rate per tube in successive passes. There is a sharp rise in the tube-side heat transfer coefficient calculated by the correlation by Soliman *et al.* (1968) at qualities very close to 0.0. This is because the correlation is valid only in the quality range $0.99 > x > 0.03$, which leads to the presumably spurious rise in heat transfer coefficient for $x < 0.03$, as shown in Figure 3.3. Similarly there is a sharp drop in the heat transfer coefficient calculated by Traviss *et al.* (1973) for qualities close to 0.0 as the correlation is valid only for $x > 0.1$. We see that even though there

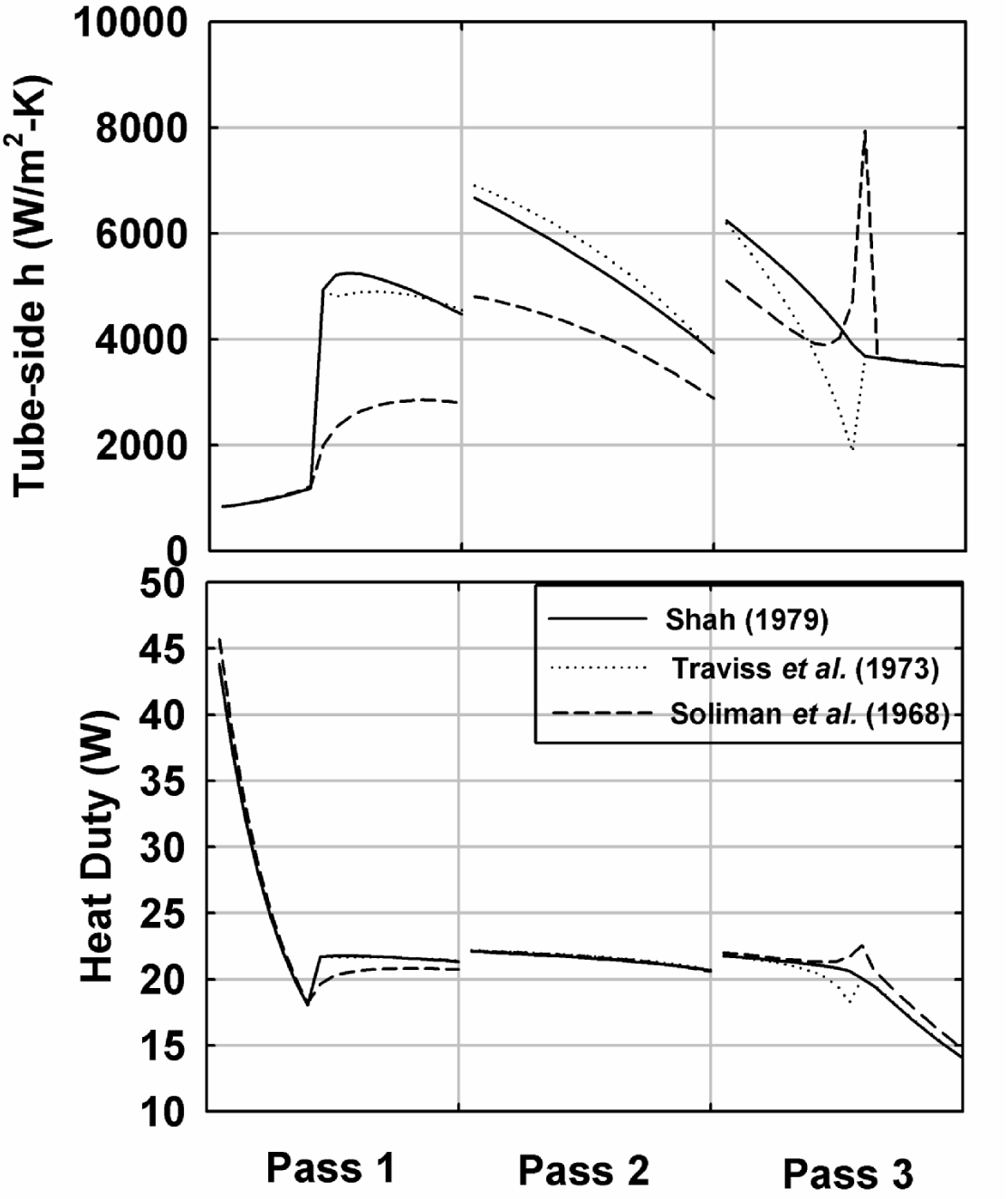

Figure 3. 3 Effect of various Two-phase Heat Transfer Correlations

is a slight difference in the tube-side heat transfer coefficients calculated using the three correlations, there is very little difference in the heat duty because the air-side thermal resistance is dominant. For example, at the inlet to the second pass, the tube-side heat

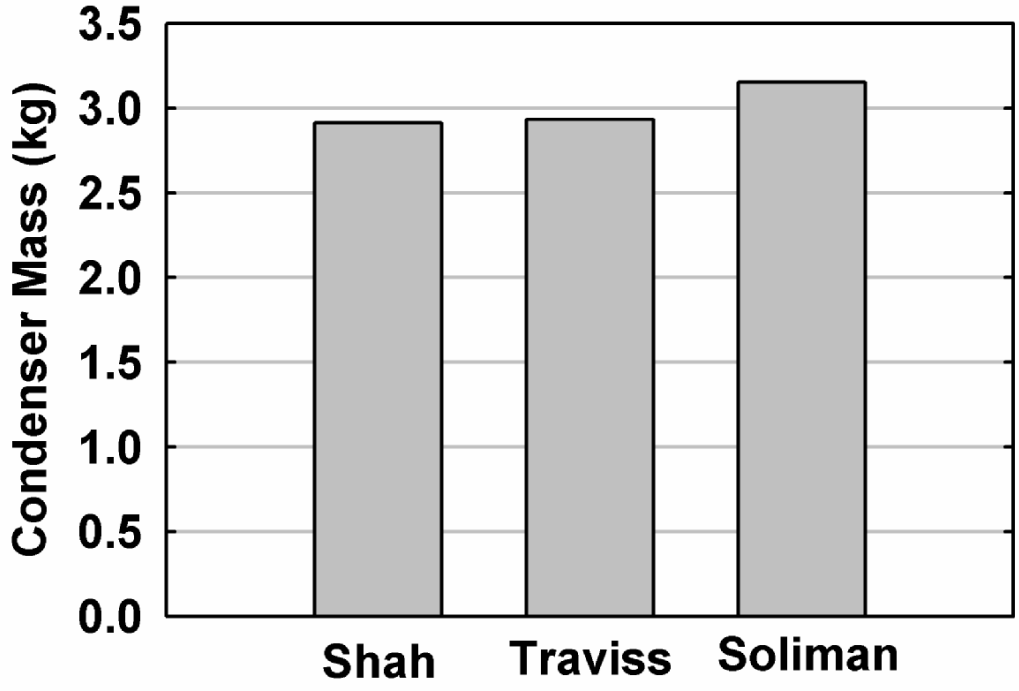

Figure 3. 4 Effect of Two-phase Heat Transfer Correlation on Condenser Mass

transfer coefficients calculated using correlations by Shah (1979), Traviss *et al.* (1973) and Soliman *et al.* (1968) are 6677 W/m^2-K, 6906.8 W/m^2-K and 4811 W/m^2-K and the corresponding hAs for the segment are 19.9 W/K, 20.6 W/K and 14.4 W/K, whereas the corresponding air-side hA is 3.0 W/K, clearly indicating that the heat duty should be insensitive to small variations in condensation heat transfer coefficients. Consequently, the condenser mass required to deliver the design heat duty is almost the same for the three correlations. This is seen from Figure 3.4, which shows that the mass required is 2.91 kg with the Shah (1979) correlation, 2.93 kg with the Traviss *et al.* (1973) correlation and 3.15 kg with the Soliman *et al.* (1968) correlation. For all further analyses, the tube-side condensation heat transfer coefficient is calculated using the correlation by Shah (1979).

It is helpful to obtain an understanding of the variation in refrigerant and air-side heat transfer coefficients across the condenser before a systematic parametric optimization of the geometry can be initiated. Figure 3.5 and 3.6 show the tube-side, air-side and overall heat transfer coefficient and heat duty variation along the length of the condenser. The tube-side heat transfer coefficient is low near the condenser inlet region because the refrigerant enters the condenser as superheated vapor. At about half way through the first pass, the refrigerant starts condensing and the tube-side heat transfer coefficient exhibits a sharp increase. In the two-phase region, the tube-side heat transfer coefficient gradually decreases as the refrigerant quality decreases because of the increase in the liquid fraction and the consequent decrease in flow velocities.

There is no significant change in the air-side heat transfer coefficient. The air-side heat transfer coefficients are slightly higher in the condenser inlet region, due to high local heat dissipation rates resulting in higher air outlet temperatures. An increase in the mean air temperature (which is an average of the inlet and outlet air temperatures) leads to an increase in the thermal conductivity of air, which causes an increase in the air-side heat transfer coefficient. The air-side heat transfer coefficient is slightly lower near the condenser outlet region for the same reason. As there is no significant variation in the air-side heat transfer coefficient, the fin efficiency remains fairly constant ($0.870 < \eta_{fin} < 0.871$).

Because the air-side heat transfer coefficient is fairly constant ($178.0 < h_{air} < 179.6$ W/m^{2}K), the overall heat transfer coefficient variation follows the tube-side heat transfer coefficient variation even though the air-side resistance is the governing resistance. The minimum and maximum values of the overall heat transfer coefficient are

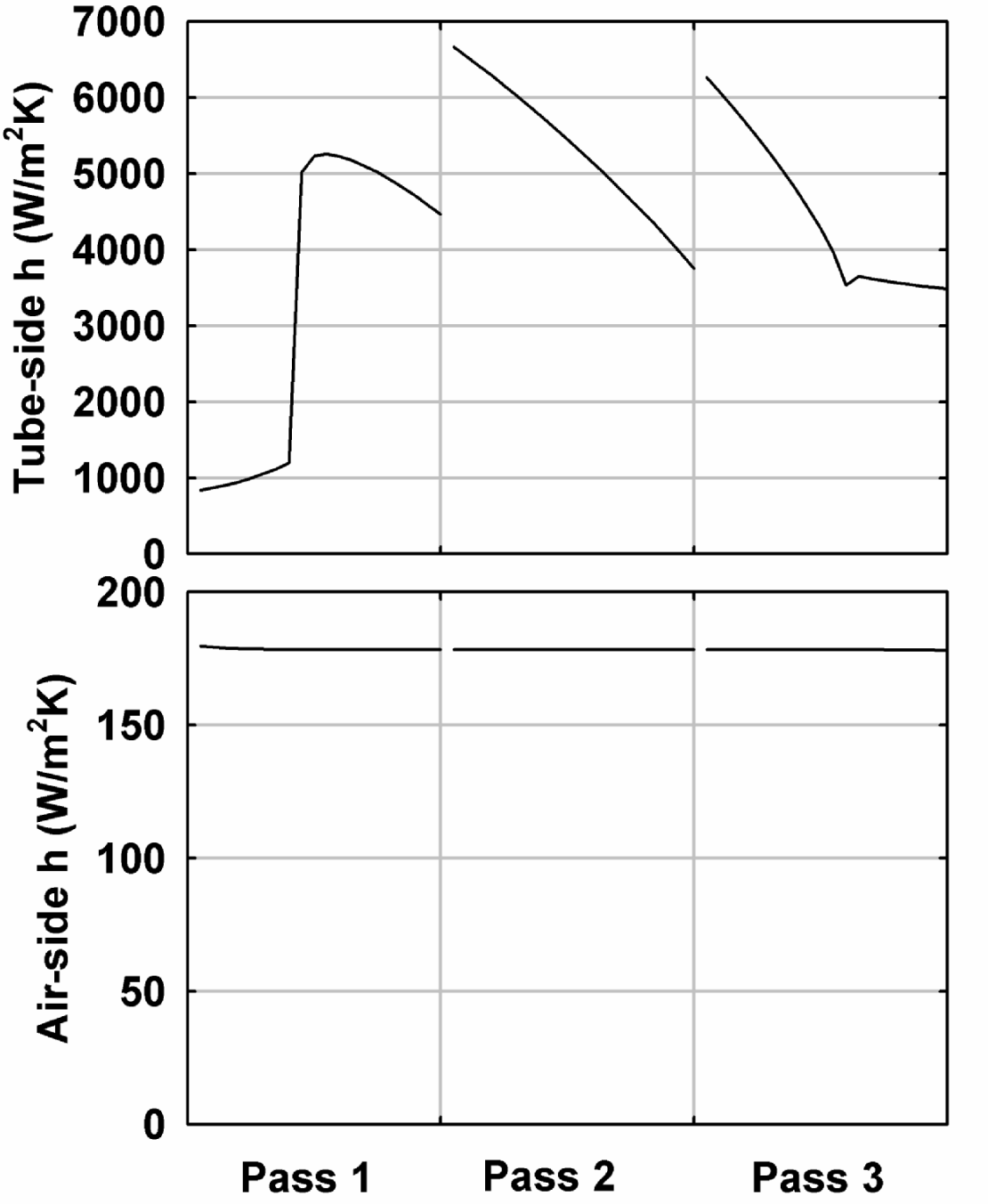

Figure 3. 5 Tube-side and Air-side Heat Transfer Coefficients

91 W/m^{2}K and 159 W/m^{2}K respectively. The bare tube outer heat transfer area is 1.28 m^2, while the fins provide a surface area of 8.70 m^2, resulting in an effective heat transfer area of 8.78 m^2. Thus the fins enhance the heat transfer area by a factor of 7. The

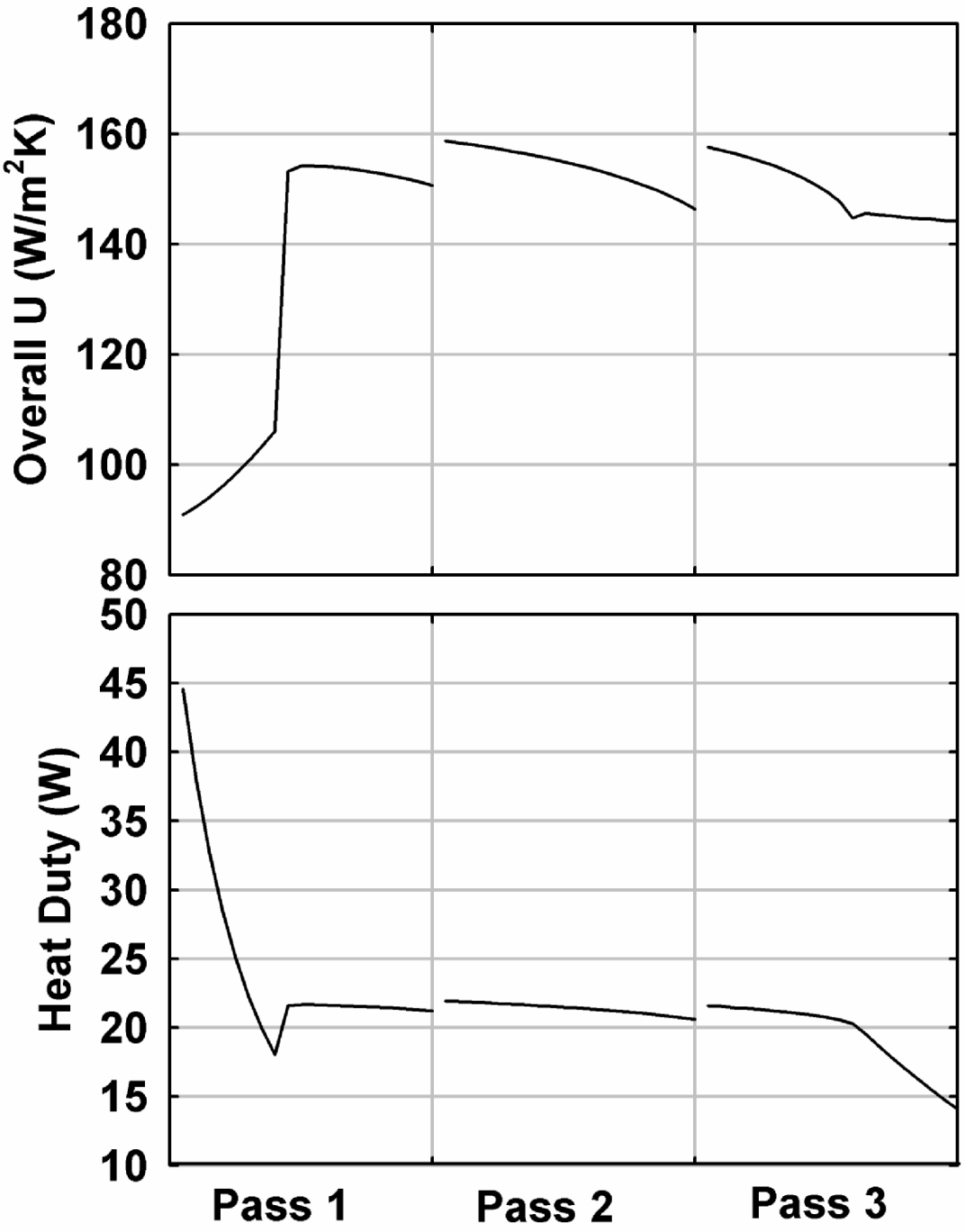

Figure 3. 6 Overall Heat Transfer Coefficient and Heat Duty

minimum and maximum values of the heat exchanger UA across the condenser are 798 W/K and 1394 W/K respectively. The heat dissipated in the desuperheating, condensation and subcooling regions are 3.90 kW (26.9%), 9.94 kW (68.5%) and 0.67 kW (4.6%)

respectively. The condenser mass required for the desuperheating, condensation and subcooling regions are 0.62 kg (21.3%), 2.11 kg (72.5%) and 0.18 kg (6.2%) respectively.

This variation in heat transfer coefficients has a direct bearing on the heat dissipation rate along the condenser length. Though the heat transfer coefficients are relatively lower near the refrigerant inlet region, the heat dissipation rate is the highest in this region due to a large temperature difference between the refrigerant and air. The heat dissipation decreases sharply with decrease in refrigerant temperature in the superheated region and is lower than that in the two-phase region at the end of the superheated region. This is because at the end of the superheated region, the refrigerant temperature is close to the saturation temperature but the heat transfer coefficients are much lower due to single-phase vapor flow. The heat dissipation rate remains fairly constant in the two-phase region and decreases slightly in the subcooled region due to the lower refrigerant heat transfer coefficient and the decreasing temperature difference between the refrigerant and air. Though there is a step increase in the heat transfer coefficient with each pass, this increase per pass is compensated by the decrease in the heat transfer area, due to the lower number of tubes per pass.

3.11 Goal of Design Optimization

With a baseline condenser designed, the goal of the design procedure is to obtain the design heat duty of 14.5 kW with minimum condenser mass. A lower condenser mass is assumed to result in a lower capital cost. For this preliminary analysis, the mass of the headers is not included in the calculation, and the variation in fabrication costs with

geometry is not accounted for.

There are a number of design parameters that affect the condenser performance. To effectively optimize heat exchanger performance based on these parameters, they are optimized in the order of their effect on the condenser performance. An initial nominal value of all the geometric parameters was assumed (baseline case, Table 3.2) and the optimal tube-side pass arrangement is obtained first. In subsequent analyses, the parameter that most strongly affected the condenser performance was optimized first, and so on. As each design parameter is varied, the total number of tubes in the heat exchanger is always kept constant, and the effect of the variation of the parameter under consideration on the condenser heat duty is compensated for by varying the heat exchanger length so as to always obtain a heat duty within 0.1% of the design heat duty. This changing tube length also affects the air-side flow area, which in turn affects the heat duty in the condenser, as discussed in subsequent sections.

The design parameters are optimized in the following order

1. Pass arrangement
2. Tube depth
3. Tube height
4. Fins per inch
5. Fin height
6. Number of webs
7. Louver angle
8. Number of louvers

3.12 Comparison of the Design Procedure to Prior Work in the Literature

Webb (1994) described a design methodology to reduce the heat exchanger size and weight for a fixed heat duty for a cross-flow spine-fin evaporator. The procedure consisted of the following steps. For fixed air and refrigerant inlet conditions and mass flow rate, the required UA to deliver the design heat duty was first calculated. For the starting configuration, the fin density and number of tube rows in the air-side direction were set to their minimum values, so as to start with a minimum mass configuration. In addition, this configuration facilitates the maximum air flow through the heat exchanger for a given allowable air-side pressure drop. (Increases in air-side hA are the most beneficial to heat exchanger performance.) The available UA was then calculated for this configuration. If the available UA was less than the required UA, the fin density was gradually increased until the required UA was obtained. For this configuration, if the air-side pressure drop was found to be higher than a pre-specified upper limit, the number of air-side tube rows was increased to the next higher value and the design procedure was repeated until a configuration that satisfies all the design requirements was obtained.

The above-mentioned design procedure arrived at a suitable heat exchanger configuration by systematically varying a set of geometric parameters. It was seen that an effective heat exchanger design was obtained by a judicious change of the key design parameters, without trying out all possible heat exchanger configurations. It was demonstrated that such an approach taking into consideration the thermal behavior of the heat exchanger saved considerable time over a rigorous mathematical optimization procedure across all possible parametric variations..

The present study uses a similar approach, guided by the expected effects of changes in parameters on heat transfer, pressure drop, and mass. As the parameters are changed, the effects on these dependent variables are documented, which guides the choice of the following parameters. The following sections describe the progression of the condenser configuration as the most suitable value for each parameter is chosen.

.

3.13 Pass Arrangement

The number of passes was varied keeping the total number of tubes constant. During this exercise the number of tubes in each pass was assigned so as to result in approximately equal pressure drops in each pass. The various pass arrangements considered are listed in Table 3.3. An increase in the number of passes decreases the number of tubes in each pass, resulting in a decrease in the refrigerant cross sectional flow area. This results in higher refrigerant flow velocities through each tube, which in turn increases the refrigerant-side heat transfer coefficient. This helps in reducing the total mass of the condenser.

Figure 3.7 shows that the condenser mass decreases with an increase in the

Table 3. 3 Pass Arrangements

Number of passes	Pass arrangement
1	32
2	20,12
3	15,11,6
4	13,10,5,4
5	10,9,6,4,3
6	9,7,6,4,3,3

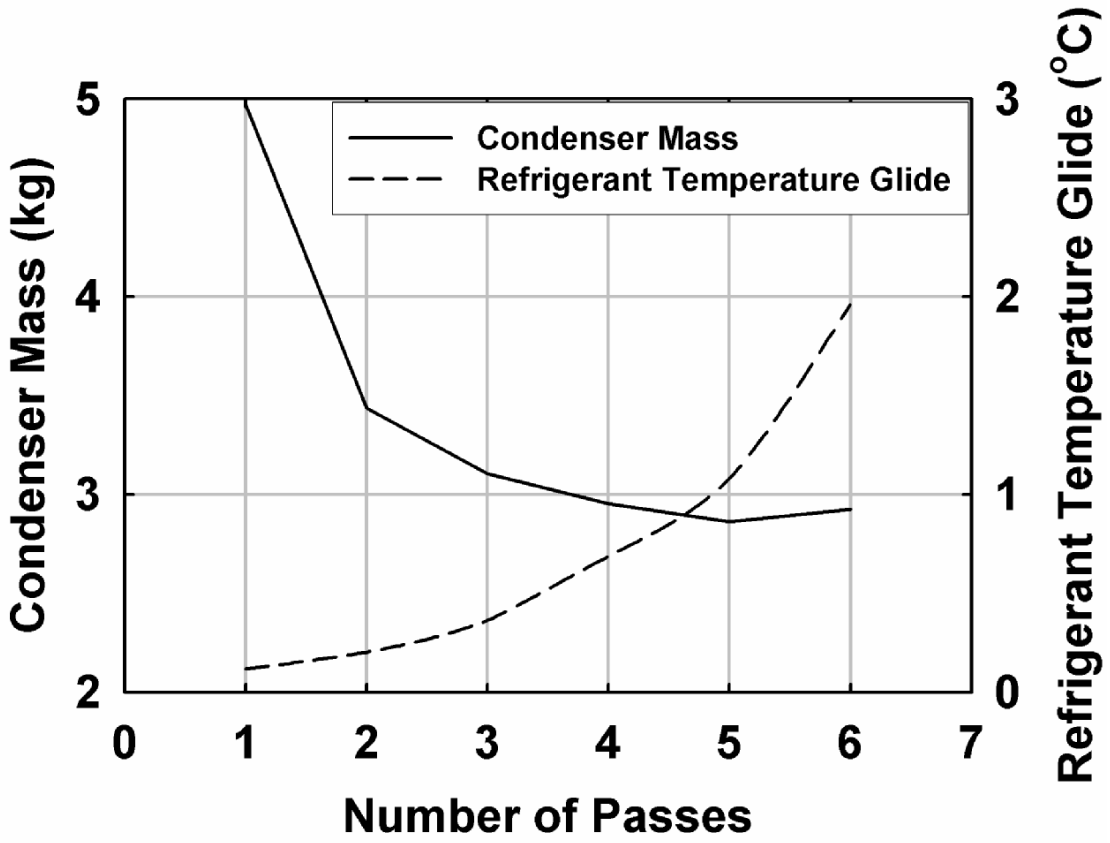

Figure 3. 7 Effect of Number of Passes

number of passes. However the rate of decrease is higher initially and decreases with additional passes because the increase in tube-side heat transfer coefficient and its impact on the overall UA is not significant for a further increase in the number of passes. Thus, for example, with one pass, the condenser mass is 4.97 kg and decreases to 2.95 kg for 4 passes, but with a further increase to 6 passes, the mass decreases only to 2.92 kg. The increase in the refrigerant flow velocity also leads to higher refrigerant pressure drop. This results in a higher temperature glide during condensation of the refrigerant, from 0.12°C for one pass to 1.96°C for 6 passes, i.e., greater than the allowable 1°C glide.

As the number of passes is increased, the tube length is decreased to compensate for the additional heat transfer per unit area and thus maintain a constant heat duty. This decreased length also reduces the air-flow area, leading to higher air velocities. This

increases the average air-side heat transfer coefficient and pressure drop from 140.9 W/m^2-K and 14.1 Pa for the one-pass configuration to 185.0 W/m^2-K and 26.9 Pa for the 6 pass configuration.

Based on these analyses, a four-pass arrangement with a tube length of 0.98 m was chosen as the optimum configuration, and delivers 14.49 kW with a 2.95 kg condenser and a refrigerant temperature glide of 0.69^{o}C. The air-side and refrigerant-side pressure drop for this configuration are 0.027 kPa and 49.4 kPa, respectively, well within the allowable limits of 0.075 kPa and 62.2 kPa respectively.

Having chosen an optimum pass arrangement, the effects of varying other parameters are systematically investigated, keeping the pass arrangement constant.

3.14 Tube depth

Increasing the tube depth increases the tube mass per unit length, and also increases the heat transfer surface area per unit length of tube. As a result of this, a shorter tube would be required to transfer the same heat duty. This reduces the total required mass of the condenser. Increasing the tube depth also increases the refrigerant cross sectional flow area, which in turn decreases the refrigerant-side heat transfer coefficient and the heat transfer capacity of the condenser. Thus, this opposing effect increases the total required mass of the condenser. Increasing the tube depth reduces the refrigerant-side pressure drop per unit length, due to an increase in the flow area for refrigerant flow. This results in a reduction in the refrigerant temperature glide.

Thus the net effect of a change in the tube depth is a combination of all of the above influences as shown in Figure 3.8. The tube mass decreases drastically initially

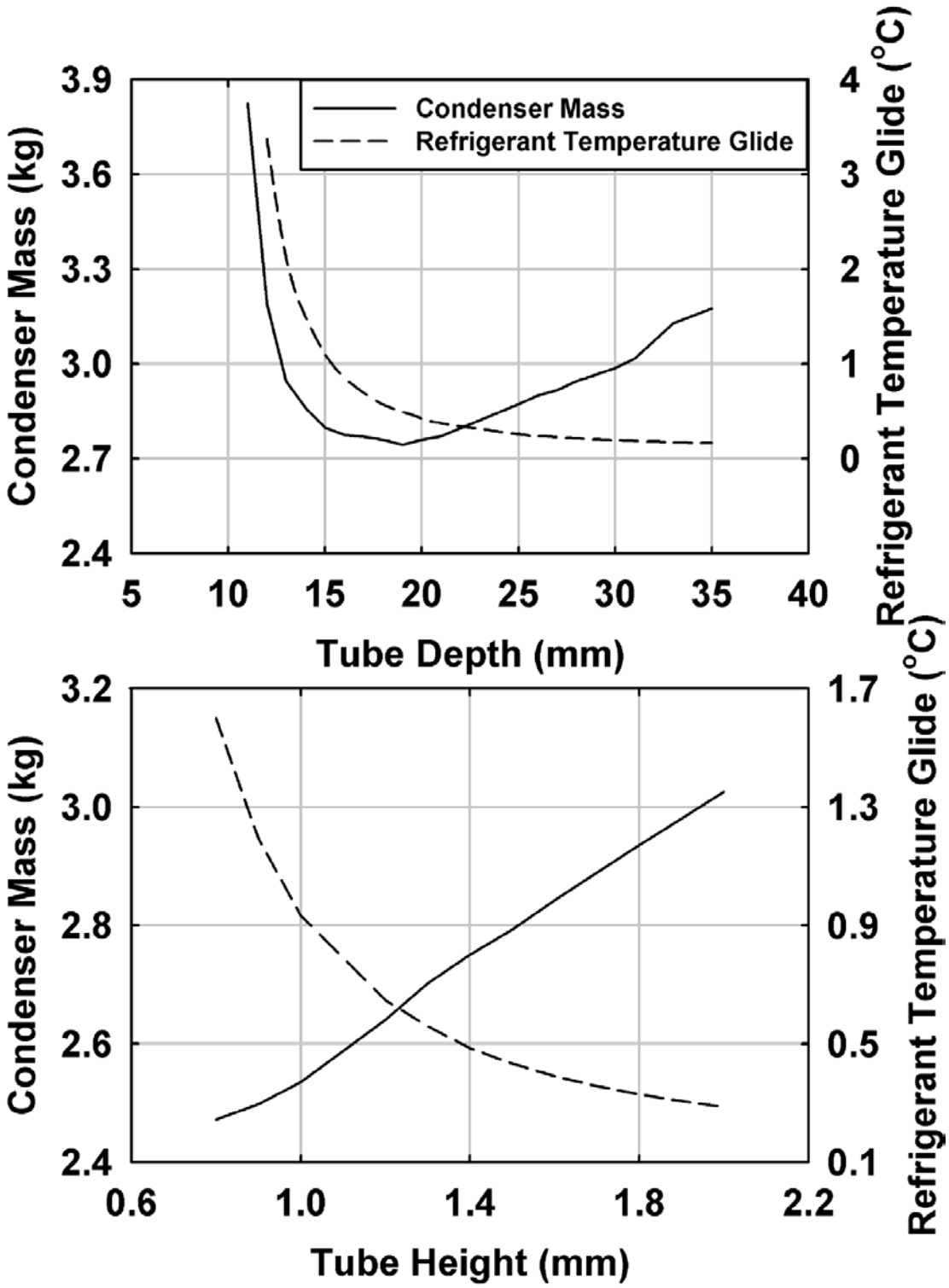

Figure 3. 8 Effect of Tube Depth and Height

from 3.82 kg at a 11 mm depth to 2.80 kg at a 15 mm depth, reaches a minimum value of 2.74 kg at 19 mm and then gradually rises with an increase in tube depth to 3.18 kg at 35

mm. This is because for a tube depth of more than 19 mm, the increase in heat transfer area is negated by the reduction in tube-side heat transfer coefficient due to reduced refrigerant flow velocity. Hence 19 mm is chosen as the optimum tube depth. Variation of the refrigerant temperature glide with tube depth is also shown in Figure 3.8. As expected, this deceases with an increase in tube depth from 3.38^{o}C at 12 mm depth to 0.16^{o}C at 35 mm depth, and is lower than the allowable value of 1^{o}C for the chosen optimum of 19 mm.

As the tube depth is varied, the tube length is also varied in order to keep the heat duty constant for each configuration considered. This change in tube length changes the air-flow area, which in turn affects the air velocities. The decrease in condenser mass from 3.82 kg (1.84 m length) at 11 mm depth to 2.74 kg (0.85 m length) at 19 mm, is partly due to the increase in the air velocity over the condenser face from 1.66 m/s to 3.62 m/s, due to a reduction in the tube length. This increase in air velocities also increases the air-side heat transfer coefficient (158.6 W/m^{2}K at 11 mm depth to 208.7 W/m^{2}K at 19 mm depth), thus enhancing condenser performance. Increasing the tube depth from 11 mm to 35 mm also increases the air-side pressure drop from 10.5 Pa (0.04" H_2O) to 335.3 Pa (1.35" H_2O), as the air has to flow through a longer path with an increase in tube depth.

The tube depth is kept constant at 19 mm for the subsequent analyses.

3.15 Tube height

Increasing the tube height increases the refrigerant cross sectional flow area, which in turn leads to a decrease in the refrigerant-side heat transfer coefficient and the

heat transfer rate. This increases the total required mass of the condenser. Increasing the tube height also increases the tube mass per unit length. The refrigerant pressure drop decreases due to an increase in the cross sectional area, which reduces the temperature glide of the refrigerant.

As the tube height is increased, the tube length is increased to compensate for the decrease in heat transfer rate per unit length of tube. This causes an increase in the air-flow area, which decreases the air velocities and hence the air-side heat transfer coefficients. The air velocity across the condenser face decreases from 3.99 m/s to 3.36 m/s as the tube height is increased from 0.8 mm to 2.0 mm due to the increase in tube length from 0.81 m to 0.88 m. The air-side pressure drop decreases from 74.23 Pa (0.30" H_2O) for a 0.8 mm height to 66.6 Pa (0.28" H_2O) for a 2.0 mm height due to the increase in air-flow area.

Based on these effects, the tube mass required increases with an increase in tube height, while the refrigerant temperature glide decreases, as shown in Figure 3.8. The condenser mass increases from 2.47 kg at a 0.8 mm height to 3.03 kg at a 2.0 mm height, while the refrigerant temperature glide decreases from 1.6^{o}C at a 0.8 mm height to 0.29^{o}C at 2.0 mm height.

From these plots it is clear the smallest possible tube height that maintains the refrigerant temperature glide below 1^{o}C should be selected. Thus a tube height of 1.0 mm is chosen, and maintained constant for subsequent analyses. The mass of the condenser is 2.64 kg at the 1.0 mm tube height.

3.16 Fin Density

Increasing the fin density increases the condenser mass and the air-side heat transfer area per unit length of tube, decreasing the tube length required to transfer the same heat duty. This effect helps in reducing the total required mass of the condenser. Increasing the fin density also decreases the free flow area for air, which in turn increases the air velocity and the air-side heat transfer coefficient, which helps in reducing the total required mass of the condenser. In addition, as the fin density is increased, even at the same air flow velocity, a larger fraction of the air flow occurs through the louvers in a boundary layer (Webb 1994). This results in a higher air-side heat transfer coefficient, which again helps in reducing the mass of the condenser. As condensation requires a smaller tube length at higher fin densities, the refrigerant pressure drop, and in turn, the refrigerant temperature glide decreases. A higher fin density, however, increases the fan power required.

The combination of these effects is seen in Figure 3.9, which shows the effect of a change in fin density on tube mass and refrigerant temperature glide. Both the tube mass and the refrigerant temperature glide decrease with an increase in the fin density. As the fin density increases from 3 fins per cm to 12 fins per cm, the condenser mass decreases from 5.36 kg to 1.81 kg due to a significant decrease in the tube length from 2.27 m to 0.38 m, while the refrigerant temperature glide decreases from 2.68^{o}C to 0.50^{o}C. With a fin density increase from 3 fins per cm to 12 fins per cm, the tube mass decreases from 3.07 kg to 0.52 kg, while the fin mass decreases from 2.29 kg to 1.29 kg because even though there are more fins per unit length, the total tube length is much smaller. Figure 3.9 shows the increase in fan power with fin density. The fan power increases

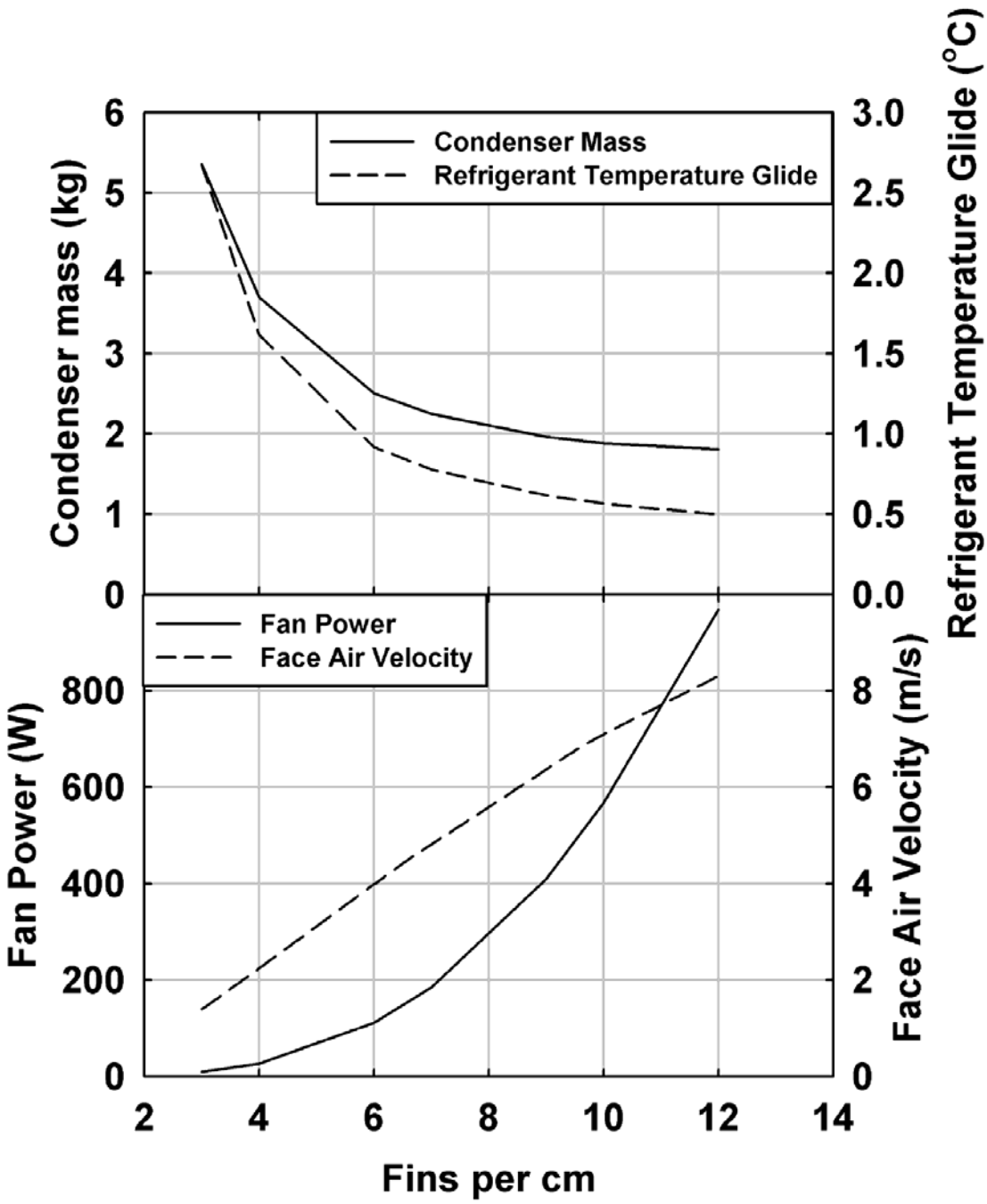

Figure 3. 9 Effect of Fin Density

substantially from 9.2 W at 3 fins per cm to 969.0 W at 12 fins per cm. The decrease in tube length also increases the face air velocity from 1.4 m/s for 3 fins/cm to 8.3 m/s for 12 fins/cm. A fin density of 6 fins per cm was chosen to keep the face velocity below the maximum allowable value of 4 m/s. At 6 fins per cm, the condenser mass is 2.61 kg, the

refrigerant temperature glide is 0.92^{o}C, and the fan power required is 111.3 W.

This value of fin density is maintained constant throughout the rest of the optimization procedure.

3.17 Fin height

Increasing the fin height increases the condenser mass per unit length and the air-side heat transfer area per unit length of tube, which decreases the tube length required to transfer the same heat duty. Increasing the fin height also increases the free flow area for the air, which leads to lower air velocities and decreases the air-side heat transfer coefficient. This effect increases the condenser mass required to obtain the design heat duty. The increase in fin height also decreases the fin efficiency due to an increased temperature difference between the fin base and tip. The average fin efficiency decreases from 0.97 at a 5 mm fin height to 0.72 at a 20 mm fin height.

The combination of these effects is shown in Figure 3.10. The tube mass first decreases with an increase in fin height from 2.83 kg at a 5 mm height to 2.57 kg at a 11 mm height, reaches a minimum value at 11 mm and then increases to 2.91 kg at 20 mm height. The effect of a change in fin height on the face air velocity is also shown in Figure 3.10. As expected, the face air velocity decreases from 5.19 m/s to 2.92 m/s as the fin height increases from 5 mm to 20 mm.

The refrigerant temperature glide is indirectly affected due to a decrease in the tube length with increase in fin height, and decreases with an increase in fin height, as shown in Figure 3.10.

Based on these graphs, a fin height of 11 mm is selected as the optimum value.

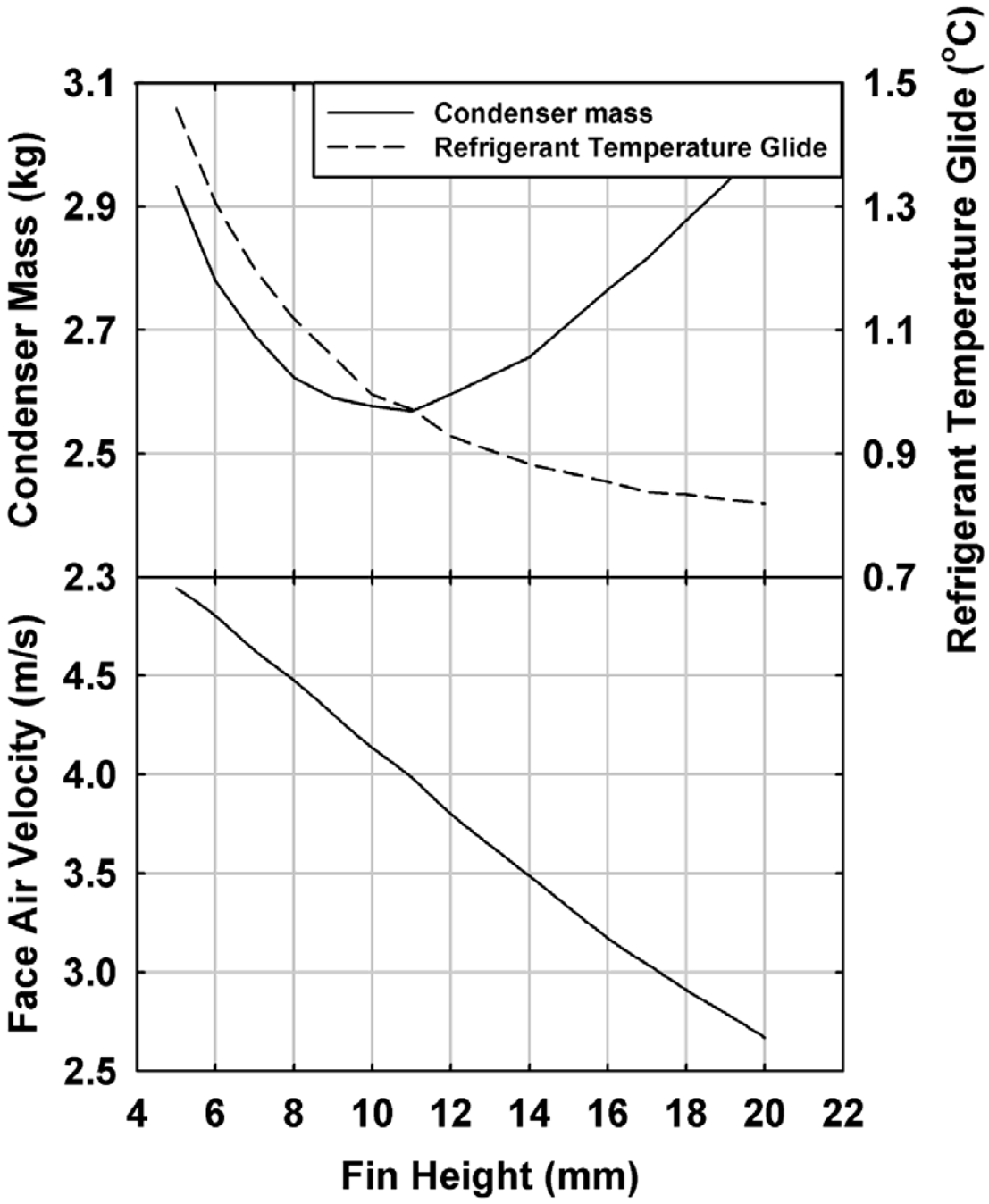

Figure 3.10 Effect of Fin Height

The tube mass required is the lowest for this value of fin height, and the refrigerant temperature glide and the face air velocity are within acceptable limits.

3.18 Number of webs

Increasing the number of webs in the condenser tube increases the condenser

mass per unit length and decreases the refrigerant cross sectional flow area, which results in a higher tube-side heat transfer coefficient. This helps in reducing the total required mass of the condenser, but also results in a higher refrigerant-side pressure drop and increases the refrigerant temperature glide.

The net effect of the change in the number of webs is shown in Figure 3.11. The tube mass initially decreases with an increase in number of webs from 2.55 kg at 5 webs to 2.47 kg at 12 webs, reaches a minimum value at 12 webs and then increases to 2.54 kg at 20 webs. Thus, because the refrigerant-side heat transfer resistance is not dominant, the increase in tube mass with additional webs is greater than the decrease in condenser mass due to an improved heat transfer coefficient. As expected, the refrigerant temperature glide increases with an increase in the number of webs from 0.68^{o}C for 5 webs to 2.41^{o}C for 20 webs.

The improved heat transfer rate with increasing webs reduces the required tube length from 0.90 m for 5 webs to 0.78 m for 20 webs. The decrease in tube length reduces the condenser face area, resulting in an increase in the face air velocity from 3.9 m/s for 5 webs to 4.49 m/s for 20 webs. Among the cases where the face air velocity is lower than the allowable value of 4 m/s, the tube mass is minimum when the number of webs is 6. This is chosen as the optimum value. The condenser mass and refrigerant temperature glide for this optimum value are 2.54 kg and 0.73^{o}C respectively.

3.19 Louver Geometry

At sufficiently high Reynolds number values, the air flow tends to occur in a boundary layer parallel to the louver. This results in the development of a laminar

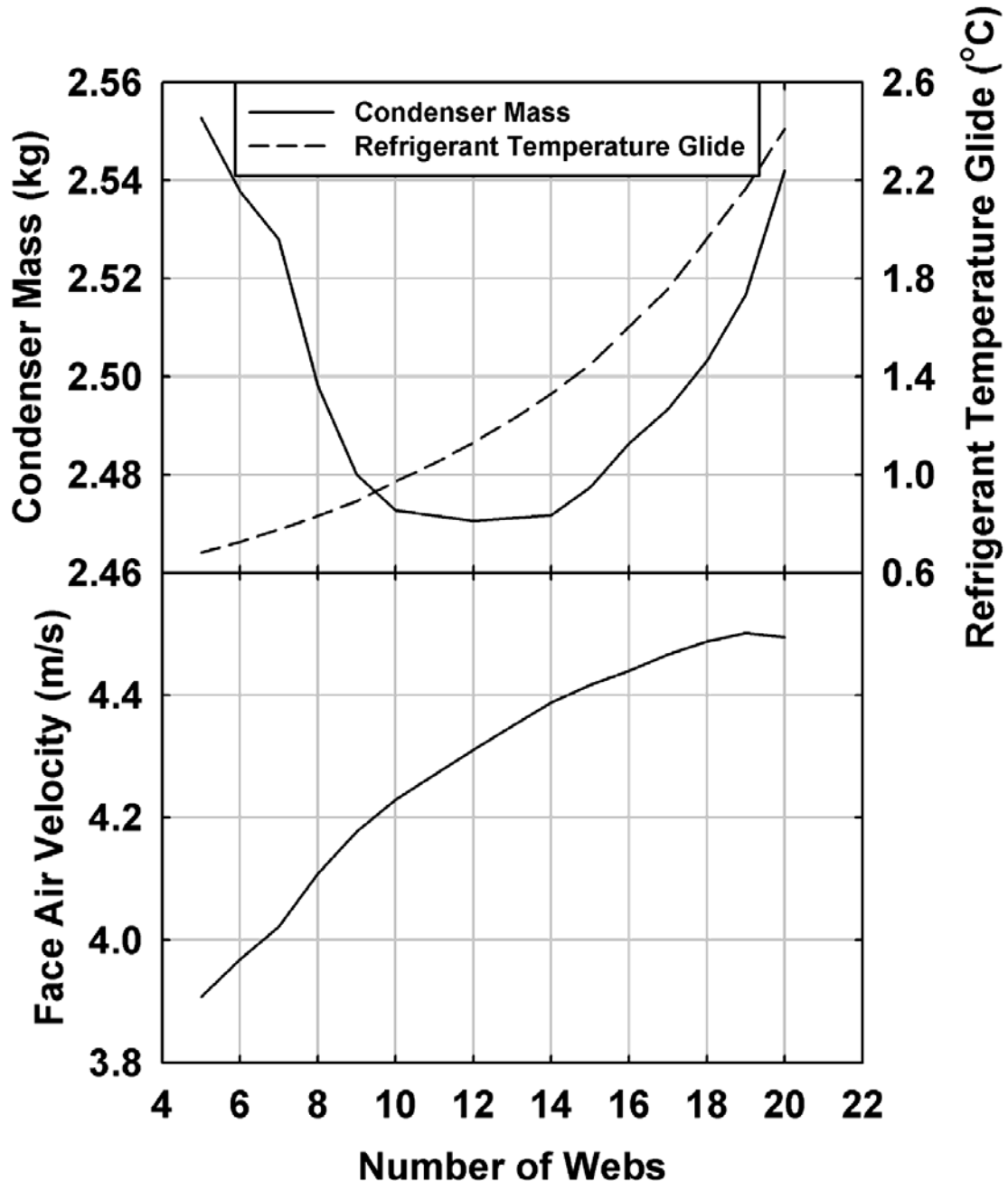

Figure 3. 11 Effect of Number of Webs

boundary layer in the short louver width followed by its dissipation in the wake region between the louvers (Webb 1994). This results in significantly higher air-side heat transfer coefficients for louvered fins as compared to smooth fins. Increasing the louver angle increases the air-side heat transfer coefficient, as a larger louver angle results in a more interrupted boundary layer. This helps in reducing the total required mass of the

condenser. But increasing the louver angle also increases the air-side pressure drop and the fan power required.

Figure 3.12 shows that the condenser mass decreases with an increase in louver angle as expected, from 3.59 kg at 10^o to 2.10 kg at 60^o. Figure 3.11 shows that the fan power increases with an increase in the louver angle from 41.5 W at 10^o to 176.6 W at 60^o. The tube length decreases from 1.26 m for a louver angle of 10^o to 0.73 m for 60^o. This decrease in tube length leads to a decrease in the refrigerant temperature glide with increase in louver angle from 1.00°C at 10^o to 0.62°C at 60^o (Figure 3.11). The decrease in tube length also increases the face air velocity from 2.8 m/s for 10^o to 4.8 m/s at 60^o.

A louver angle of 30^o provides the lowest tube mass for which the face air velocity is lower than the maximum allowable value of 4 m/s. Hence 30^o is chosen as the optimum louver angle. The condenser mass, refrigerant temperature glide and fan power are 2.54 kg, 0.73°C and 103.1 W, respectively at this louver angle.

An increase in the number of louvers per cm also increases the air-side heat transfer coefficient due to the presence of a more interrupted boundary layer, thus reducing the total required mass of the condenser. However increasing the number of louvers per cm also increases the air-side pressure drop, resulting in higher fan power. Figure 3.13 shows the effect of the change in the number of louvers. As expected, the tube mass decreases with an increase in the number of louvers from 3.12 kg for 5 louvers per cm to 2.33 kg for 20 louvers per cm. Figure 3.12 shows that the fan power required increases with an increase in the number of louvers, from 16.3 W for 5 louvers per cm to 234.3 W for 20 louvers per cm. The refrigerant temperature glide decreases gradually from 0.87°C at 5 louvers per cm to 0.68°C at 20 louvers per cm due to a decrease in

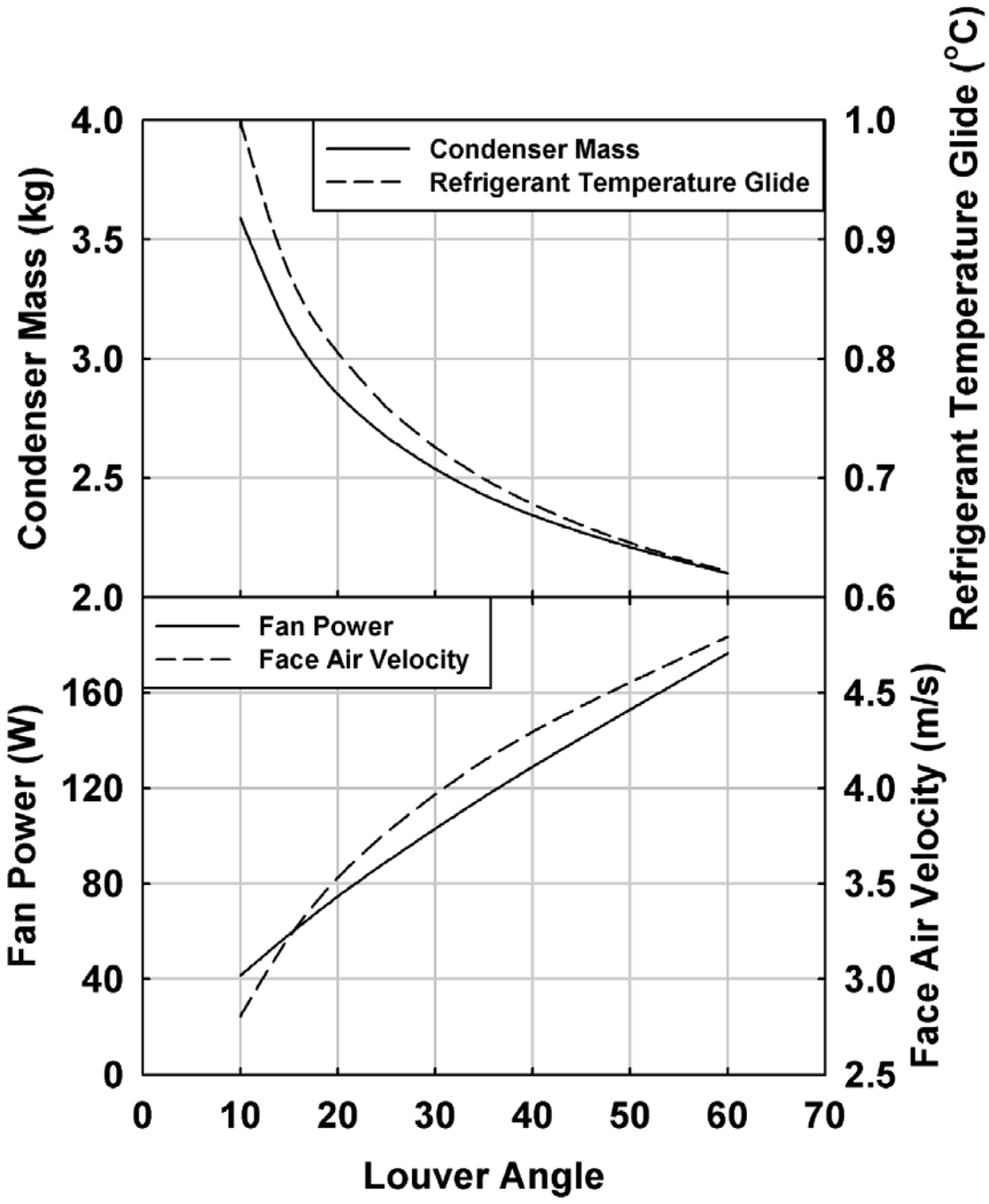

Figure 3. 12 Effect of Louver Angle

tube length from 1.09 m to 0.82 m. The face air velocity increases from 3.23 m/s for 5 louvers per cm to 4.3 m/s for 20 louvers/cm due to the decrease in tube length. The number of louvers per cm was chosen to be 13 to obtain the lowest tube mass for which the face air velocity is within acceptable limits. At this value, the condenser mass,

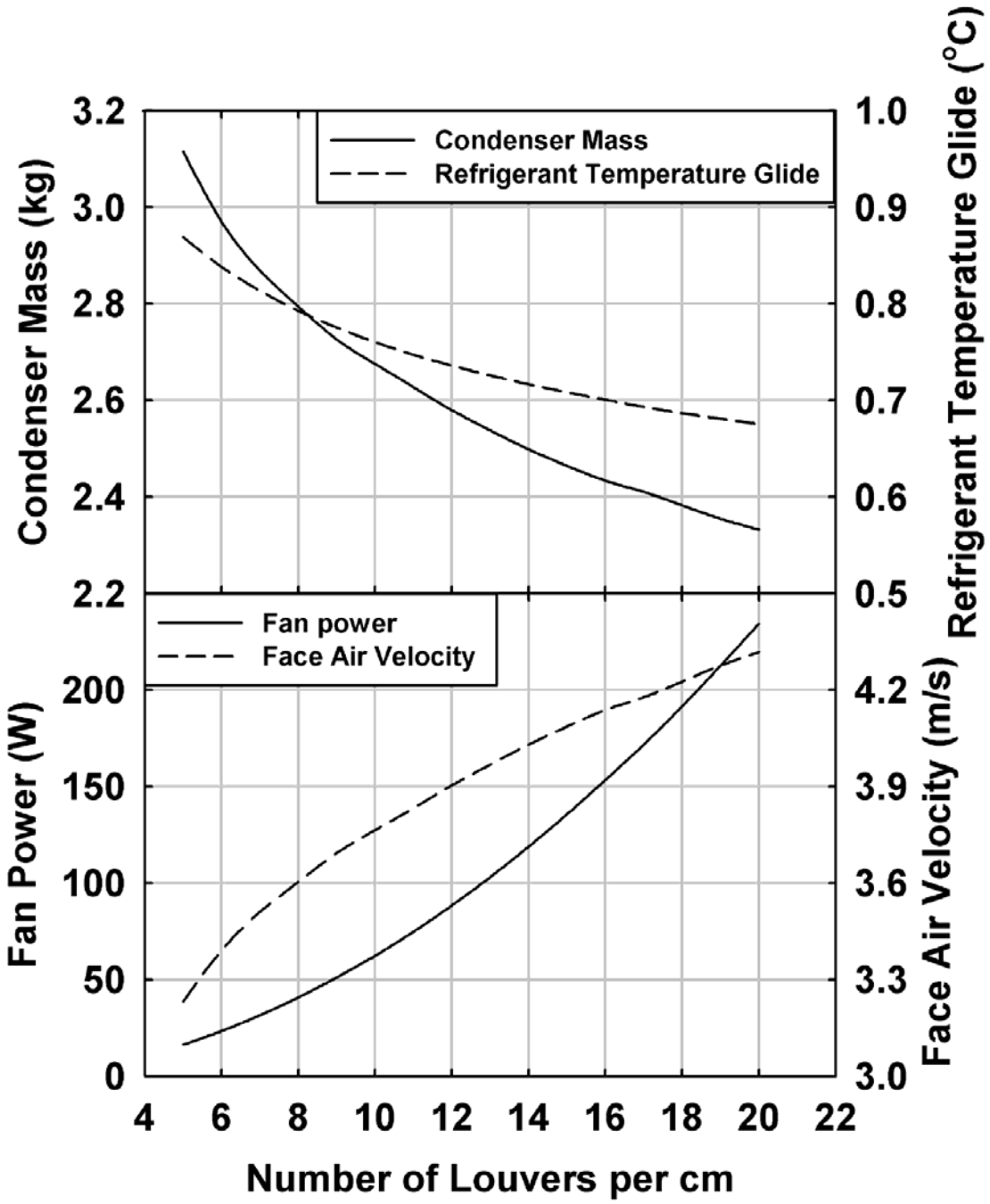

Figure 3. 13 Effect of Number of Louvers per cm

refrigerant temperature glide and fan power are 2.54 kg, 0.73°C and 103.1 W respectively.

3.20 Final Optimized Geometry

The final optimized values of all the geometric parameters are shown in Table 3.4. Figure 3.14 shows the variation in the key parameters of the condenser as each of the design parameters are successively varied, as discussed above. The condenser mass reduces as each parameter is optimized. Figure 3.14 also depicts the variation of the condenser height and length with each parameter. The final optimized values of the condenser length and height are lower than the baseline values. Table 3.4 outlines the variation of the various condenser performance parameters through the design procedure. The

Table 3. 4 Optimum Values of the Geometric Parameters

Tube side		Fin		Louver	
Inner tube height	1.0 mm (0.04 in)	Fin pitch	1.667 mm (0.066 in)	Louver angle	30^{o}
Inner tube depth	19 mm (0.75)	Fin height	11 mm (0.43 in)	Number of louvers per cm	13
Number of webs	6	Fin thickness	0.127 mm (0.005 in)	Louver width	0.8 mm (0.044 in)
Thickness of webs	0.318 mm (0.0125 in)	Fin depth	19.6 mm (0.77 in)		
Tube wall thickness	0.318 mm (0.0125 in)				
Tube length	0.89 m (2.9 ft)				
Pass arrangement	13, 10, 5, 4				

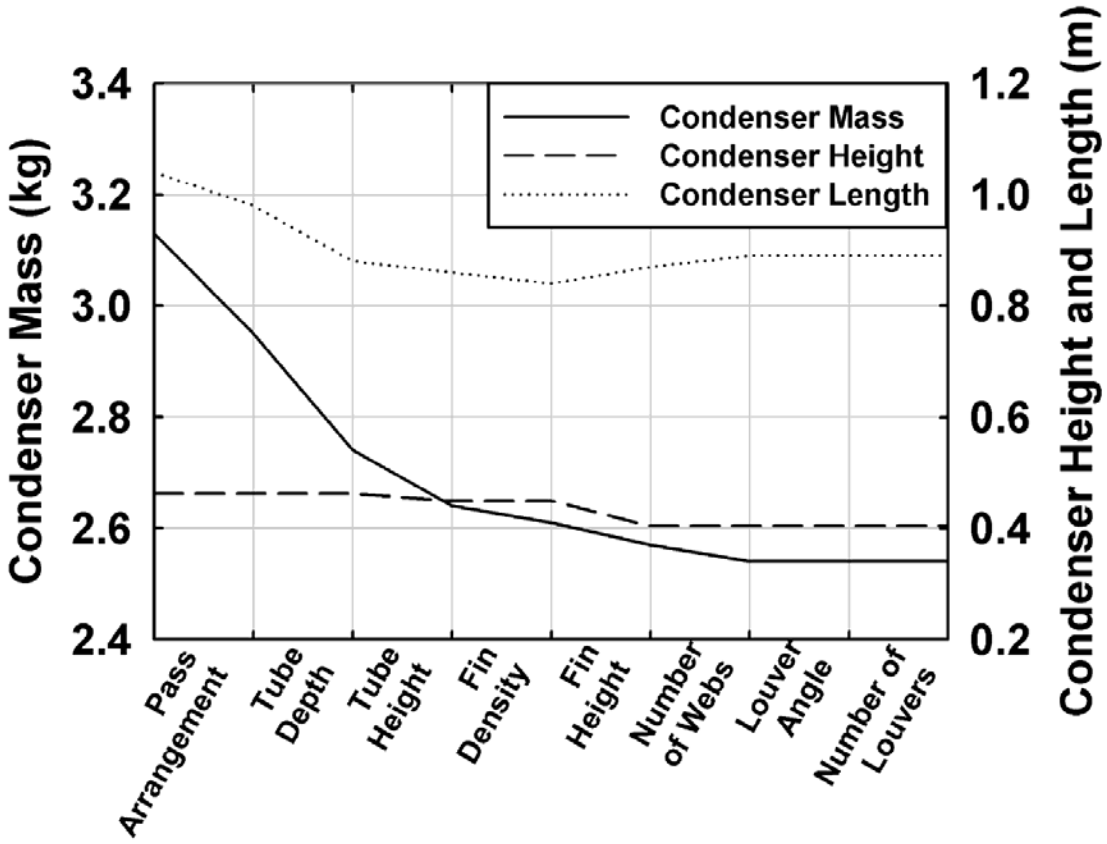

Figure 3. 14 Variation of the Condenser Mass, Height and Length through the Optimization procedure

optimum condenser configuration thus obtained has 19% lower mass than the baseline configuration for the same heat duty.

In order to verify that the geometry obtained is indeed the best possible one under the current design constraints, each of the geometric parameters was individually perturbed from its current optimum value. The result of this analysis is presented in Table 3.5. It is seen that for the variation of each of the geometric parameters, either the required condenser mass is higher than the optimum case, or one of the design constraints is violated. This confirms that the geometry obtained for the current optimization procedure provides a lower condenser mass than other geometries for the set design constraints.

Table 3. 5 Verification of the Optimization Procedure

Geometric Parameter Varied	Mass (kg)	Ref T_{glide} (^oC)	Face Air Velocity (m/s)	Fan Power (W)	Length (m)	Height (m)	Comment
Optimum Configuration	2.54	0.73	3.97	103.1	0.89	0.404	
Pass Arrangement 4 passes → 3 passes	2.58	0.48	4.05	105.9	0.87	0.404	Face Air Velocity greater than the allowable limit
Pass Arrangement 4 passes → 5 passes	2.44	1.58	4.29	113.5	0.82	0.404	Face Air Velocity greater than the allowable limit
Tube Depth 19 → 18 mm	2.56	0.85	3.75	87.4	0.94	0.404	Condenser mass greater than the Optimum Configuration
Tube Depth 19 mm → 20 mm	2.535	0.63	4.16	119.6	0.85	0.404	Face Air Velocity greater than the allowable limit
Tube Height 1.0 mm → 0.9 mm	2.47	0.91	4.09	105.9	0.870	0.401	Face Air Velocity greater than the allowable limit
Tube Height 1.0 mm → 1.1 mm	2.60	0.60	3.87	101.1	0.90	0.411	Condenser mass greater than the Optimum Configuration
Fin Density 6 fins/cm → 5 fins/cm	2.94	0.89	3.15	56.3	1.12	0.404	Condenser mass greater than the Optimum Configuration
Fin Density 6 fins/cm → 7 fins/cm	2.28	0.62	4.78	170.6	0.74	0.404	Face Air Velocity greater than the allowable limit
Fin Height 11 mm → 10 mm	2.26	0.64	4.99	170.1	0.77	0.372	Face Air Velocity greater than the allowable limit
Fin Height 11 mm → 12 mm	2.32	0.61	4.57	169.9	0.71	0.436	Face Air Velocity greater than the allowable limit
Number of Webs 6 → 5	2.55	0.68	3.91	101.1	0.90	0.404	Condenser mass greater than the Optimum Configuration
Number of Webs 6 → 7	2.53	0.78	4.02	104.8	0.88	0.404	Face Air Velocity greater than the allowable limit
Louver Angle 30^o → 25^o	2.67	0.76	3.77	89.3	0.94	0.404	Condenser mass greater than the Optimum Configuration
Louver Angle 30^o → 35^o	2.43	0.70	4.15	116.4	0.85	0.404	Face Air Velocity greater than the allowable limit

3.21 Cost Analysis

It was seen in the preceding analysis that as the condenser mass is decreased, typically the fan power increases, even if the air-side velocity and pressure drop are maintained within the chosen limits. To investigate the effect of the increased fan power on operating cost, an approximate estimate of the cost of operating a residential air-conditioning unit in its expected lifetime of 10 years for 3000 hours/year operation was calculated. Here, the costs of maintenance and for the operation of the indoor blower were not considered. The compressor was assumed to operate at a power of 4 kW (ideal power) with an assumed electrical to mechanical conversion efficiency of 90%. The compressor power of 4 kW was obtained by considering that this design was for a 3-ton (10.5 kW) cooling load and a nominal 14.5 kW condenser duty (which yields the 4 kW compressor load). The fan was assumed to operate at 60% efficiency. The results of this approximate analysis are shown in Table 3.6. The operating cost of the compressor was found to be $6667, assuming an electric power rate of 5 c/kWh based on prevailing local utility rates. The fan operating cost, on the other hand, was $90 for the baseline configuration and $258 for the optimum configuration. Thus the cost of operating the fan was found to be 1.3% and 3.9% of the compressor operating cost for the baseline and optimum configurations, respectively.

It is clear from this analysis that the cost of operating the fan is not significant as compared to the cost of operating the compressor, which suggests that minimizing condenser mass does not carry with it a significant operating cost penalty. However the 19% reduction in condenser mass from 3.13 kg to 2.54 kg during the optimization procedure leads to significant reduction in capital costs. A more conclusive judgment

Table 3. 6 Cost Analysis for an Air-conditioning System

	Baseline Condenser Configuration	Optimum Condenser Configuration
Compressor Operation Cost	6667	6667
Fan Operation Cost	90	258
Percentage Cost on Fan Operation	1.3%	3.9%

about this issue can be made best by conducting a life-cycle cost analysis; however, such an analysis is not particularly meaningful when only one component is optimized. A comprehensive optimization of the capital and operating costs of the condenser, evaporator, fan, blower and other auxiliary systems was considered to be outside the scope of the present study.

3.22 Uncertainty Analysis

The air-side heat transfer coefficient was calculated using the correlation by Kim and Bullard (2002a). The values of heat transfer coefficient predicted by this equation are accurate to within ±14.5%. The condenser mass was calculated for the maximum and minimum values of air-side heat transfer coefficient, obtained by increasing and decreasing the air-side heat transfer coefficient by 14.5%, respectively. It was also ensured that the other design constraints were satisfied by the condenser geometry for this increased and decreased air-side heat transfer coefficient. The condenser mass was found to be 3.03 kg and 2.41 kg for the minimum and maximum values of the air-side heat transfer coefficient. It may be recalled that the condenser mass calculated using the air-side heat transfer coefficient predicted by the correlation was 2.54 kg. The decrease in condenser mass at the upper bound of the heat transfer coefficient is smaller than the

corresponding increase at the lower bound because in the upper bound the fin density is reduced for 6 fins/cm to 5.3 fins/cm to maintain the face air velocity below 4 m/s. Thus, the effect of uncertainties in air-side heat transfer coefficient on the condenser mass is not negligible.

The tube-side heat transfer coefficient during condensation of the refrigerant is calculated using the correlation by Shah (1979). This correlation has an error of ±15.4% in the calculated value of the heat transfer coefficient. The condenser mass was calculated for minimum and maximum values of two-phase heat transfer coefficients obtained by adjusting for the percentage error in the heat transfer coefficient due to the accuracy of the correlation. The condenser mass calculated for the minimum and maximum values of the tube-side condensation heat transfer coefficients were 2.60 kg and 2.48 kg respectively. It can be seen that the condenser mass changes by 2.4% from value predicted by the correlation when the uncertainties are taken into account. When the air-side uncertainties were considered, as discussed above, the predicted value changed by 5.1% and 19.3% for the upper and lower bounds, respectively. Thus, uncertainties in air-side heat transfer coefficient affect the condenser mass more significantly than the uncertainties in condensation heat transfer coefficient prediction.

Chapter 4

EFFECT OF AIR FLOW MALDISTRIBUTION

4.1 Need for Air Flow Mal-distribution Study

Figure 1.2 shows a typical condenser unit of an air conditioning system. The condenser coils are vertically placed along the four sidewalls of the condenser unit. Air flow over the condenser coils is generated by an induced-draft fan placed at the top of the unit. This configuration results in a non-uniform air flow through the condenser coils. Hence a uniform air flow distribution, which is assumed in most theoretical studies, is an idealization. A study of the condenser performance for mal-distributed air flow conditions is therefore required to better approximate the operation of an air-cooled condenser under realistic conditions.

4.2 Heat Transfer Coefficient Variation for Uniform Air Flow

Before analyzing the performance of the condenser for mal-distributed air flows, it would be instructive to study the heat transfer coefficient variation along the condenser length for the optimum geometry obtained in the previous chapter, under uniform air flow. Figure 4.1 and 4.2 show the air-side, tube-side and overall heat transfer coefficient and the heat duty variation along the length of the condenser for uniform air flow. The air-side heat transfer coefficient is fairly constant along the entire condenser length ($221.8\ W/m^2K < h_{air} < 223.9\ W/m^2K$). There is a slight decrease in the air-side heat transfer coefficient at the refrigerant inlet and exit region of the condenser. This decrease is because there is a drop in the heat duties at these points, due to the temperature drop in

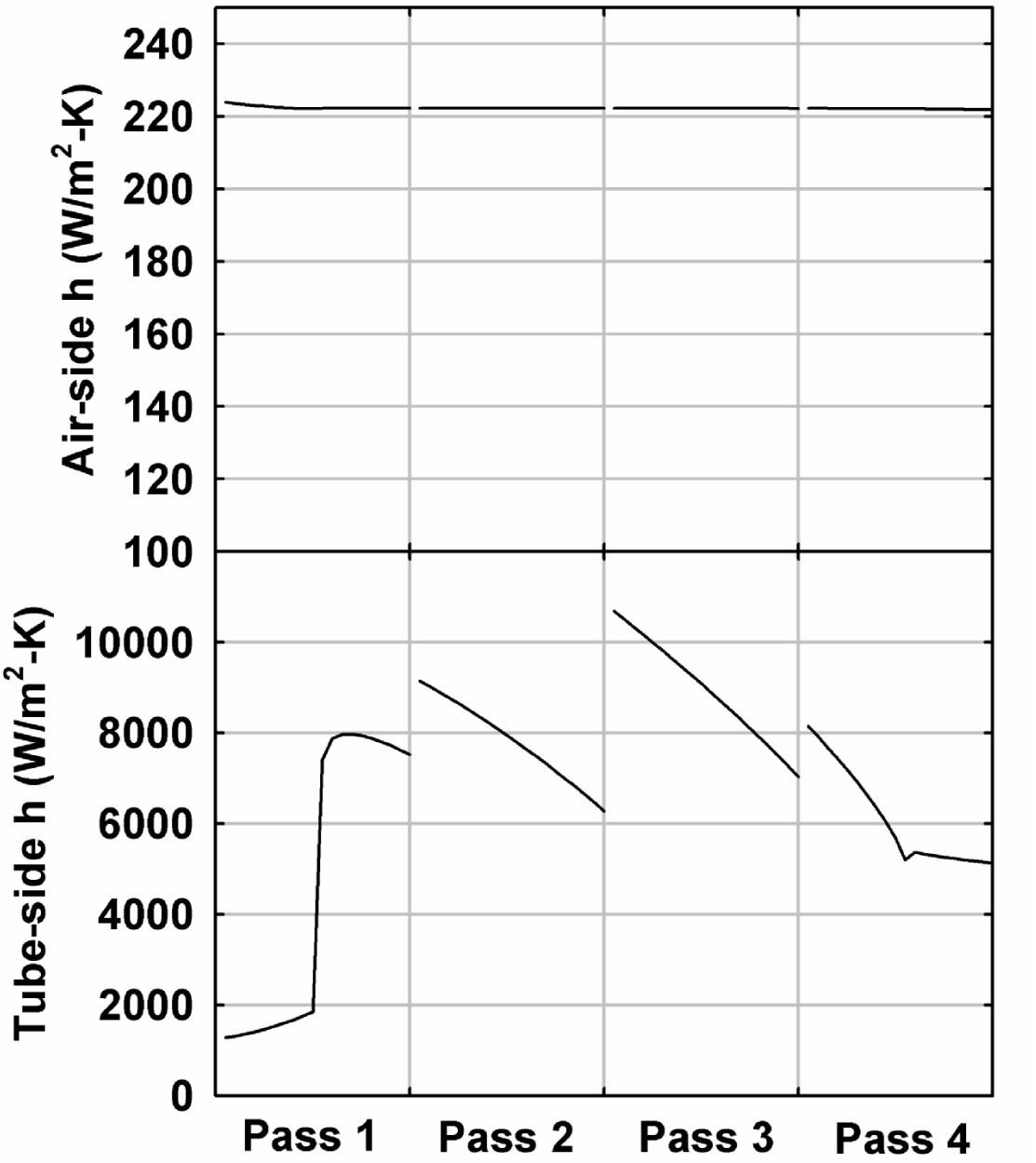

Figure 4. 1 Air-side and Tube-side Heat Transfer Coefficient Variation

the refrigerant during single-phase cooling. This causes a slight drop in the average air temperature, and consequently, a slight drop in the thermal conductivity of air. This drop in thermal conductivity decreases the air-side heat transfer coefficient.

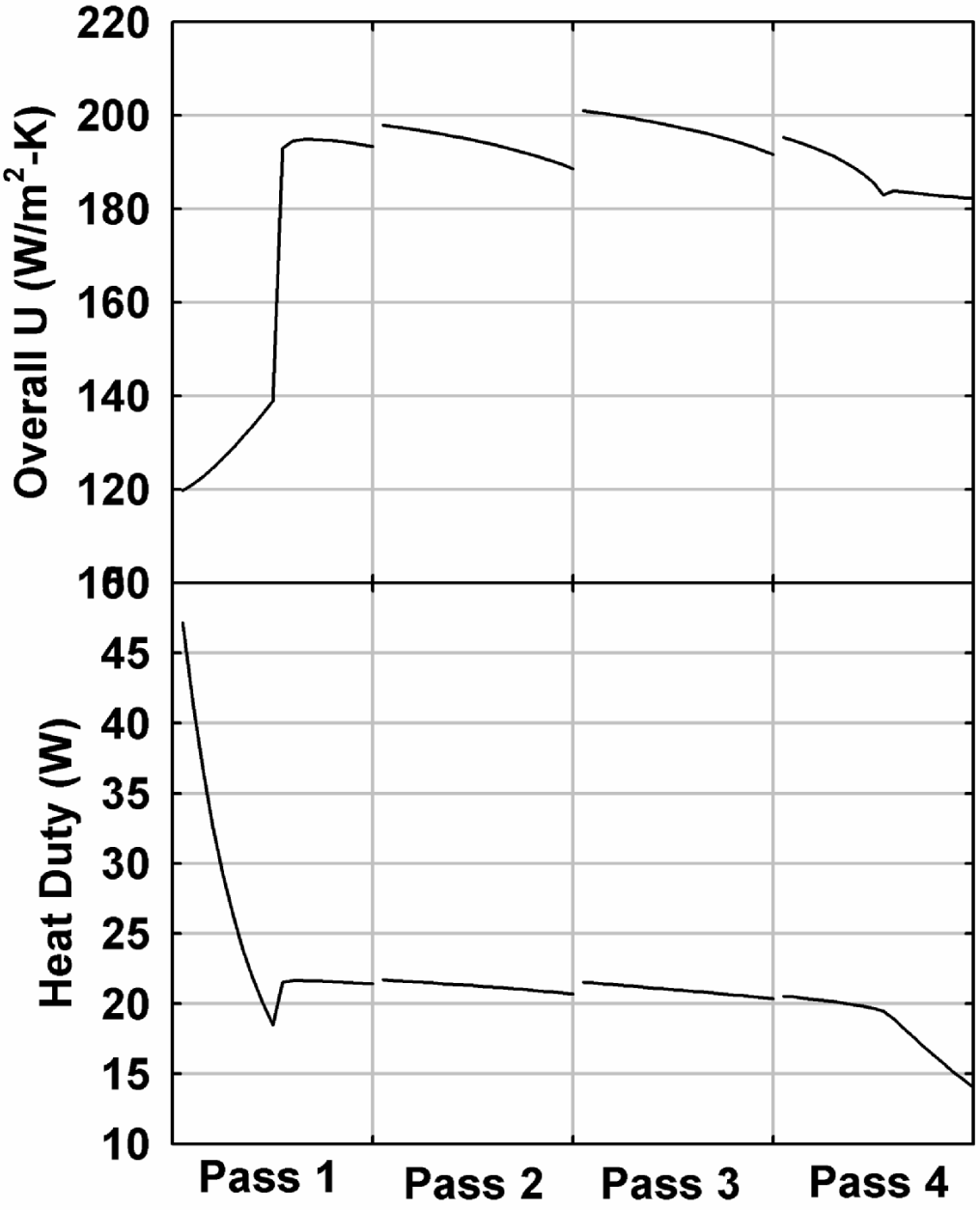

Figure 4. 2 Overall Heat Transfer Coefficient and Heat Duty Variation

Because the refrigerant enters the condenser as a superheated vapor, the vapor heat transfer coefficient on the tube-side is low at the condenser inlet region. The tube-side heat transfer coefficient at the condenser inlet is 1282 W/m^2K. At about halfway through the first pass, the refrigerant reaches the saturation temperature and starts to condense,

and the tube-side heat transfer coefficient increases sharply to 7977 W/m^{2}K. The tube-side heat transfer coefficient then gradually decreases to 7516 W/m^{2}K at the end of the first pass, due to the decrease in refrigerant quality and the resultant reduction in flow velocity. The tube-side heat transfer coefficient then rises to 9144 W/m^{2}K at the inlet to the second pass, due to a reduction in the number of tubes per pass (from 13 in the first pass to 10 in the second) causing an increase in the refrigerant flow velocity. This trend in the tube-side heat transfer coefficient is maintained until about halfway through the fourth (last) pass, when the entire refrigerant inventory is condensed and the refrigerant starts flowing as subcooled liquid. In the subcooled region, the liquid heat transfer coefficient on the tube-side is lower than the condensation heat transfer coefficient, and remains fairly constant (5133 W/m^2-K < $h_{subcooled}$ < 5367 W/m^2-K) until the exit of the condenser. The single-phase heat transfer coefficient in the sub-cooled region is larger than the heat transfer coefficient in the superheated region because of better heat transfer characteristics of the liquid refrigerant as compared to vapor.

The overall heat transfer coefficient is much lower than the tube-side heat transfer coefficient due to low air-side heat transfer coefficient. However, as the air-side heat transfer coefficient is fairly constant, the nature of the overall heat transfer coefficient variation along the condenser length is very similar to the variation of the tube-side heat transfer coefficient. Thus the overall heat transfer coefficient is 119.8 W/m^{2}K at the refrigerant inlet and sharply rises to 194.8 W/m^{2}K at about halfway through the first pass as the refrigerant starts condensing. The overall heat transfer coefficient then gradually decreases to 193.4 W/m^{2}K at the end of the first pass, due to a decrease in the refrigerant quality. The overall heat transfer coefficient rises to 197.9 W/m^{2}K at the inlet of the

second pass due to a decrease in the number of tubes per pass in the second pass. This trend in the overall heat transfer coefficient variation is continued in the second and third passes, and the overall heat transfer coefficient at inlet to the fourth pass is 195.3 W/m^{2}K. The overall heat transfer coefficient then rapidly decreases to 183.9 W/m^{2}K at the end of refrigerant condensation, and then gradually decreases in the refrigerant single-phase region to 182.2 W/m^{2}K at the refrigerant exit.

The variation of the heat transferred in each segment of the condenser along the condenser length is shown in Figure 4.2. The heat duty per segment is very high at the refrigerant inlet region due to a large temperature difference between the refrigerant and the air. Once the refrigerant reaches the two-phase region, the refrigerant-to-air temperature difference remains fairly constant ($\approx 15^{o}$C) and the heat duty variation is similar to the variation in the overall heat transfer coefficient. The heat duty decreases again in the subcooled region, because of a drop in the refrigerant-to-air temperature difference due to refrigerant subcooling.

4.3 Air Flow Mal-distributions Considered

The effect of non-uniform air flow distribution on the condenser performance was studied. The air flow was linearly deviated by varying extents from the uniform case keeping the mean air flow rate constant. The deviation from uniform air flow distribution ϕ was defined as,

$$\phi = \frac{\dot{m}_{top} - \dot{m}_{mean}}{\dot{m}_{mean}} \qquad (59)$$

where, $\dot{m}_{top}$ is the local air flow rate at the top of the condenser coil.

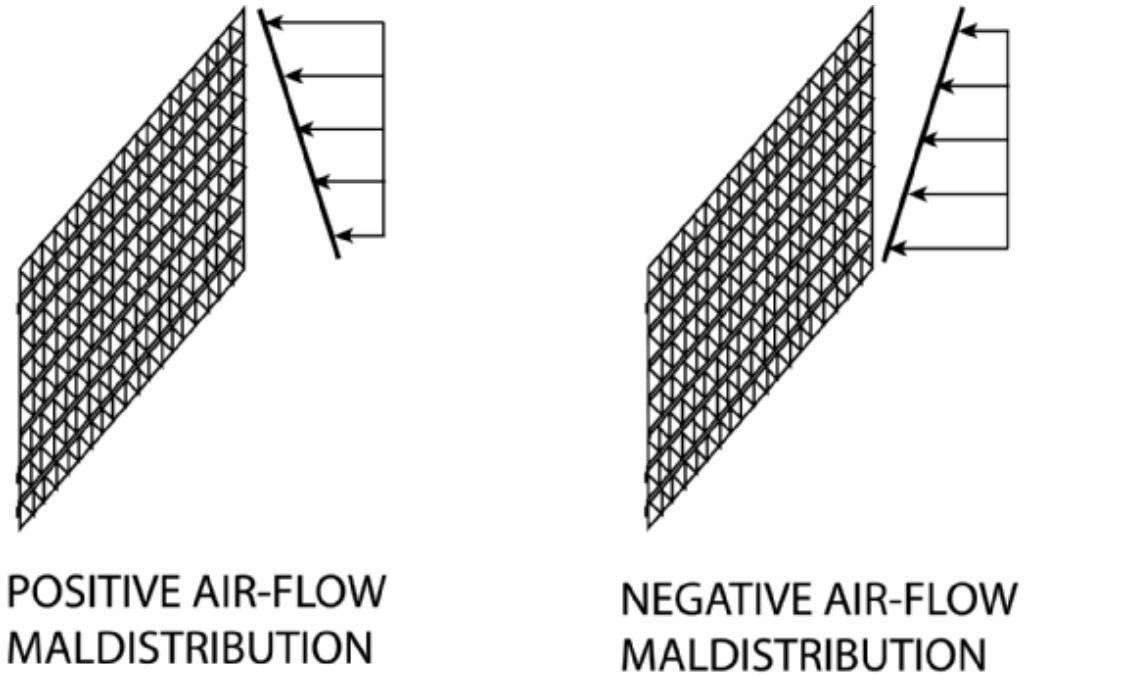

Figure 4. 3 Positive and Negative Air Flow Mal-distributions

Thus the deviation is positive when the local air flow rate is maximum at the top and minimum at the bottom of the condenser, and negative when the local air flow rate is minimum at the top and maximum at the bottom of the condenser. This is illustrated in Figure 4.3.

4.4 Effect of Negative Air Flow Mal-distribution on Condenser Performance

A study of the heat transfer coefficient variation along the condenser length for mal-distributed air flows provides a good insight into the reasons for the change in condenser performance due to mal-distribution. Figure 4.4 and 4.5 show the variation of the air-side, tube-side and overall heat transfer coefficients and heat duty along the condenser length for a representative air flow mal-distribution of ϕ = -0.3. Thus, the air flow rate is 30% lower at the top (refrigerant inlet region) and 30% higher at the bottom

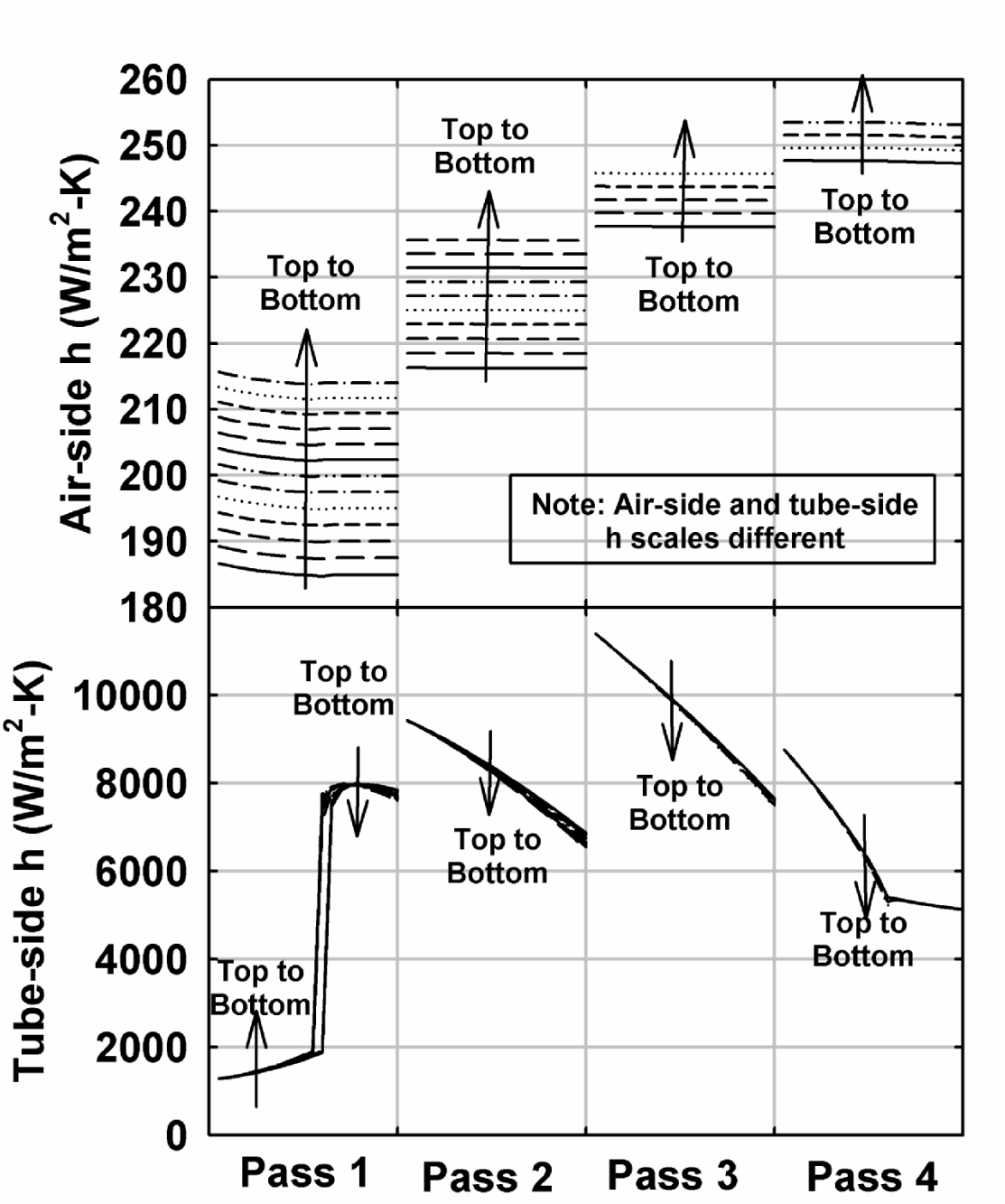

Figure 4. 4 Effect of Negative Air Flow Mal-distribution on Air-side and Tube-side Heat Transfer Coefficient

(refrigerant outlet region) of the condenser. The air velocity is 2.78 m/s at the top of the condenser and 5.16 m/s at the bottom.

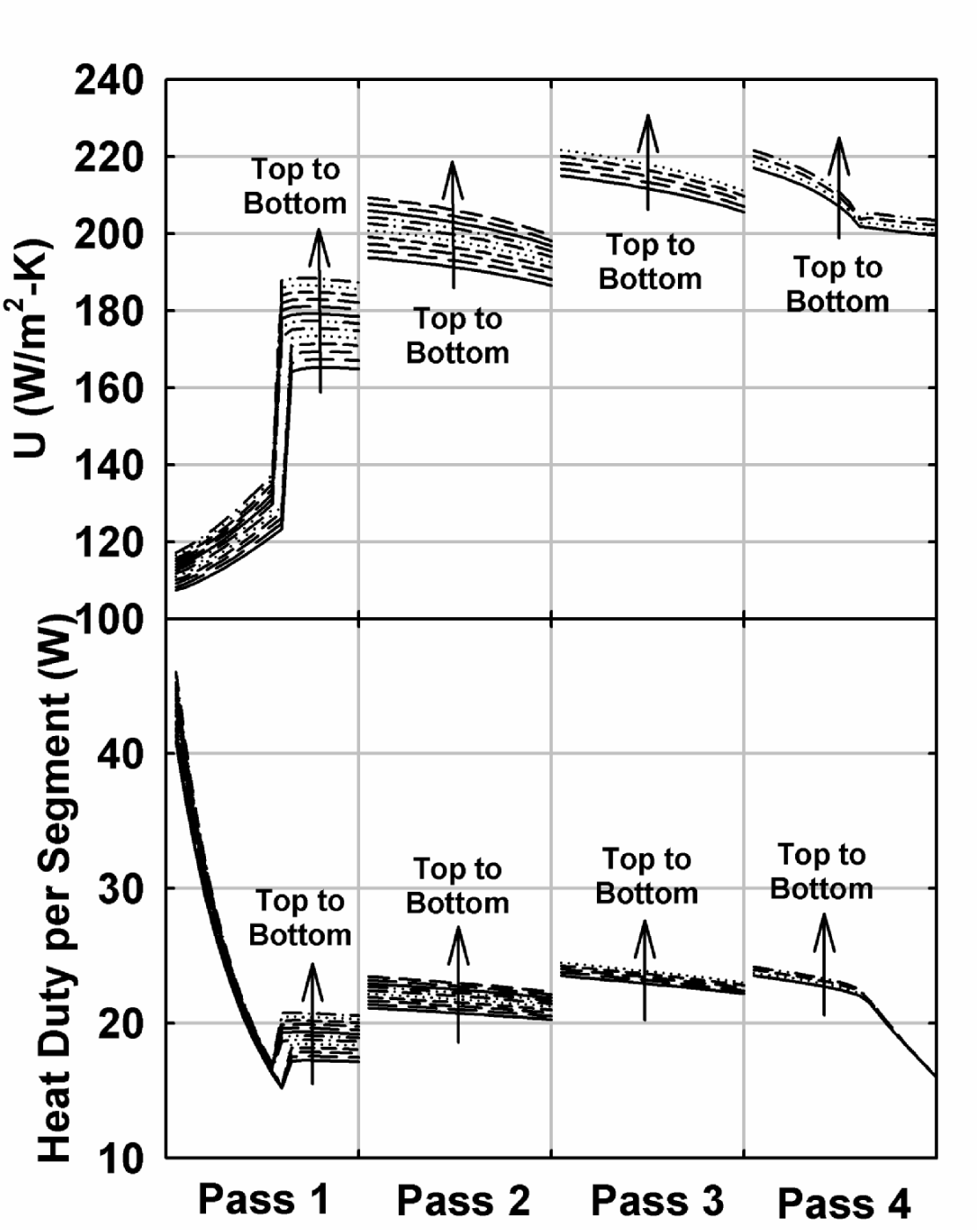

Figure 4. 5 Effect of Negative Air Flow Mal-distribution on Overall U and Heat Duty

The air-side heat transfer coefficient steadily increases from the top-most tube to the bottom-most tube in the condenser, due to increased air flow rates. The air-side heat

transfer coefficient at the refrigerant inlet region of the top-most tube is 186.7 W/m^2K, while the air-side heat transfer coefficient at the corresponding position on the lower-most tube (refrigerant exit region) is 253.1 W/m^2K. The variation of air-side heat transfer coefficients within each refrigerant tube is similar to the variation in the uniform air flow case, i.e it is fairly constant.

The effect of air flow mal-distribution is less pronounced in the variation of tube-side heat transfer coefficient than that in the air-side heat transfer coefficient. The nature of the tube-side heat transfer coefficient variation in any given refrigerant tube is similar to the uniform air flow case. However unlike for uniform air flow distribution, here the tube-side heat transfer coefficient in the upper tubes in any pass is slightly higher than those in the lower tubes, in the two-phase and the subcooled region. At the refrigerant exit, the tube-side heat transfer coefficient in the top-most tube in the last pass is 5137.4 W/m^2K (subcooled), while the tube-side heat transfer coefficient is 5125.0 W/m^2K (subcooled) in the lower-most tube in the last pass. This is because the refrigerant temperature is slightly higher in the upper tubes, due to the lower heat dissipation as a result of lower air flow rates over these tubes. In the two-phase region, the tube-side heat transfer coefficients are slightly larger in the upper tubes because due to lower heat dissipation rates, the refrigerant quality is slightly higher in the upper tubes with the correspondingly higher heat transfer coefficient. At the exit to the first pass, the refrigerant is in the two-phase region and the tube-side heat transfer coefficient at the top-most tube in the first pass is 7840.7 W/m^2K ($x = 0.84$), while at the lower-most tube in the same pass, it is 7602.5 W/m^2K ($x = 0.77$). However, in the superheated region, the tube-side heat transfer coefficient is found to decrease slightly from the top row to the

bottom row in the pass because the mean refrigerant temperature is higher for the lower tubes due to the lower air flow. The tube-side heat transfer coefficient in the top-most tube at the refrigerant inlet region is 1279.5 W/m^2K (superheated), while it is 1281.1 W/m^2K (superheated) for the lower-most tube in that pass. Also, the transition from superheated to two-phase, and two-phase to subcooled regions occurs slightly earlier in the lower tubes of a pass, due to higher heat dissipation rates in them. This can be seen in Figure 4.4.

For each tube, the air-side heat transfer coefficient is fairly constant, while the tube-side heat transfer coefficient varies to a larger extent as explained above. Hence, along the tube, the nature of the variation of the overall heat transfer coefficient is similar to that of the tube-side heat transfer coefficient. However, among different tubes, the variation in the air-side heat transfer coefficient being the significant resistance has a pronounced effect on the overall heat transfer coefficient. For tubes in the same pass, the overall heat transfer coefficient is lower in the upper tubes, due to lower air-side heat transfer coefficients. At the inlet to the first pass, the overall heat transfer coefficient is 107.4 W/m^2K for the top-most tube in the pass, while it is 117.2 W/m^2K for the lower-most tube in the pass. The highest overall heat transfer coefficient occurs in the lower-most tube of the condenser, where the air flow rate, and therefore the air-side heat transfer coefficient is maximum, even though the corresponding refrigerant heat transfer coefficient is only characteristic of single-phase liquid flow.

The variation of the segment heat duty along the condenser length is shown in Figure 4.5. The nature of the heat duty variation along a tube is similar to that in the case of uniform air flow. However within any pass, the heat dissipation is lower in the upper

tubes of a pass, due to lower air flow rates. At the refrigerant inlet region in the first pass, the heat dissipation per segment is 40.9 W for the top-most tube, while it is 46.0 W for the lower-most tube in the first pass. Though the overall heat transfer coefficient and the air flow rate are lowest in the refrigerant inlet region of the condenser, the heat dissipation is the highest due to a large refrigerant-to-air temperature difference. However, this heat dissipation in the refrigerant inlet region is lower than that in the uniform air flow case, due to the lower air flow in this case. In the uniform air flow case, the heat duty in the refrigerant inlet region was 47.2 W, i.e., 13% higher than in this case. In the refrigerant exit region, the heat dissipation rates are higher in the mal-distributed air flow case than for uniform air flow due to the higher air flow rates in this region. The heat dissipation rate in the refrigerant exit region is 15.99 W in the top-most tube of the last pass and 16.03 W in the lower-most tube, while the heat dissipation rate is 14.04 W in the refrigerant exit region for uniform air flow.

It should be noted that, in the parts where the condenser receives low air flow rates, the heat dissipation rate is not drastically affected, as the refrigerant-to-air temperature difference is higher in these regions. However, the heat dissipation in the parts of the condenser having lower refrigerant-to-air temperature difference was enhanced due to higher air flow rates. Thus a negative air flow mal-distribution tends to neutralize the imbalance in the heat dissipation rates in various parts of the condenser. This results in better condenser performance than the uniform air flow case. In the uniform air flow case, a condenser of length 0.89 m was required to achieve the design heat duty, while a tube length of 0.88 m was found to be sufficient to deliver the design heat duty in the mal-distributed case with air flow mal-distribution of $\phi = -0.3$. The

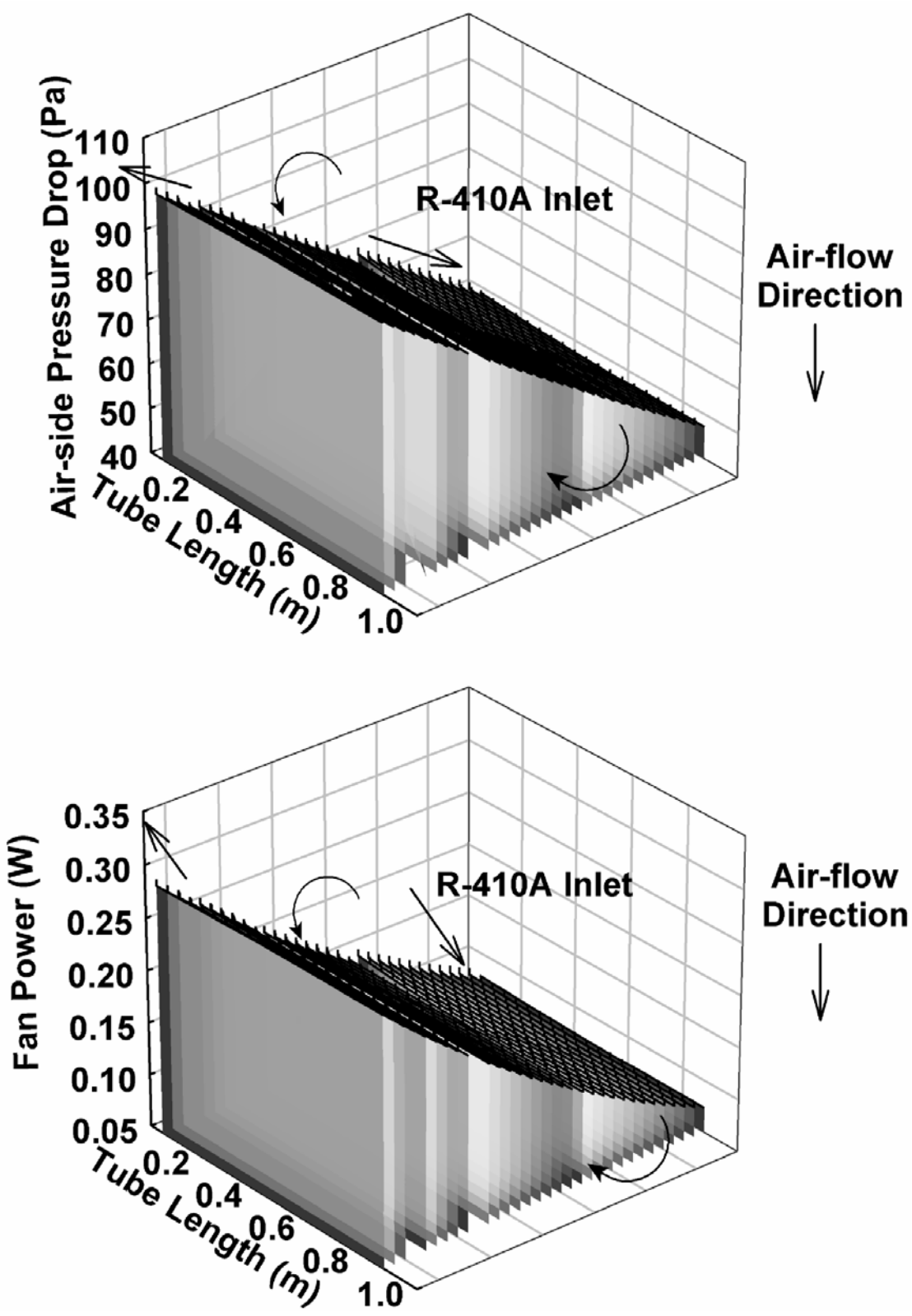

Figure 4. 6 Effect of Negative Air Flow Mal-distribution on Air-side pressure drop and Fan Power

corresponding condenser masses are 2.54 kg for the uniform air flow case, and 2.52 kg for the mal-distributed air flow case.

Figure 4.6 shows the variation in the air-side pressure drop and fan power along the condenser length. We see that both the air-side pressure drop and the fan power required are higher at regions of higher air flow rate. The air-side pressure drop at the inlet to the top-most tube is 48.73 Pa, while it is 99.93 Pa at the corresponding position in the lower-most tube. The fan power per segment at the inlet to the top-most tube is 0.078 W, while it is 0.290 W at the corresponding location in the bottom-most tube. The total fan power required for this case is 108.5 W, while that for the uniform air flow case is 103.1 W.

4.5 Effect of Positive Air Flow Mal-distribution on Condenser Performance

Figure 4.7 and 4.8 show the variation of the tube-side, air-side and overall heat transfer coefficients and heat duty along the condenser length for an air flow mal-distribution of $\phi = 0.3$. Thus, the air flow rate is 30% higher at the top (refrigerant inlet region) and 30% lower at the bottom (refrigerant outlet region) of the condenser. The air velocity is 5.16 m/s at the top of the condenser and 2.78 m/s at the bottom.

The air-side heat transfer coefficient steadily decreases from the top-most tube to the bottom-most tube in the condenser, due to reduced air flow rates. The air-side heat transfer coefficient is 251.3 W/m^2K at the refrigerant inlet region of the top-most tube, and 181.7 W/m^2K at the corresponding position on the lower-most tube (refrigerant exit region). The variation of air-side heat transfer coefficients within each refrigerant

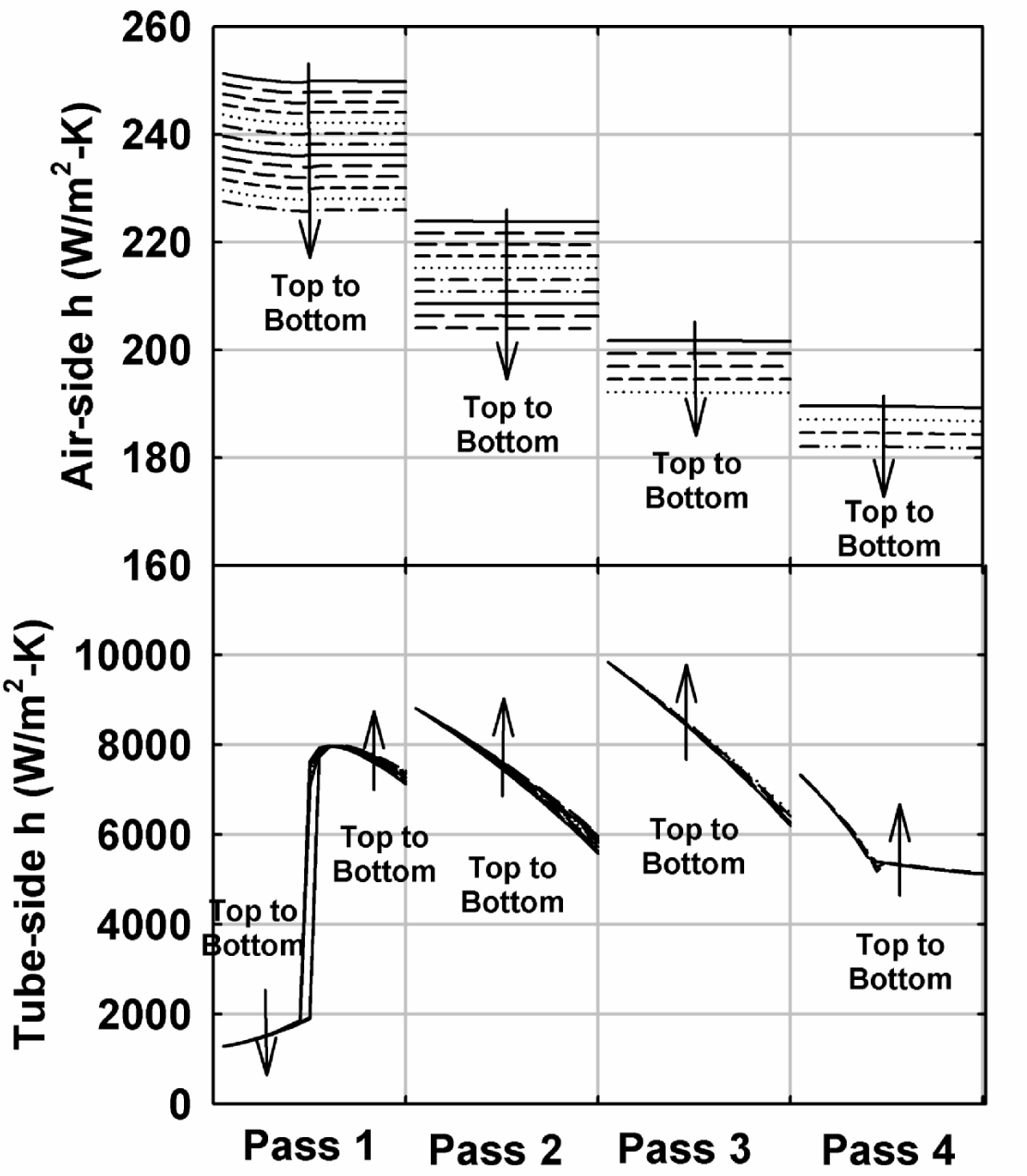

Figure 4. 7 Effect of Positive Air Flow Maldistribution on Air-side and Tube-side h

tube is similar to the variation in the uniform air flow case, i.e it is fairly constant.

The effect of air flow mal-distribution is less pronounced on the variation of tube-side heat transfer coefficient than that on the air-side heat transfer coefficient. The nature of the tube-side heat transfer coefficient variation in any given refrigerant tube is similar

to the uniform air flow case. However unlike for uniform air flow distribution, here the tube-side heat transfer coefficient in the upper tubes in any pass is slightly lower than those in the lower tubes, in the two-phase and the subcooled region. At the refrigerant exit, the tube-side heat transfer coefficient in the top-most tube in the last pass (subcooled region) is 5120.7 W/m^2K, while the tube-side heat transfer coefficient is 5138.4 W/m^2K in the lower-most tube in the last pass. This is because the refrigerant temperature is slightly lower in the upper tubes, due to higher heat dissipation as a result of higher air flow rates over these tubes. In the two-phase region, the tube-side heat transfer coefficients are slightly lower in the upper tubes because due to the higher heat dissipation rates, the refrigerant quality is slightly lower in the upper tubes with the correspondingly lower h. At the exit to the first pass, the refrigerant is in the two-phase region and the tube-side heat transfer coefficient at the top-most tube in the first pass is 7130.6 W/m^2K ($x = 0.65$), while at the lower-most tube in the same pass it is 7410.9 W/m^2K ($x = 0.72$). However, in the superheated region, the tube-side heat transfer coefficient is found to increase slightly from the top row to the bottom row in the pass because the mean refrigerant temperature is lower for the lower tubes due to higher airflow. The tube-side heat transfer coefficient in the top-most tube at the refrigerant inlet region is 1283.4 W/m^2K (superheated), while it is 1282.4 W/m^2K (superheated) for the lower-most tube in that pass. Also, the transition from superheated to two-phase, and two-phase to subcooled regions occurs slightly earlier in the upper tubes of a pass, due to higher heat dissipation rates in them. This can also be seen in Figure 4.7.

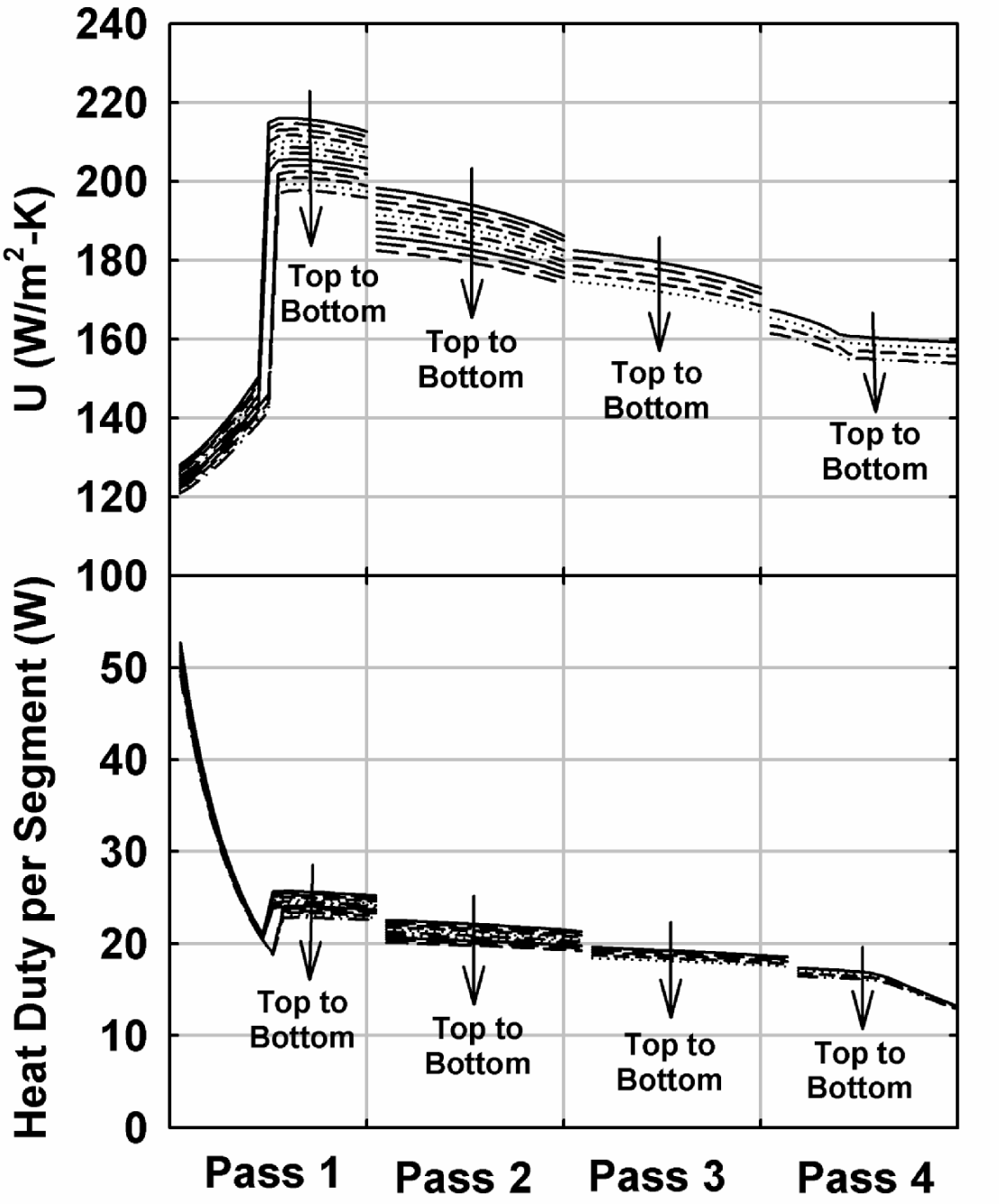

Figure 4. 8 Effect of Positive Air Flow Mal-distribution on Overall U and Heat Duty

For each tube, the air-side heat transfer coefficient is fairly constant, while the tube-side heat transfer coefficient varies to a larger extent as explained above. Hence along the tube, the nature of the variation of the overall heat transfer coefficient is similar to that of

the tube-side heat transfer coefficient. However, among different tubes, the variation in the air-side heat transfer coefficient being the significant resistance has a pronounced effect on the overall heat transfer coefficient. For tubes in the same pass, the overall heat transfer coefficient is higher in the upper tubes, due to higher air-side heat transfer coefficients. At the inlet to the first pass, the overall heat transfer coefficient is 128.1 W/m^2K for the top-most tube in the pass, while it is 121.6 W/m^2K for the lower-most tube in the pass. The highest overall heat transfer coefficient occurs in the top-most tube of the condenser, where the air flow rate, and therefore, the air-side heat transfer coefficient is maximum, even though the corresponding refrigerant heat transfer coefficient is only characteristic of single-phase vapor flow.

The variation of the segment heat duty along the condenser length is shown in Figure 4.8. The nature of the heat duty variation along a tube is similar to that in the case of uniform air flow. However within any pass, the heat dissipation is higher in the upper tubes of a pass, due to higher air flow rates. At the refrigerant inlet region in the first pass, the heat dissipation per segment is 52.7 W for the top-most tube, while it is 49.2 W for the lower-most tube in the first pass. As the overall heat transfer coefficient, the air flow rate and the refrigerant-to-air temperature difference are highest in the refrigerant inlet region of the condenser, the heat dissipation is highest in this region. Also, this heat dissipation in the refrigerant inlet region is higher than that in the uniform air flow case, due to the higher air flow rate in this case. In the uniform air flow case, the heat duty in the refrigerant inlet region was 47.2 W i.e., 23% lower than in this case. In the refrigerant exit region, the heat dissipation rates are lower in the mal-distributed air flow case than for uniform air flow due to the lower air flow rates in this region. The heat dissipation

rate in the refrigerant exit region is 11.77 W in the top-most tube of the last pass and 11.55 W in the lower-most tube, while the heat dissipation rate is 14.04 W in the refrigerant exit region for uniform air flow.

It should be noted that in the parts where the local heat dissipation rates are higher due to higher refrigerant-to-air temperature difference in the uniform air flow case, the heat dissipation rates are further improved due to higher air flow rates. The heat dissipation in the parts of the condenser having lower refrigerant-to-air temperature difference is further decreased due to lower air flow rates. Thus a positive air flow mal-distribution tends to aggravate the imbalance in the heat dissipation rates in various parts of the condenser. This results in poorer condenser performance than the uniform air flow case. In the uniform air flow case, a condenser of length 0.89 m was required to achieve the design heat duty, while a tube length of 0.92 m was required to deliver the design heat duty in the mal-distributed case with air flow mal-distribution of $\phi = 0.3$. The corresponding condenser masses are 2.54 kg for the uniform airflow case and 2.62 kg for the mal-distributed air flow case.

Figure 4.9 shows the variation in the air-side pressure drop and fan power along the condenser length. We see that both the air-side pressure drop and the fan power required are higher at regions of higher air flow rate. The air-side pressure drop at the inlet to the top-most tube is 96.92 Pa, while it is 44.91 Pa at the corresponding position in the lower-most tube. The fan power per segment at the inlet to the top-most tube is 0.285 W, while it is 0.070 W at the corresponding location in the bottom-most tube. The total

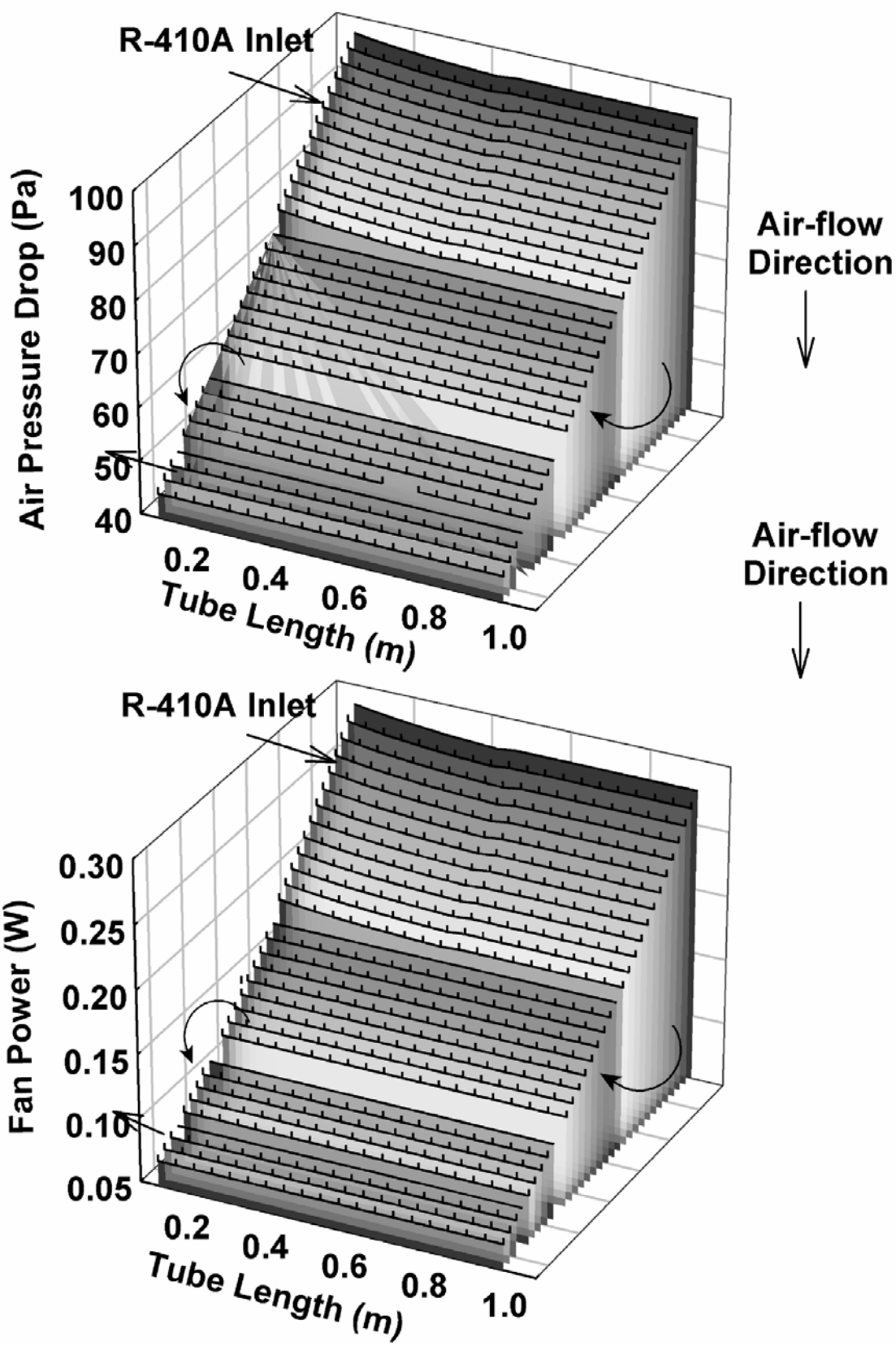

Figure 4. 9 Effect of Positive Air Flow Mal-distribution on Air-side Pressure Drop and Fan Power

fan power required for this case is 103.4 W, while it is 103.1 W for the uniform air flow case and 108.5 W for an air flow maldistribution of degree $\phi = -0.3$.

4.6 Summary of Condenser Performance for Mal-distributed Air Flow Conditions

Similar to the analyses described previously, the condenser performance was analyzed for air flow mal-distributions ranging from $-0.5 < \phi < 0.5$. In all these cases, the average air flow rate was always maintained constant at 1.62 kg/s (3000 cfm). The results of these analyses are plotted in Figure 4.10.

Starting with uniform air flow case, as the degree of air flow mal-distribution is made more negative the condenser performance improves initially and the condenser mass required to transfer the design heat duty of 14.5 kW decreases. The condenser mass is minimum for an air flow mal-distribution of $\phi = -0.2$. As the air flow mal-distribution is made further negative, the condenser performance drops and the condenser mass required to deliver the design heat duty increases. This is because for very adverse negative air flow mal-distributions, the air-side heat transfer coefficients near the top of the condenser are so small that they significantly affect the overall heat dissipation, and hence lower the condenser performance.

As the condenser performance improves, the condenser length required to deliver the design heat duty goes down. This reduces the condenser face area which results in an increase in the face air velocity. Thus the face air velocity is maximum (4.00 m/s) for an air flow mal-distribution of -0.2 and is lower for other cases with larger condenser lengths. A higher face velocity also results in higher air-side pressure drops, which causes an increase in the fan power required. Figure 4.10 also shows the face air velocity and the

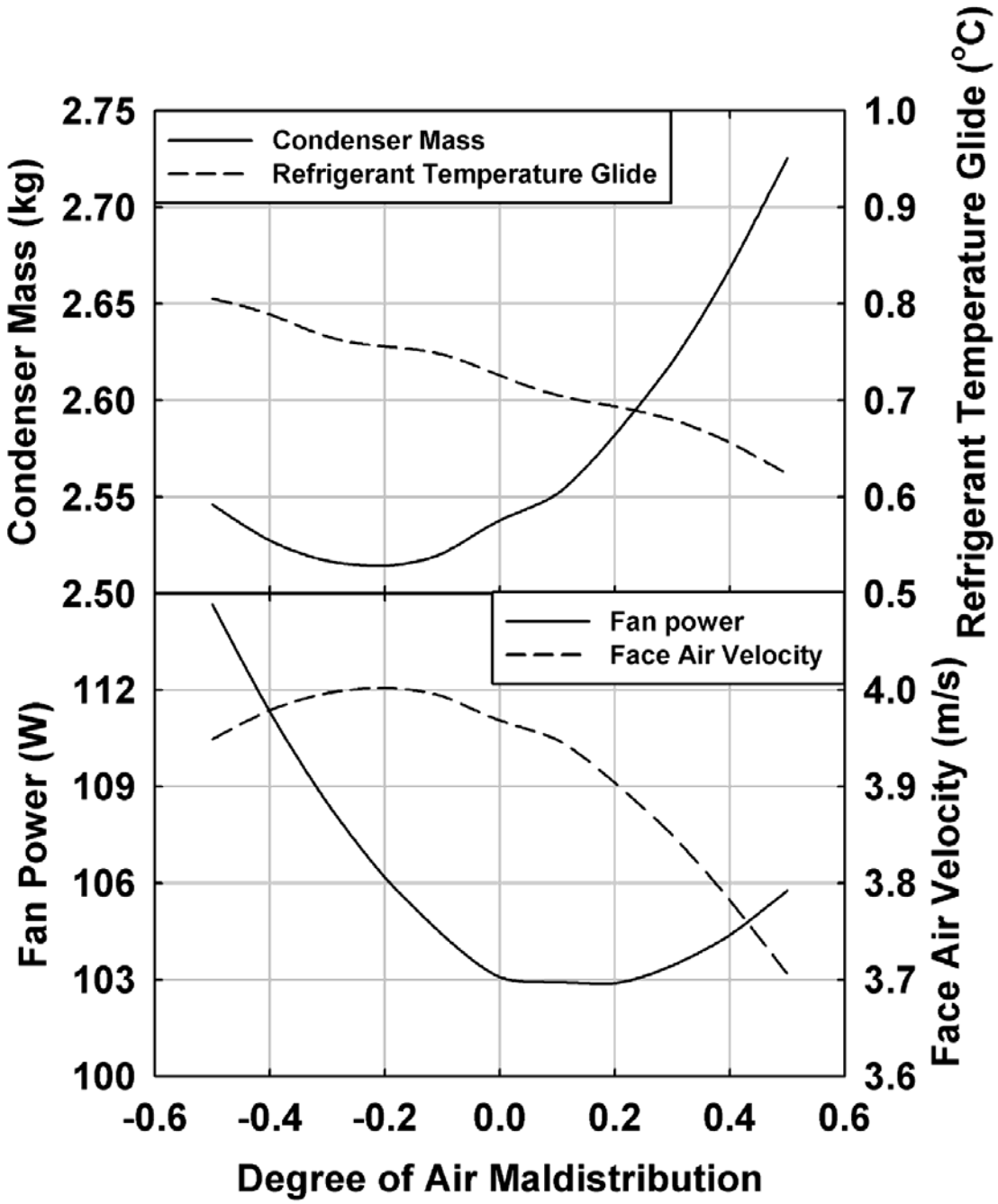

Figure 4. 10 Effect of Air Flow Mal-distribution

fan power required for various air flow mal-distributions. The fan power decreases from 114.6 W for ϕ = -0.5 to 105.8 W for ϕ = 0.5. Also, the refrigerant temperature glide is seen to decrease with more positive air flow mal-distributions. The refrigerant

temperature glide is 0.81^{o}C for an air flow mal-distribution of degree -0.5, 0.73^{o}C for uniform air flow and 0.62^{o}C for an air flow mal-distribution of 0.5.

The results obtained from the present analysis are quite similar to the results of air flow mal-distribution studies conducted earlier by various researchers for conventional heat exchanger geometries. For example, Lee *et al.* (2003) numerically found the maximum reduction in the heat transfer rate due to air flow mal-distribution to be 6% for finned-tube evaporators (for a two-dimensional concave air velocity distribution with about 50% deviation from the mean value). Rabas (1987) found the maximum deviation in the condenser performance was 7% due to air flow mal-distribution (for a parabolic air flow mal-distribution with 50% deviation from the mean air velocity). Chiou (1983) estimated a 5-10% decrease in heat transfer rate due to air flow mal-distribution in automobile air-conditioning condensers. In the present study, the maximum reduction in the average heat transfer rate due to air flow mal-distribution was found to be 7% (for ϕ = 0.5).

Chapter 5

CONDENSER DESIGN FOR MAL-DISTRIBUTED AIR FLOWS

5.1 Need for Design Modifications for Mal-distributed Air Flows

In the previous chapter, it was seen that the condenser performance drops for certain air flow mal-distributions. As the air flows available to condensers in real-life applications are mal-distributed, it is necessary to overcome this drop in performance through appropriate modifications in condenser design. One solution is to simply increase the condenser length by adding a factor of safety to the design calculations. This however increases the material and refrigerant costs and defeats the entire purpose of the optimization procedure. Another method is to have non-uniform air-side geometry such as a non-uniform fin density and fin height so that the condenser performance is improved. This method to further improve condenser performance is discussed in the present chapter.

5.2 Fin Density Non-uniformities Considered

The fin density was varied linearly for every row keeping the mean fin density constant at 6 fins per cm. However, it should be noted that the structural strength of the condenser could decrease with extremely low fin densities; hence practical designs should have a lower limit on the fin density at any point in the condenser. The fin density deviation was defined as,

$$f_{dev} = \frac{fd_{top} - fd_{mean}}{fd_{mean}} \qquad (60)$$

Thus for a positive fin density deviation, the fin density is maximum at the top and minimum at the bottom, while for a negative fin density deviation the fin density is minimum at the top and maximum at the bottom. For a fin density deviation of -0.5, the fin density is 50% lower at the top (refrigerant inlet region) of the condenser and 50% higher at the bottom, that is, 3 fins per cm at the top and 9 fins per cm at the bottom.

5.3 Condenser Performance for a Non-uniform Fin Density

It is instructive to study the variation in heat transfer coefficients under non-uniform fin densities to understand the condenser performance in that case. Figure 5.1 and 5.2 show the variation of the tube-side, air-side and overall heat transfer coefficients and the heat duty for a fin density deviation of 0.2 under an air flow mal-distribution of degree 0.3. In this case the fin density at the top of the condenser is 7.2 fins per cm, while the fin density at the bottom of the condenser is 4.8 fins per cm. The average fin density is maintained at a constant value of 6 fins per cm. The face air velocity is 5.16 m/s at the top of the condenser and 2.78 m/s at the bottom. (The air velocity through the heat exchanger will be different in this case than the uniform fin density case with mal-distributed air flow due to the different fin density. But face velocity is the same because it is computed upstream of the heat exchanger core and only depends on the face area)

The air-side heat transfer coefficient steadily decreases from the top-most tube to the bottom-most tube in the condenser, due to reduced air flow rates and reduced fin

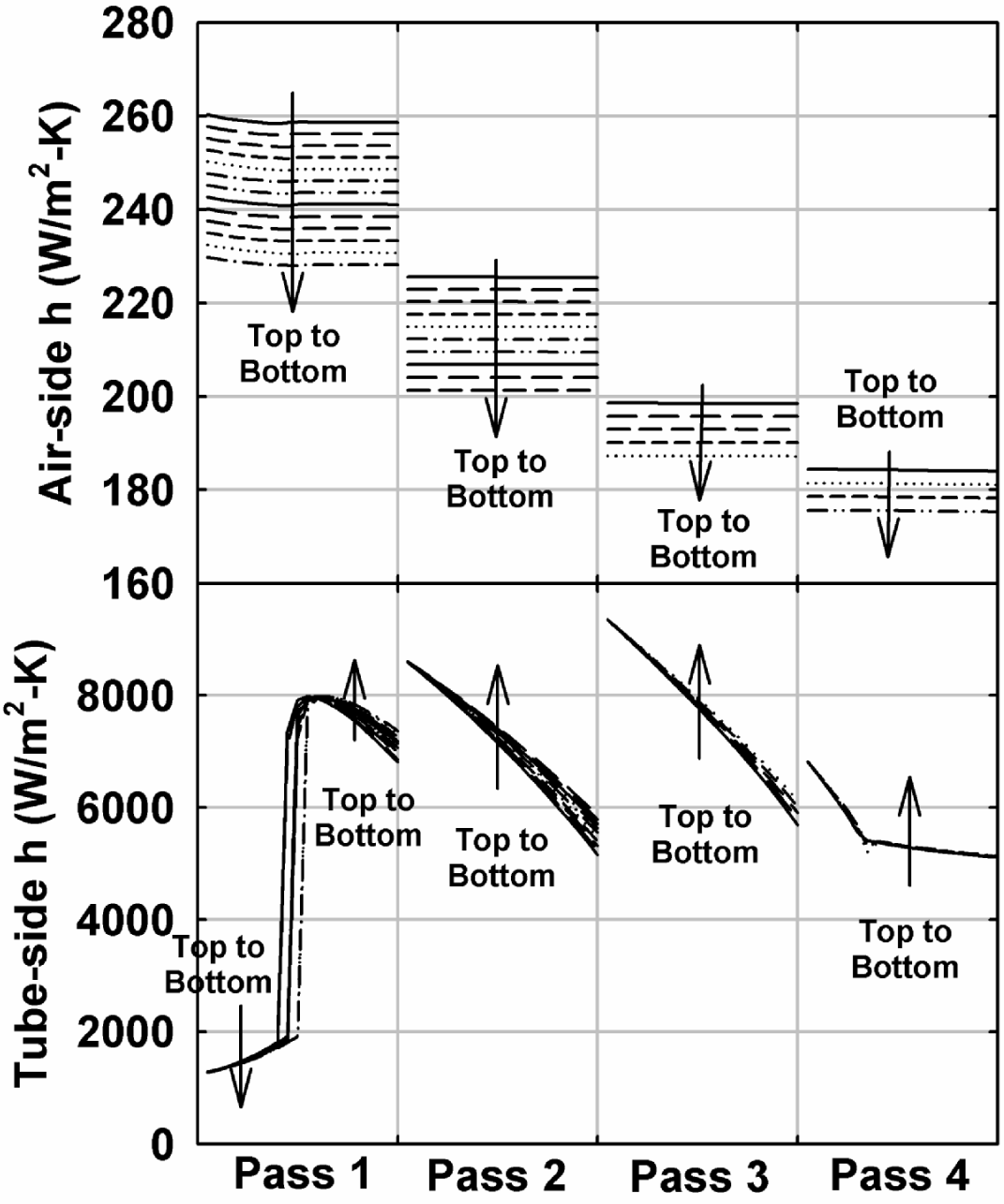

Figure 5.1 Effect of Fin Density Non-uniformity on Air-side and Tube-side h densities. The air-side heat transfer coefficient at the refrigerant inlet region of the top-most tube is 260.3 W/m^{2}K, while the air-side heat transfer coefficient at the corresponding position on the lower-most tube (refrigerant exit region) is 175.3 W/m^{2}K.

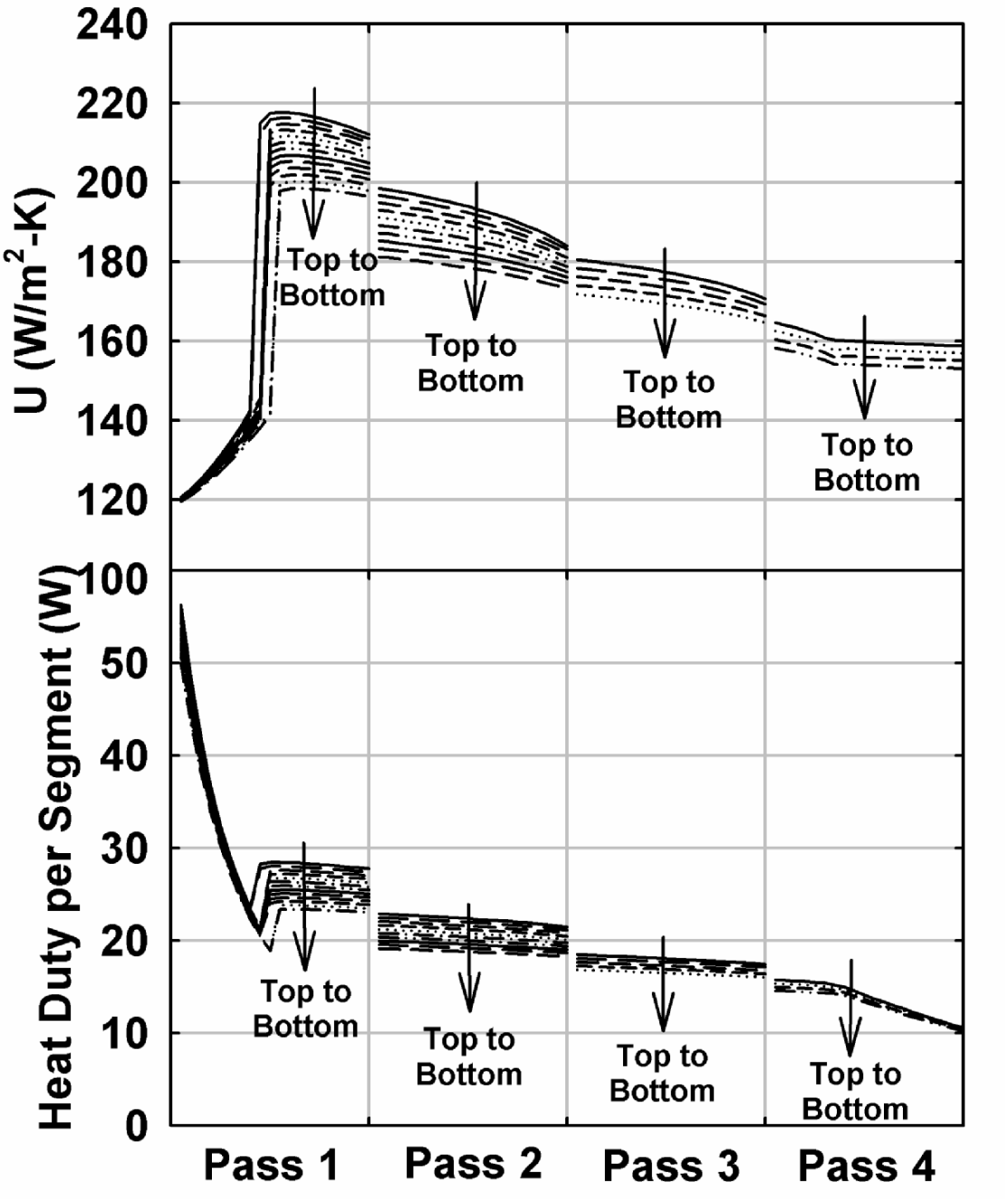

Figure 5.2 Effect of Fin Density Non-uniformity on Overall U and Heat Duty

The variation of air-side heat transfer coefficients along each refrigerant tube is similar to the variation in the uniform air flow case, that is, it is fairly constant. The disparity in the air-side heat transfer coefficients in the top and bottom extremes of the condenser is even

more than that in the case of uniform fin densities under the same mal-distributed air flow. This is because in addition to having a higher air flow rate, the upper tubes also have a higher fin density, thus further enhancing the air-side heat transfer coefficients at the top.

As in the case of uniform fin densities under mal-distributed air flow conditions, the effect of fin density variation is less pronounced on the variation of tube-side heat transfer coefficient than that on the air-side heat transfer coefficient. The nature of the tube-side heat transfer coefficient variation in any given refrigerant tube is similar to the uniform fin density case with an air flow mal-distribution of degree 0.3. However, in this case, the difference between the tube-side heat transfer coefficients at the top-most and lower-most tubes in the same pass is more than that in the case of uniform fin density. This is because, in this case the heat dissipation is even higher in the upper tubes because in addition to a higher air flow rate, the upper tubes also have a higher fin density leading to a higher heat dissipation from the upper tubes. At the refrigerant exit (subcooled region), the tube-side heat transfer coefficient in the top-most tube in the last pass is 5111.7 W/m^2K, while the tube-side heat transfer coefficient is 5134.7 W/m^2K in the lower-most tube in the last pass. This is because the refrigerant temperature is slightly lower in the upper tubes, due to higher heat dissipation as a result of higher air flow rates and higher fin densities over these tubes. In the two-phase region, the tube-side heat transfer coefficients are slightly lower in the upper tubes because due to higher heat dissipation rates, the refrigerant quality is slightly lower in the upper tubes. At the exit to the first pass, the refrigerant is in the two-phase region and the tube-side heat transfer coefficient at the top-most tube in the first pass is 6813.9 W/m^2K ($x = 0.60$), while at the

lower-most tube in the same pass is 7365.1 W/m^{2}K (x = 0.71). However, in the superheated region, the tube-side heat transfer coefficient is found to increase with a decrease in refrigerant temperature. As a result, the tube-side heat transfer coefficients are found to be higher for the upper tubes in a pass. The tube-side heat transfer coefficient in the top-most tube at the refrigerant inlet region is 1284.6 W/m^{2}K (superheated), while the tube-side heat transfer coefficient is 1282.5 W/m^{2}K (superheated) for the lower-most tube in that pass. Also, as in the case of uniform fin densities under mal-distributed air flows of degree 0.3, the transition from superheated to two-phase and two-phase to subcooled occur slightly earlier in the upper tubes of a pass, due to higher heat dissipation rates in them.

Along each tube, the air-side heat transfer coefficient is fairly constant, while the tube-side heat transfer coefficient varies to a larger extent. Hence within a tube, the nature of the variation of the overall heat transfer coefficient is similar to that of the tube-side heat transfer coefficient. However, among different tubes, the variation in the air-side heat transfer coefficient being the significant resistance has a pronounced effect on the overall heat transfer coefficient. For tubes in the same pass, the overall heat transfer coefficient is higher in the upper tubes, due to higher air-side heat transfer coefficients. At the inlet to the first pass, the overall heat transfer coefficient is 120.6 W/m^{2}K for the top-most tube in the pass, while it is 119.5 W/m^{2}K for the lower-most tube in the pass. The highest overall heat transfer coefficient occurs in the top-most tube of the condenser, where the air flow rate and the air-side heat transfer coefficient is maximum.

The variation of the segment heat duty along the condenser length is shown in Figure 5.2. The nature of the heat duty variation within a tube is similar to that in the case

of uniform fin densities. However within any pass, the difference between the heat dissipation rates of the upper and lower tubes is greater as in addition to a higher air flow rate, the upper tubes also have a higher fin density (providing greater surface area), thus further enhancing the heat dissipation in the upper tubes of a pass. At the refrigerant inlet region in the first pass, the heat dissipation per segment is 56.2 W for the top-most tube, while it is 50.0 W for the lower-most tube in the first pass. As the overall heat transfer coefficient, the air flow rate and the refrigerant-to-air temperature difference are the highest in the refrigerant inlet region of the condenser, the heat dissipation is highest here. Also, this heat dissipation in the refrigerant inlet region is higher than that in the uniform fin density case, due to higher fin density and the larger heat transfer coefficient due to higher air flow rates and smaller air-side cross-sectional area, which further enhances the heat transfer coefficient. In the uniform fin density case, the heat duties in the refrigerant inlet region were 52.7 W and 49.2 W, respectively, for the upper and lower tubes in this pass. In the refrigerant exit region, the heat dissipation rates are lower in the non-uniform fin density case than the uniform fin density case due to lower fin densities. The heat dissipation rate in the refrigerant exit region is 10.54 W in the top-most tube of the last pass and 10.20 W in the lower-most tube for non-uniform fin densities, while the heat dissipation rate is 11.77 W and 11.55 W in the upper and lower tubes in the refrigerant exit region for uniform fin densities (with the same mal-distributed air flow).

Though the disparity in the air-side heat transfer coefficient is higher in the case of non-uniform fin density, the average air-side heat transfer coefficient is found to be higher in this case. The average air-side heat transfer coefficient is 210.7 W/m^2K in the

case of uniform density, while it is 211.3 W/m^2K in the case of fin density deviation of -0.2 under an air flow mal-distribution of $\phi = 0.3$. As a result, the non-uniform fin density case in seen to perform better than the uniform fin density case. The condenser length required to deliver the design heat duty in the case of a uniform fin density is 0.92 m, while a length of 0.91 m is found to be sufficient in the case of non-uniform fin density with $f_{dev} = 0.2$. The corresponding condenser masses are 2.62 kg and 2.61 kg for the uniform and non-uniform fin density cases, respectively.

Figure 5.3 shows the variation in the air-side pressure drop and fan power along the condenser length. It can be seen that both the air-side pressure drop and the fan power required are higher at regions of higher air flow rate and higher fin densities. The air-side pressure drop at the inlet to the top-most tube is 135.4 Pa, while it is 30.0 Pa at the corresponding position in the lower-most tube. The fan power per segment at the inlet to the top-most tube is 0.399 W, while it is 0.047 W at the corresponding location in the bottom-most tube. The total fan power required in this case is 113.6 W, while that for a uniform fin density distribution under the same air flow condition is 103.4 W.

Figure 5.4 summarizes the condenser performance for various fin density non-uniformities ranging from -0.7 to 0.7 under an air flow with mal-distribution of degree 0.3. The condenser mass is found to be minimum for a fin density deviation of 0.2. Thus a fin density deviation of 0.2 is chosen as the optimum fin density configuration. This configuration requires a condenser mass of 2.61 kg, with a refrigerant temperature glide of 0.63^oC and fan power requirement of 113.6 W.

As the condenser length is decreased, the condenser face area decreases, resulting in an increase in the air face velocity. (It should be noted that the corresponding core

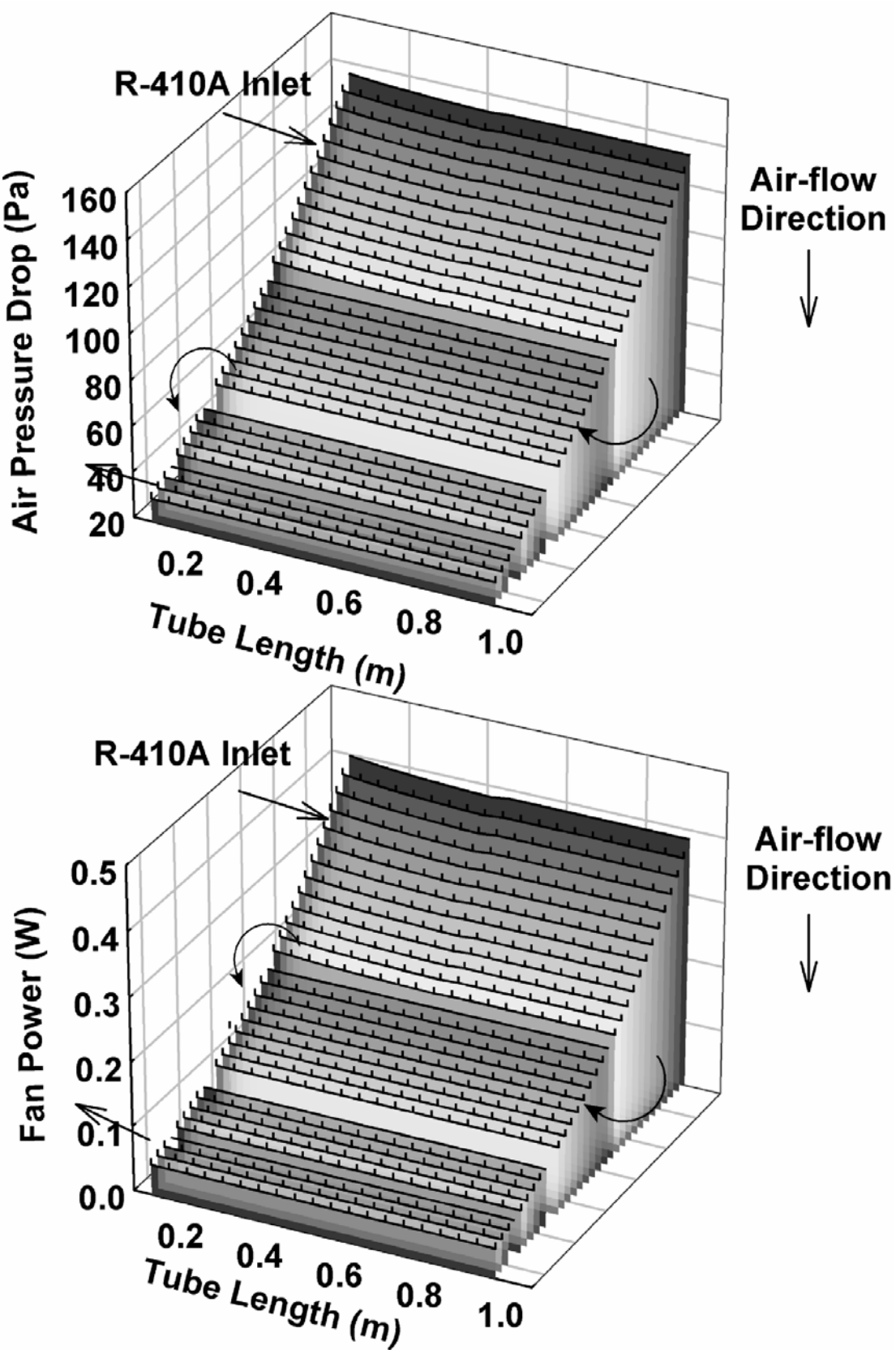

Figure 5. 3 Effect of Fin Density Non-uniformity on Air-side Pressure Drop and Fan Power

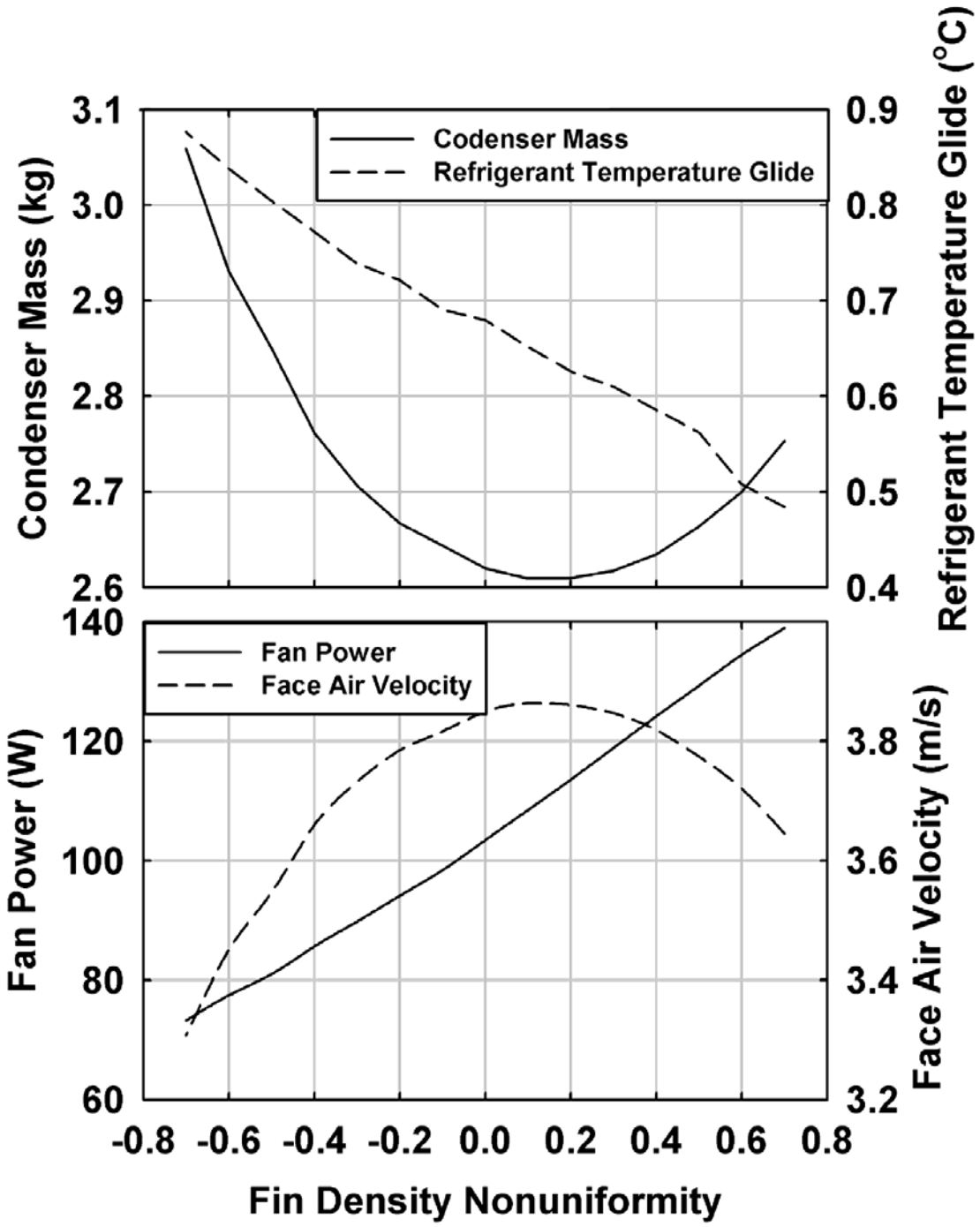

Figure 5. 4 Effect of Fin Density Non-uniformity

velocities vary across the condenser due to mal-distribution as well as the variation of fin densities). Hence the average face air velocity is maximum at 3.86 m/s for a fin non-uniformity of 0.2. The fan power however constantly increases as the fin density non-uniformity is made more positive. This is because at highly positive fin density non-

uniformities, though the face velocities are lower, the fan power is high due to the very high pressure drop combined with a high air flow rate at the top of the condenser. For a fin density distribution with f_{dev} = 0.7 and air flow distribution with ϕ = 0.3, the local face air velocity at the top of the condenser is highest at 5.12 m/s and the fin density is maximum at 10 fins per cm, resulting in extremely high air-side pressure drop and fan power. The air-side pressure drop and fan power per segment in the refrigerant inlet region of the top tube in this case is 240.9 Pa and 0.712 W, respectively, while they are 5.1 Pa and 0.008 W in the corresponding position in the lower-most tube. In the case of a negative fin density non-uniformity of f_{dev} = -0.7, the face air velocity is still maximum at the top at 5.12 m/s, but the fin density is lowest at this point at 2 fins/cm. Similarly, the fin density is maximum at 10 fins/cm at the bottom, where the local face air velocity is minimum at 3.03 m/s. Hence a negative fin density distribution tends to negate the effect of air flow maldistribution, resulting in a lower fan power. The fan power required is 138.9 W for a fin non-uniformity of 0.7 and it reduces to 73.3 W for a fin non-uniformity of -0.7.

5.4 Fin Height Non-uniformities considered

To further investigate additional modifications to the air-side geometry to address mal-distributed air flows, variations in fin height were also considered. But it should be noted that non-uniform fin heights might introduce additional complications in condenser assembly, particularly in the design of tube-side headers. Also, the introduction of multiple sizes of fins in the heat exchanger could lead to additional tooling and capital costs. These issues must be considered before variable fin heights are implemented.

For the purpose of this study, keeping the above practical considerations in mind, the fin height was varied linearly for every row keeping the mean fin height constant at 11 mm. The fin height deviation was defined as,

$$ch_{dev} = \frac{ch_{top} - ch_{mean}}{ch_{mean}} \quad (61)$$

Thus for a positive fin height deviation, the fin height is maximum at the top and minimum at the bottom, while for a negative fin height deviation the fin height is minimum at the top and maximum at the bottom. For a fin height deviation of 0.5, the fin height is 50% higher at the top (refrigerant inlet region) of the condenser, and 50% lower at the bottom, that is, 16.5 mm at the top and 5.5 mm at the bottom.

5.5 Condenser Performance for a Non-uniform Fin Height

Figure 5.5 and 5.6 show the variation of the tube-side, air-side and overall heat transfer coefficients and heat duty for a fin height deviation of 0.1, *for a fin density deviation 0.2 (i.e. the optimum fin density distribution) under an air flow mal-distribution of degree 0.3*. In this case, the fin height at the top of the condenser is 12.1 mm, while the fin height at the bottom of the condenser is 9.9 mm. The average fin height is maintained at a constant value of 11 mm. The face air velocity is 5.16 m/s at the top of the condenser and 2.78 m/s at the bottom.

The air-side heat transfer coefficient steadily decreases from the top-most tube to the bottom-most tube in the condenser, due to reduced air flow rates, reduced fin densities and reduced fin height. The air-side heat transfer coefficient at the refrigerant inlet region of the top-most tube is 251.5 W/m^2K, while the air-side heat transfer

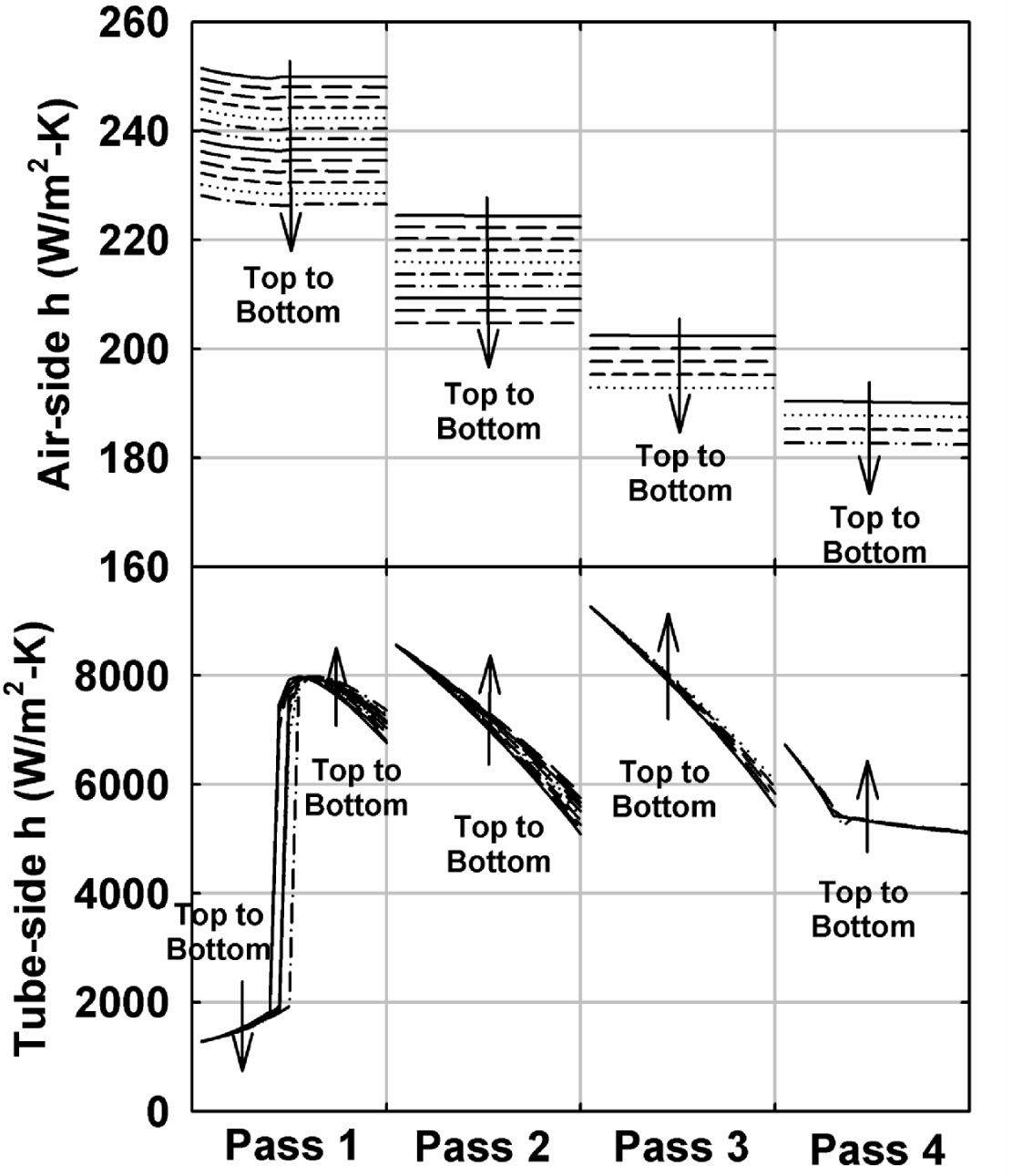

Figure 5. 5 Effect of Fin Height Deviation on Air-side and Tube-side h

coefficient at the corresponding position on the lower-most tube (refrigerant exit region) is 182.4 W/m^{2}K. The variation of air-side heat transfer coefficients within each

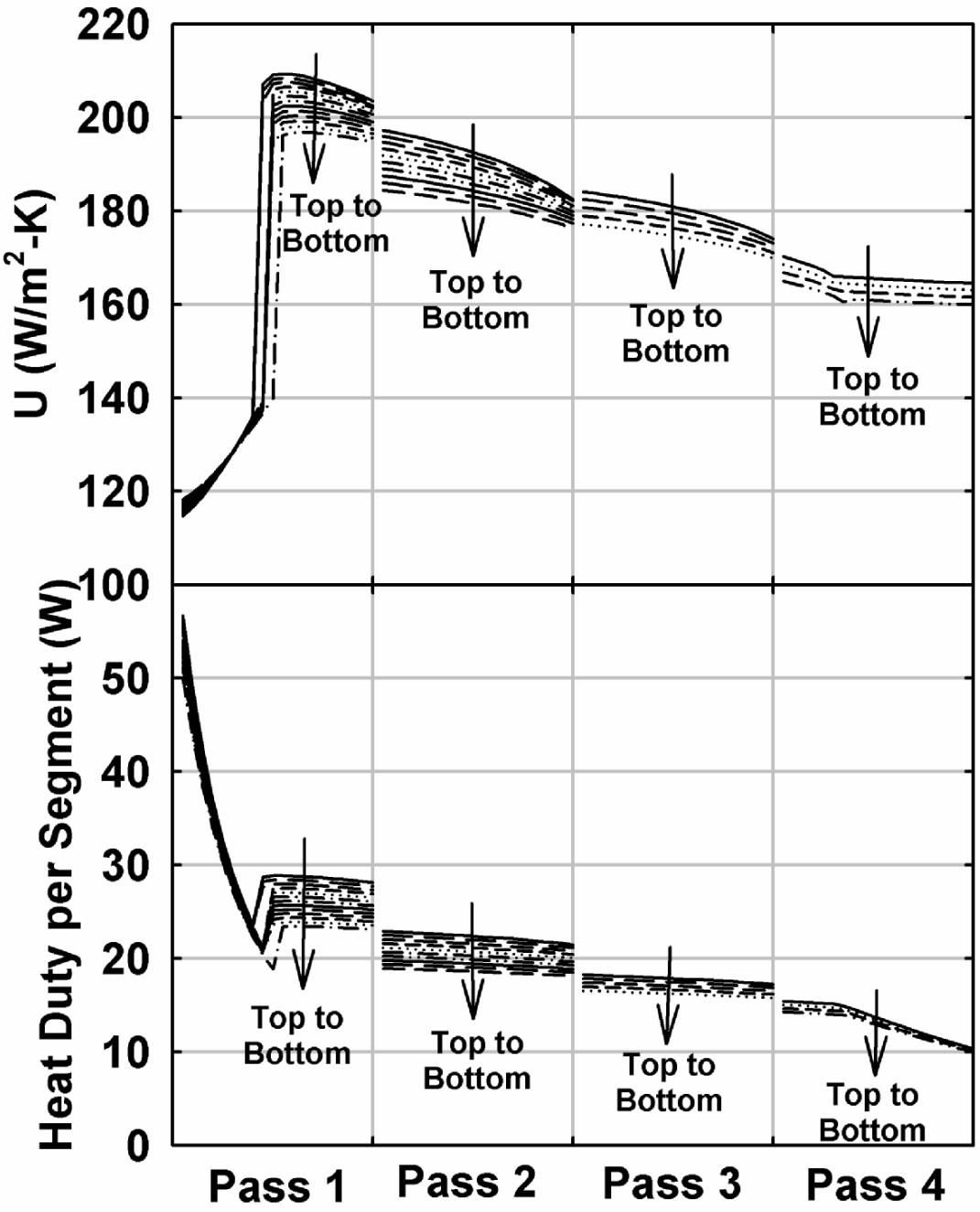

Figure 5. 6 Effect of Fin Height Deviation on Overall U and Heat Duty

refrigerant tube is similar to the variation in the uniform fin height case, that is, it is fairly constant. The disparity in the air-side heat transfer coefficients in the top and bottom extremes of the condenser is lesser than that in the case of uniform fin height under the

same mal-distributed air flow. For example, in this case the air-side heat transfer coefficient at the refrigerant inlet at the top-most tube is 251.5 W/m^2-K, while it is 182.7 W/m^2-K at the corresponding point on the bottom-most tube. For the uniform fin height case, the air-side heat transfer coefficient at the refrigerant inlet at the top-most tube is 260.3 W/m^2-K, while it is 175.6 W/m^2-K at the corresponding point on the lower-most tube. This is because the fin height is higher at the region receiving higher air flow, which reduces the air velocity. The net effect is to reduce the disparity in the air-side heat transfer coefficient between the top and bottom-most tubes. Thus, while the fin surface area is higher in the top portion of the condenser (fin surface area per unit length of tube for the top-most tube is 0.339 m^2 for ch_{dev} = 0.1, while it is 0.307 m^2 for uniform fin height distribution), the air-side heat transfer coefficient is lower.

As in the case of uniform fin height under mal-distributed air flow conditions, the effect of fin height variation is less pronounced on the variation of tube-side heat transfer coefficient than that on the air-side heat transfer coefficient. The nature of the tube-side heat transfer coefficient variation in any given refrigerant tube is similar to the uniform fin height case with an air flow mal-distribution of degree 0.3 and fin density deviation of 0.2. However, in this case, the difference between the tube-side heat transfer coefficients between the top-most and lower-most tubes in the same pass is more than that in the case of uniform fin height. This is because, in this case the heat dissipation is even higher in the upper tubes, as in addition to a higher air flow rate and higher fin density, the upper tubes also have a higher fin height leading to a higher heat dissipation from the upper tubes. It is to be noted that higher fin heights also reduce the local air velocity which tends to lower the air-side heat transfer coefficient. However in the present case, as the

fin height is increased, the enhancing effect due to the increase in heat transfer area dominates, thus increasing the heat dissipation for a higher fin height. At the refrigerant exit, the tube-side heat transfer coefficient in the top-most tube in the last pass is 5111 W/m^2K (subcooled), while the tube-side heat transfer coefficient is 5134 W/m^2K (subcooled) in the lower-most tube in the last pass. This is because the refrigerant temperature is slightly lower in the upper tubes, due to the higher heat dissipation as a result of higher air flow rates, larger fin densities and larger fin heights over these tubes. In the two-phase region, the tube-side heat transfer coefficients are slightly lower in the upper tubes because due to higher heat dissipation rates, the refrigerant quality is slightly lower in the upper tubes. At the exit to the first pass, the refrigerant is in the two-phase region and the tube-side heat transfer coefficient at the top-most tube in the first pass is 6768.8 W/m^2K ($x = 0.59$), while at the lower-most tube in the same pass is 7359.0 W/m^2K ($x = 0.70$). However, in the superheated region, the tube-side heat transfer coefficient is found to increase with a decrease in refrigerant temperature. As a result, the tube-side heat transfer coefficients are found to be higher for the upper tubes in a pass. The tube-side heat transfer coefficient in the top-most tube at the refrigerant inlet region is 1284.8 W/m^2K (superheated), while the tube-side heat transfer coefficient is 1282.6 W/m^2K (superheated) for the lower-most tube in that pass. Also, as in the case of uniform fin height, the transition from superheated to two-phase and two-phase to subcooled regions occur slightly earlier in the upper tubes of a pass, due to the higher heat dissipation rates in them.

Within each tube, the air-side heat transfer coefficient is fairly constant, while the tube-side heat transfer coefficient varies significantly. Hence within a tube, the nature of

the variation of the overall heat transfer coefficient is similar to that of the tube-side heat transfer coefficient. However, among different tubes, the variation in the air-side heat transfer coefficient being the significant resistance has a pronounced effect on the overall heat transfer coefficient. For tubes in the same pass, the overall heat transfer coefficient is higher in the upper tubes, due to higher air-side heat transfer coefficients. At the inlet to the first pass, the overall heat transfer coefficient is 114.7 W/m^2K for the top-most tube in the pass, while it is 118.2 W/m^2K for the lower-most tube in the pass. The highest overall heat transfer coefficient occurs in the top-most tube of the condenser, where the air flow rate and the air-side heat transfer coefficient is maximum.

The variation of the segment heat duty along the condenser length is shown in Figure 5.6. The nature of the heat duty variation within a tube is similar to that in the case of uniform fin height. However within any pass, the difference between the heat dissipation rates of the upper and lower tubes is more as compared to the uniform fin height case, as though the disparity in the air-side heat transfer coefficient distribution is reduced, the effect of increase in the fin area due to increase in fin height dominates. The air-side heat transfer coefficient varies from 251.5 W/m^2-K to 182.7 W/m^2-K for the top-most and bottom-most tubes for $ch_{dev} = 0.1$, while it varies from 260.3 W/m^2-K to 175.6 W/m^2-K in the uniform fin height case. The fin surface area per unit length of tube is 0.339 m^2 for $ch_{dev} = 0.1$, while it is 0.308 m^2 for uniform fin height distribution at the top-most tube. At the refrigerant inlet region in the first pass, the heat dissipation per segment is 56.7 W for the top-most tube, while it is 50.1 W for the lower-most tube in the first pass. As the overall heat transfer coefficient, the air flow rate and the refrigerant-to-air temperature difference are the highest in the refrigerant inlet region of the condenser, the

heat dissipation is highest in this region. Also, this heat dissipation in the refrigerant inlet region is higher than that in the corresponding uniform fin height case, due to higher fin height. In the uniform fin height case, the heat duty in the refrigerant inlet region was 56.2 W and 50.0 W respectively for the upper and lower extreme tubes on the pass. In the refrigerant exit region, the heat dissipation rates are lower in the non-uniform fin height case than uniform fin height case due to lower fin heights. The heat dissipation rate in the refrigerant exit region is 10.34 W in the top-most tube of the last pass and 9.98 W in the lower-most tube for non-uniform fin heights, while it is 10.54 W and 10.20 W in the upper and lower extreme tubes, respectively, in the refrigerant exit region for the corresponding uniform fin height case.

The condenser performance is seen to be slightly better than the corresponding uniform fin height case due to the reduction in disparity in the air-side heat transfer coefficient distribution. The condenser length required to deliver the design heat duty in the case of a uniform fin height is 0.913 m, while a length of 0.912 m is found to be sufficient in the case of non-uniform fin height with deviation 0.1. The corresponding condenser masses are 2.610 kg and 2.608 kg for the uniform and non-uniform fin height cases.

Figure 5.7 shows the variation in the air-side pressure drop and fan power along the condenser length. It can be seen that both the air-side pressure drop and the fan power

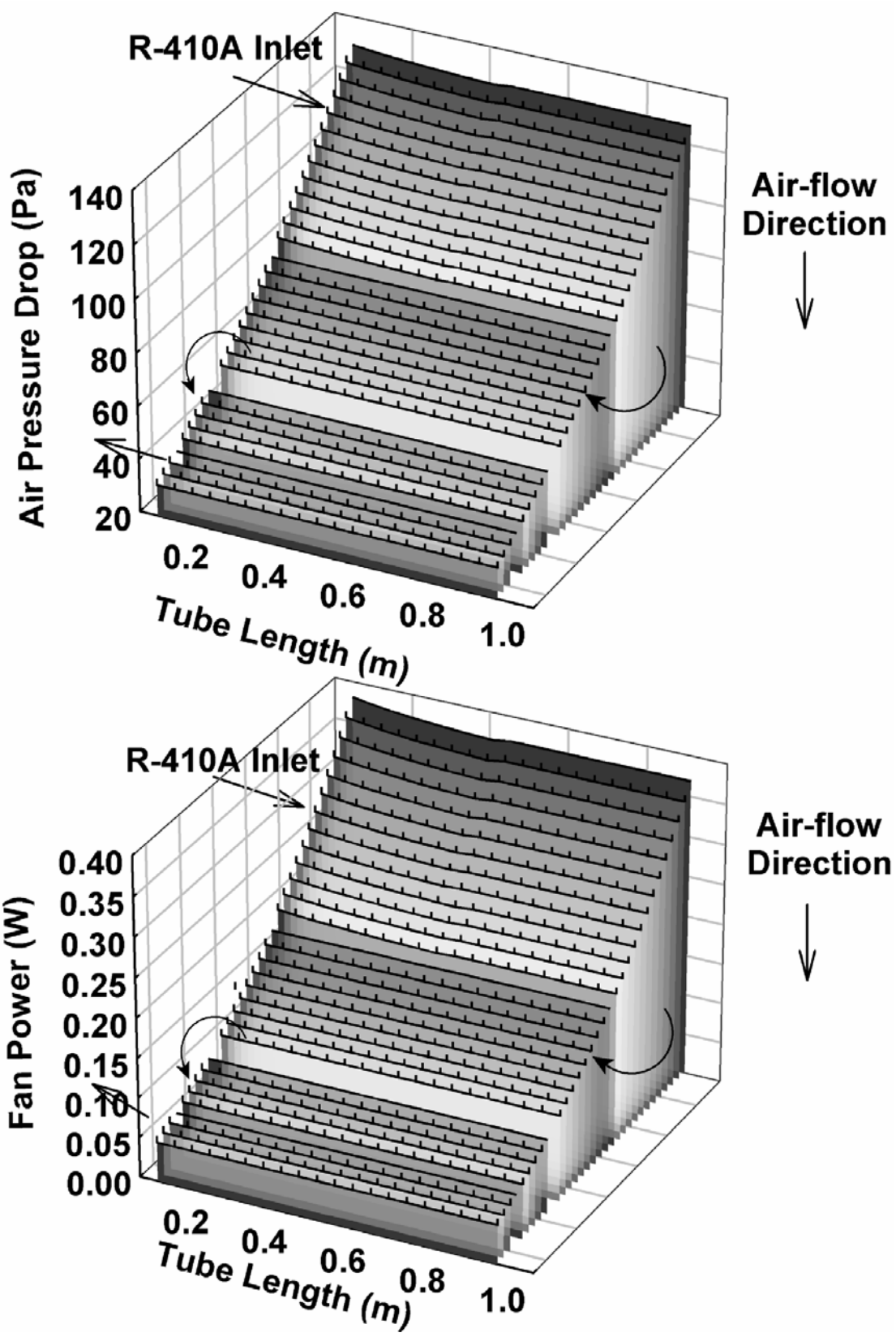

Figure 5. 7 Effect of Fin Height Deviation on Air-side Pressure Drop and Fan Power

required are higher at regions of higher air flow rate and higher fin densities in spite of the additional flow area provided in the upper rows due to the larger fin height. The air-side pressure drop at the inlet to the top-most tube is 129.4 Pa, while it is 31.9 Pa at the corresponding position in the lower-most tube. The fan power per segment at the inlet to the top-most tube is 0.381 W, while it is 0.050 W at the corresponding location in the bottom-most tube. The total fan power for this case is 112.0 W, while that for the uniform fin height case is 113.6 W.

Figure 5.8 summarizes the condenser performance for various fin height non-uniformities ranging from -0.7 to 0.7 *under an air flow mal-distribution of degree 0.3 and fin density non-uniformity of degree 0.2.* The condenser mass is found to be minimum for a fin height deviation of 0.1. Thus a fin height deviation of 0.1 is chosen as the optimum fin height configuration. This configuration requires a condenser mass of 2.608 kg, with a refrigerant temperature glide of 0.62^{o}C and fan power requirement of 112.0 W.

As the condenser length is decreased, the condenser face area decreases resulting in an increase in the air face velocity. Hence the face air velocity is maximum at 3.86 m/s for a fin height non-uniformity of 0.1. The fan power however constantly increases as the fin height non-uniformity is made more negative. This is because at highly negative fin height non-uniformities, though the face velocities are lower, the fan power is high due to the very high pressure drop (in the top-most tube, 221.6 Pa for ch_{dev} = -0.7, while 135.4 Pa for uniform fin height distribution) combined with a high air flow rate at the top of the condenser. The air-side pressure drop at the refrigerant inlet region of the top-most condenser is 221.6 Pa for a ch_{dev} = -0.7, while it is 135.4 Pa for a uniform fin height

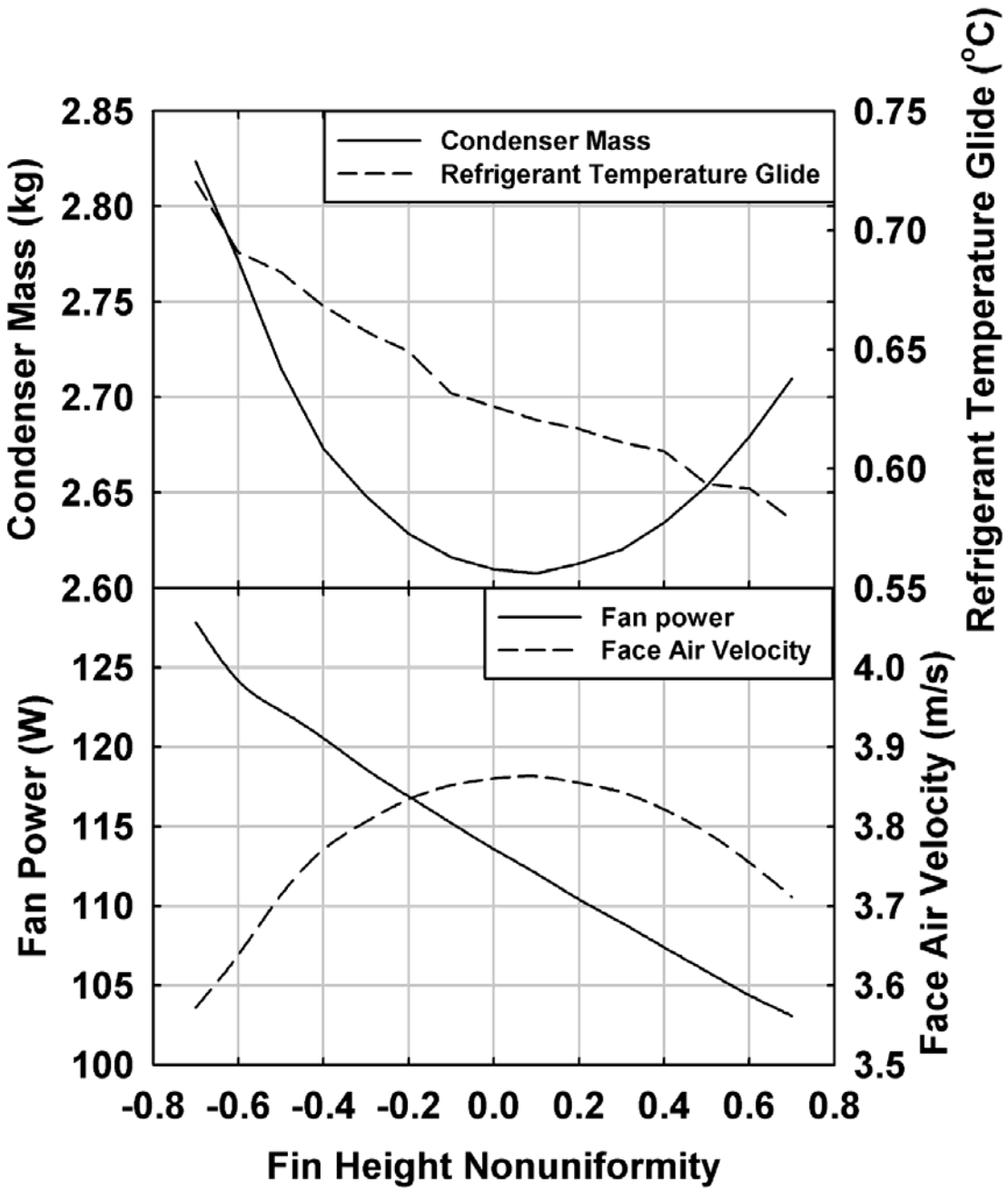

Figure 5. 8 Effect of Fin Height Deviations

distribution. The fan power required is 127.8 W for a fin height non-uniformity of -0.7, and decreases to 103.1 W for a fin height non-uniformity of 0.7.

Thus the optimum air-side geometry for an air flow mal-distribution of degree $\phi = 0.3$ is a fin density deviation f_{dev} of -0.2 and a fin height deviation ch_{dev} of 0.1.

5.6 Optimum Air-side Geometry for various Air Flow Mal-distributions

An air-side geometry optimization study, like the one described in the previous four sections was conducted for air flows of mal-distribution ranging from -0.5 to 0.5. The

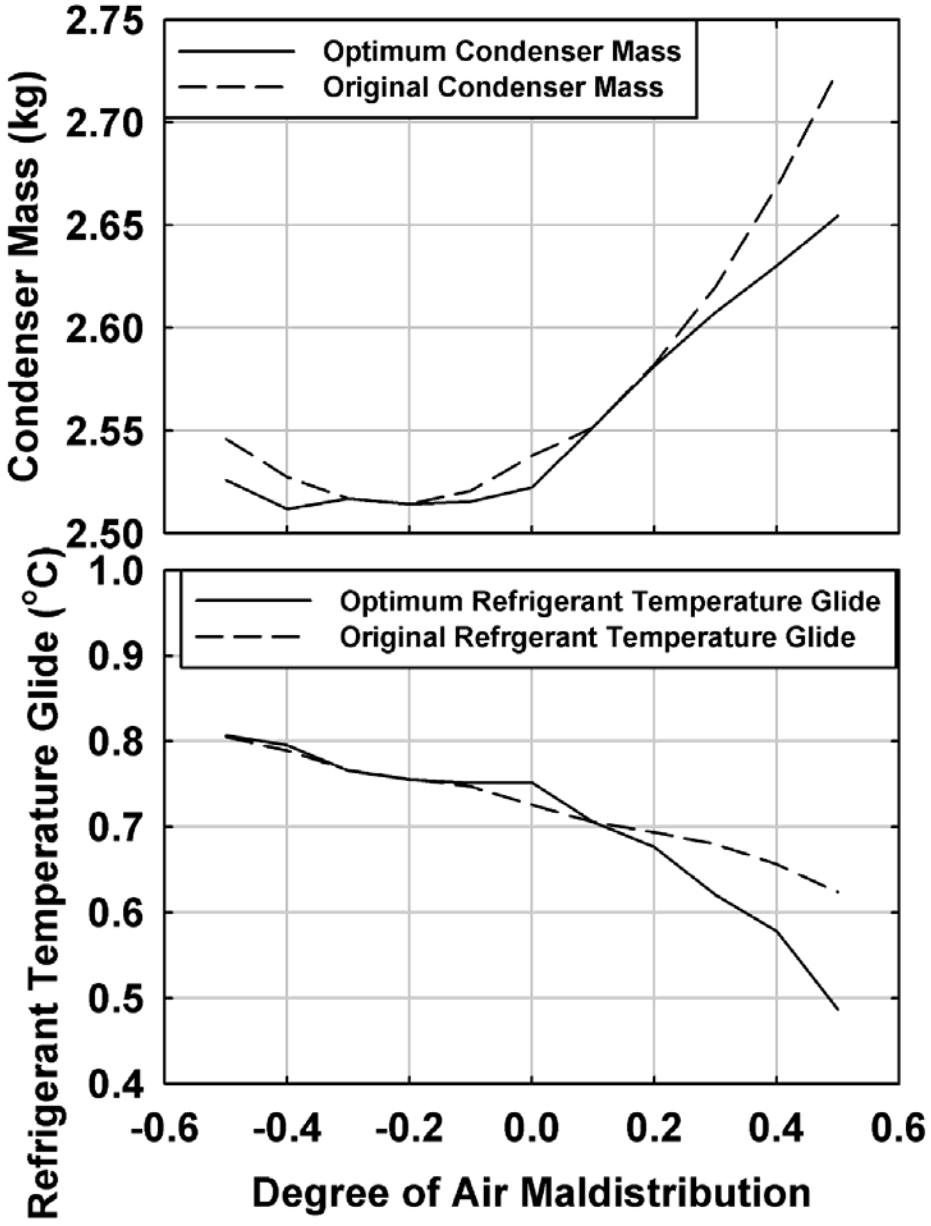

Figure 5. 9 Performance of the Optimum Geometry

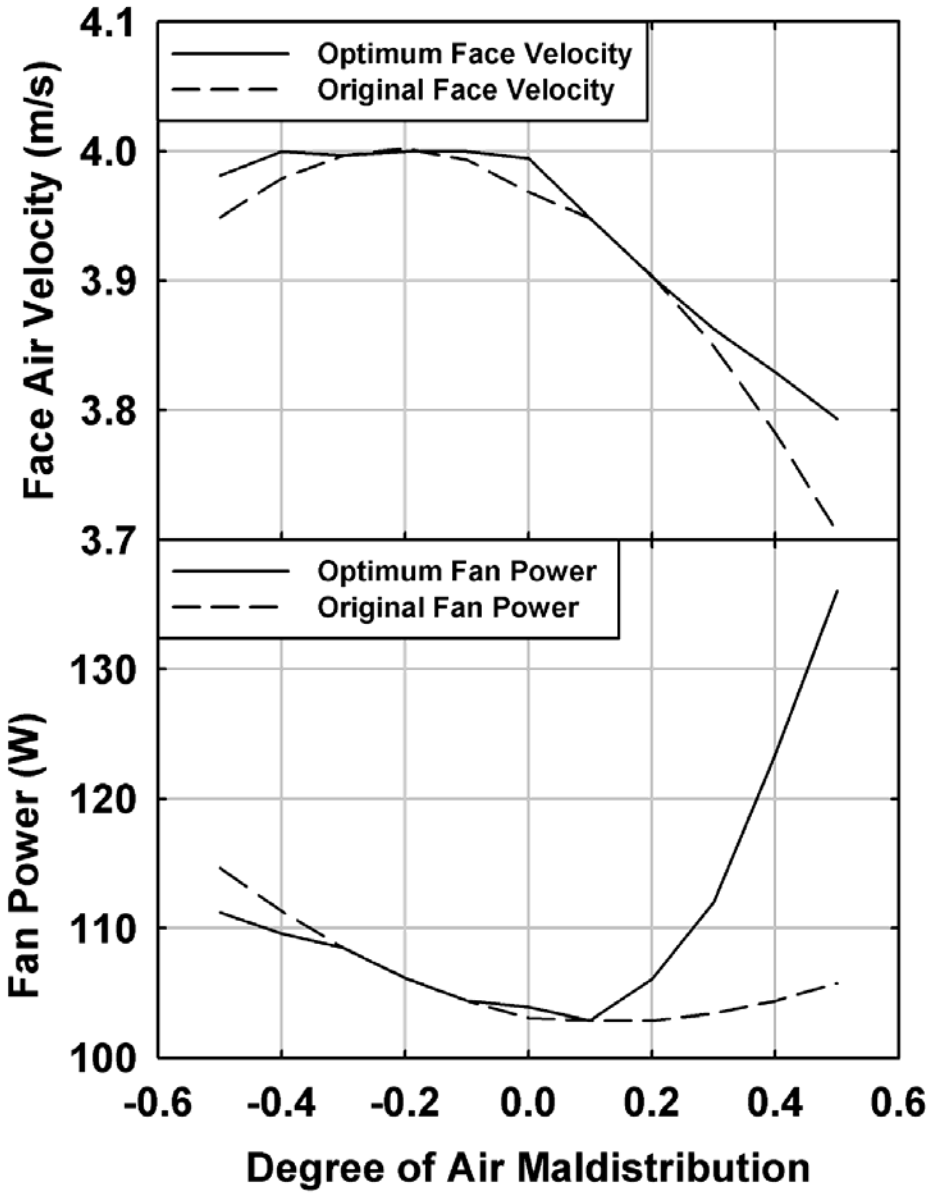

Figure 5. 10 Performance of the Optimum Geometry

results of these optimization studies are summarized in Figures 5.9 and 5.10. It is seen that the condenser mass required is reduced by the air-side geometry optimizations for the extreme air flow mal-distributions. For an air flow mal-distribution of $\phi = 0.5$, the required condenser mass is 2.73 kg for uniform air-side geometry, but can be reduced to 2.65 kg through air-side geometry optimizations. Similarly, for an air flow mal-

distribution of -0.5 the required condenser mass is reduced from 2.55 kg to 2.53 kg through air-side geometry optimization.

The refrigerant temperature glide is significantly lower in the case of air flow mal-distribution of degree 0.5. The refrigerant temperature glide in the case of uniform air-side geometry is 0.62^{o}C and decreases to 0.49^{o}C by air-side geometry optimization.

The face air velocity is higher in the optimum air-side geometry cases, because these have a lower tube length and hence a lower condenser face area. This also results in higher fan power requirement for the optimum cases. This is shown in Figure 5.10.

This analysis shows that the maximum reduction in the condenser mass due to air-side geometry modifications is from 2.73 kg to 2.64 kg for an air flow mal-distribution of 0.5. However in section 3.10, the condenser masses calculated for the baseline geometry using the correlations by Shah (1979), Traviss *et al.* (1973) and Soliman *et al.* (1968) were 2.91 kg, 2.93 kg and 3.15 kg respectively. Thus the change in condenser mass due to the use of different tube-side heat transfer coefficient correlations is more than that due to the use of non-uniform air-side geometries. Therefore, uncertainties in heat transfer correlations should be recognized while choosing geometric parameters. It can still be concluded, however, that given a heat transfer correlation, the minima in condenser mass will occur at the same combination of parameters as chosen here, although the actual mass required would vary by an amount dependent on the uncertainty in the heat transfer correlation.

Chapter 6

CONCLUSIONS AND RECOMMENDATIONS

6.1 Conclusions

An analysis of the heat duty, pressure drop and other performance parameters of a multilouver fin, microchannel condenser for a variety of geometry and inlet conditions was performed in this study. The refrigerant-side and air-side heat transfer coefficients and pressure drop were computed using correlations from the literature. For a uniform air flow case, a design procedure was developed to obtain the condenser geometry that delivers the required heat duty of 14.5 kW with lowest condenser mass. The design procedure led to a 19% reduction in the required condenser mass.

The performance of the optimum geometry obtained for uniform air flow conditions was then tested under linearly mal-distributed air flow conditions. An air flow mal-distribution of degree $\phi = 0.5$ (i.e. higher air flow rate near refrigerant inlet) was found to increase the required condenser mass by 7%, while an air flow mal-distribution of degree $\phi = -0.2$ was found to reduce the required condenser mass by 1%. The air-side geometrical parameters, viz. fin density and fin height were linearly varied to obtain a geometry that delivers the design heat duty with minimum condenser mass under mal-distributed air flow conditions. The required condenser mass was reduced by as much as 3% due to judicious allocation of fin density and fin height across the condenser. In fact, for certain cases, the optimum geometry obtained for mal-distributed air flows was found to have a lower mass than the original condenser, designed for uniform air flow. Thus air flow mal-distributions could be turned to a benefit, by careful design.

The design procedure presented in the current work can be used as a tool for efficient microchannel condenser design. A set of design constraints were used in the current work. These constraints could be modified to suit the specific application. Also the ease of manufacture and first cost of the optimum geometry needs to be considered, while designing for a real-life application.

6.2 Recommendations for Further work

This work represents a preliminary step in the analysis and design of microchannel tube, multilouver fin condensers under realistic air flow conditions. While air flow mal-distributions from the top to bottom of the condenser were considered here, potential lateral mal-distributions and non linear vertical distributions of air flow should also be investigated. Also the modifications made in the air-side geometry to improve condenser performance might affect the upstream inlet air flow pattern available to the condenser. The condenser design for mal-distributed air flow could be further improved to account for this cross effect of change in inlet air flow pattern due to modifications in downstream air-side geometry. Furthermore, in all case investigated here, the air inlet temperature was assumed to be uniform across the condenser. Mal-distributed temperatures should be investigated in further studies. Refrigerant flow across different tubes within a pass was also assumed to be uniform in this study; however in actual condensers, refrigerant flow non-uniformities exist due to poor header design and fabrication. An investigation of the effect of refrigerant mal-distribution on condenser performance would complement this study. It should be noted that the design procedure for uniform air flow optimized one geometric parameter at a time and did not account for

the cross-effects between various parameters. While a perturbation of the final chosen parameters was conducted to validate the choice of these values, these cross-effects would perhaps be best captured using a more elaborate optimization procedure that optimizes all the geometric parameters simultaneously, albeit at a much greater computational expense. Finally, the results from this study should be validated experimentally, and the effect of condenser design optimization on the system-level performance of an air-conditioning system should be investigated. As part of this, the capital costs involved in implementing the design geometries with non-uniform air-side geometries should be studied.

REFERENCES

Beiler, M. G. and Kroger, D. G. (1996), "Thermal performance reduction in air-cooled heat exchangers due to nonuniform flow and temperature distributions," *Heat Transfer Engineering*, **17** (1): 82-92.

Berryman, R. J. and Russell, C. M. B. (1987), "Effect of Maldistribution of Airflow on Air-Cooled Heat Exchanger Performance," *Maldistribution of Flow and Its Effect on Heat Exchanger Performance. Presented at the 24th National Heat Transfer Conference and Exhibition.*, Pittsburgh, PA, USA, ASME, New York, NY, USA, pp. 19-23.

Bhatti, M. S. and Shah, R. K. (1987). Turbulent and transition flow convective heat transfer in ducts. Handbook of single-phase convective heat transfer. S. Kakac, R. K. Shah and W. Aung, Wiley-Interscience**:** 4.1-4.166.

Butterworth, D. (1975), "A comparison of some void-fraction relationships for co-current gas-liquid flow," *International Journal of Multiphase Flow*, **1** (6): 845-50.

Chiou, J. P. (1983), "Effect of the Air Flow Nonuniformity on the Thermal Performance of Automobile Air Conditioning Condenser," *International Congress & Exposition - Society of Automotive Engineers*, Detroit, MI, Engl, SAE, Warrendale, Pa, USA, p. 830542.

Churchill, S. W. (1977a), "Comprehensive Correlating Equations for Heat, Mass and Momentum Transfer in Fully Developed Flow in Smooth Tubes," *Industrial & Engineering Chemistry, Fundamentals*, **16** (1): 109-116.

Churchill, S. W. (1977b), "Friction-Factor Equation Spans All Fluid-Flow Regimes," *Chemical Engineering (New York)*, **84** (24): 91-92.

Elgowainy, A. (2001), "Effect of airflow nonuniformity on the thermal performance and pressure drop in tube-fin heat exchanger of an air-conditioning system," *35th National Heat Transfer Conference*, Anaheim

Friedel, L. (1979), "New friction pressure drop correlations for upward, horizontal and downward two-phase pipe flow," *HTFS Symposium*, Oxford

Garimella, S. and Coleman, J. W. (1998), "Design of cross-flow condensers for ammonia-water absorption heat pumps," *Proceedings of the 1998 ASHRAE Winter Meeting. Part 2 (of 2), Jan 18-21 1998*, San Francisco, CA, USA, ASHRAE, Atlanta, GA, USA, pp. 1553-1564.

Garimella, S., Coleman, J. W. and Wicht, A. (1997), "Tube and fine geometry alternatives for the design of absorption-heat-pump heat exchangers," *Journal of Enhanced Heat Transfer*, **4** (3): 217-235.

Garimella, S. and Wicht, A. (1995), "Air-cooled condensation of ammonia in flat-tube, multi-louver fin heat exchangers," *Proceedings of the 1995 ASME International Mechanical Engineering Congress and Exposition, Nov 12-17 1995*, San Francisco, CA, USA, ASME, New York, NY, USA, pp. 47-58.

Jiang, Y. and Garimella, S. (2001), "Compact air-coupled and hydronically coupled microchannel heat pumps," *2001 ASME International Mechanical Engineering Congress and Exposition, Nov 11-16 2001*, New York, NY, United States, American Society of Mechanical Engineers, pp. 227-239.

Kim, J.-H. and Groll, E. A. (2003), "Performance comparisons of a unitary split system using microchannel and fin-tube outdoor coils," *ASHRAE Transactions Technical*

and Symposium Papers, Kansas City, MO, United States, Amer. Soc. Heating, Ref. Air-Conditoning Eng. Inc., pp. 219-229.

Kim, M.-H. and Bullard, C. W. (2002a), "Air-side thermal hydraulic performance of multi-louvered fin aluminum heat exchangers," *International Journal of Refrigeration*, **25** (3): 390-400.

Kim, M.-H. and Bullard, C. W. (2002b), "Performance evaluation of a window room air conditioner with microchannel condensers," *Journal of Energy Resources Technology, Transactions of the ASME*, **124** (1): 47-55.

Lee, J., Kwon, Y.-C. and Kim, M. H. (2003), "An improving method for analyzing a fin and tube evaporator containing a zeotropic mixture refrigerant with air mal-distribution," *International Journal of Refrigeration*, **26** (6): 707-720.

Lemmon, E. W., McLinden, M. O. and Huber, M. L. (2002). Reference Fluid Thermodynamic and Transport Properties, NIST.

Natarajan, N. M. and Lakshmanan (1972), "Laminar flow in rectangular ducts: Prediction of velocity profiles and friction factor," *Indian Journal of Technology*, **10** (12): 435-438.

Purday, H. F. P. (1949). An introduction to the mechanics of viscous flow; film lubrication, the flow of heat by conduction and heat transfer by convection. New York, Dover.

Rabas, T. J. (1987), "Effect of nonuniform inlet flow and temperature distributions on the thermal performance of air-cooled condensers," *Maldistribution of Flow and Its Effect on Heat Exchanger Performance. Presented at the 24th National Heat Transfer Conference and Exhibition.*, Pittsburgh, PA, USA, ASME, New York, NY, USA, pp. 29-35.

Rohsenow, W. M., Hartnett, J. P. and Gani´c, E. N. (1985). Handbook of heat transfer fundamentals. New York, McGraw-Hill.

Shah, M. M. (1979), "General correlation for heat transfer during film condensation inside pipes," *International Journal of Heat and Mass Transfer*, **22** (4): 547-556.

Shah, R. K. and Bhatti, M. S. (1987). Laminar Convective Heat Transfer in Ducts. Handbook of Single-Phase Convective Heat Transfer. S. Kakac, R. K. Shah and W. Aung, Wiley-Interscience**:** 3.1-3.137.

Shah, R. K. and London, A. L. (1978). Laminar flow forced convection in ducts : a source book for compact heat exchanger analytical data. New York, Academic Press.

Soler, A. I., Singh, K. P. and Ng, T.-L. (1983), "Effect of nonuniform inlet air flow on air cooler heat exchange performance," *ASME-JSME Thermal Engineering Joint Conference Proceedings*, Honolulu, HI, USA, ASME, New York, NY, USA, pp. 537-542.

Soliman, M., Schuster, J. R. and Berenson, P. J. (1968), "A general heat transfer correlation for annular flow condensation," *Journal of Heat Transfer*, **90**: 267-276.

Traviss, D. P., Rohsenow, W. M. and Baron, A. B. (1973), "Forced-Convection Condensation Inside Tubes: A Heat Transfer Equation for Condenser Design," **79** (Part 1): 157-165.

Webb, R. L. (1994). Principles of enhanced heat transfer. New York, John Wiley & Sons Inc.